Screening of electrode materials for microbial fuel cells operating with *S. oneidensis* and *G. sulfurreducens*

Dissertation

zur Erlangung des Doktorgrades der Technischen Fakultät

der Albert-Ludwigs-Universität Freiburg im Breisgau

Vorgelegt von

Elena Kipf (Dipl.-Ing.)

Freiburg im Breisgau 2019

Dekan

Prof. Dr. Rolf Backofen

Referenten

Prof. Dr. Roland Zengerle (Freiburg)

Prof. Dr. Johannes Gescher (Karlsruhe)

Tag der Abgabe: 04.09.2019

Tag der Prüfung: 16.12.2019

Elena Kipf

IMTEK - Institut für Mikrosystemtechnik

Professur für Anwendungsentwicklung

Technische Fakultät

Albert-Ludwigs-Universität Freiburg im Breisgau

Für meine Eltern

Abstract

Microbial fuel cells are an upcoming ecological and sustainable technology to generate electricity from abundant organic residues or wastewater without the need for expensive noble-metal catalysts. Electroactive microorganisms function as biocatalysts by oxidizing organic biomass and transferring the released electrons to the anode electrode as external electron acceptor in order to sustain their bacterial metabolism.

One aim of this thesis is to identify anode materials which yield high current densities. The comparison of anode materials from literature is difficult, since the studies differ in their operating conditions, measurement techniques, inoculation strategies and fuel cell constructions. Therefore, systematic and extensive anode material screenings under application-relevant steady-state conditions are presented here, using the two strains *Shewanella oneidensis* and *Geobacter sulfurreducens*. Both are model organisms for microbial fuel cells, but rely on different electron transfer mechanisms: diffusive mediated electron transfer via self-secreted shuttles (*S. oneidensis*) and direct electron transfer via outer membrane cytochromes of cells attached to the electrode (*G. sulfurreducens*). In that context, it is of major interest to find out if these model organisms perform differently with the anode materials due to their distinct electron transfer mechanisms.

In chapter 2 of this thesis, a systematic screening of carbon-based anode materials for microbial fuel cells with *S. oneidensis* is presented. Under anoxic conditions nanoporous activated carbon cloth is a superior anode material in terms of current density normalized to the projected anode area and anode volume (24.0 ± 0.3 µA cm^{-2} and 482 ± 7 µA cm^{-3} at −0.2 V vs. SCE, respectively). The good performance can be attributed to the high specific surface area of the material, which is available for mediated electron transfer through self-secreted flavins. Under aerated conditions, *S. oneidensis* achieves an about three times higher current density with activated carbon cloth (79 ± 5 µA cm^{-2} at -0.2 V vs. SCE) and an about six times higher current density with graphite felt (78 ± 1 µA cm^{-2} at -0.2 V vs. SCE), however at the expense of the coulombic efficiency. These higher current densities compared to anoxic operation might be related to the formation of a thicker biofilm under aeration. Interestingly, under aerated conditions no influence of the specific surface area regarding the achieved current densities was observed, which is attributed to a shift from

primary indirect electron transfer by mediators to direct electron transfer via adherent cells. Furthermore, with activated carbon cloth it could be shown that an aerated initial growth phase enhances the current density under subsequent anoxic conditions fivefold when compared to a similar experiment that was conducted under permanently anoxic conditions.

Chapter 3 of this thesis presents a comparison of the two model organisms *G. sulfurreducens* and *S. oneidensis* with two selected anode materials. High-surface-area activated carbon cloth and low-surface-area graphite felt were compared in terms of polarization curves under quasi-steady-state conditions. Unexpectedly, *G. sulfurreducens* exhibits similar current densities up to 700 µA cm^{-2} independent of the anode material. This is ∼50 % higher than steady-state values reported previously. The negligible influence of the electrode material on the electrical performance of *G. sulfurreducens* is attributed to the fact that it performs only direct electron transfer, but forms thick biofilms. In contrast, *S. oneidensis*, relying mainly on mediated electron transfer, apparently makes better use of high-surface-area activated carbon and achieves higher current densities compared to graphite felt. This underlines the importance of tailoring anode materials according to the used organisms.

In order to further examine the effect of the anode material on the achievable current density with *G. sulfurreducens*, a systematic investigation of different carbon- and metal-based anode materials was conducted in chapter 4 of this thesis, using a pure culture of the model organism *G. sulfurreducens*. The highest limiting current density of 756 ± 15 µA cm^{-2} at −0.253 ± 0.037 V vs. SCE was achieved with graphite foil using a step-wise galvanostatic technique. But also the application of completely different anode materials such as activated carbon cloth, stainless steel and graphite felt led to similar high limiting current densities, suggesting that *G*. *sulfurreducens* is able to use a large range of substantially different anode materials as external electron acceptor. Additionally, it could be shown that a step-wise galvanostatic polarization to record polarization curves yields similar current densities as potentiostatic control at −0.400 V vs. SCE with the investigated carbon-based materials. However, in case of stainless steel a significantly lower current density was achieved using step-wise galvanostatic polarization compared to potentiostatic control at -0.400 V vs. SCE, which is attributed to a strong polarization of stainless steel especially in the low current density region of the polarization curve. This effect is assumedly associated with the formation of an oxide layer with elevated electrical resistance on the metal surface as reported previously.

In conclusion, it could be demonstrated that for *S. oneidensis* the achievable current density depends significantly on the specific surface area of the material, which is

presumably available for the self-secreted flavins acting as electron shuttles. This result is beneficial for applications in which pure cultures of *S. oneidensis* are employed, such as in the bioproduction of platform chemicals using unbalanced fermentation, or in a biosensor. In contrast to *S. oneidensis*, *G. sulfurreducens* achieves substantially higher current densities with a wide range of different anode materials, without any influence of the specific surface area of the materials observed. This finding opens up the possibility to use a great variety of anode materials and to concentrate on robust and inexpensive materials that meet all criteria for future scale-up. In the context of recent literature that reports clogging and fouling of expensive, complex 3-dimensional anodes resulting in the same or even less current densities than 2-dimensional anodes, the in this thesis investigated flat anode materials are promising with regard to future practical application. These results indicate that the anode material needs to be selected according to the applied electroactive microorganism.

On the cathode side of a microbial fuel cell typically the oxygen reduction reaction takes place. To avoid the use of expensive noble-metal catalysts, the application of enzymes as biocatalysts has moved more and more into the focus. Nevertheless, time-consuming and cost-intensive enzyme purification as well as the limited enzyme lifetime due to intrinsic protein degradation are severe drawbacks of this technology. In that respect, previous research has shown that the lifetime of an immersed laccase cathode can be extended by the periodic supply of crude enzyme-containing supernatant of the fungus *T. versicolor.* A further aim of this thesis is therefore to transfer this promising approach to an application-relevant air-breathing cathode design.

A novel concept of an air-breathing enzymatic cathode combined with the continuous supply of unpurified laccase-containing supernatant of *T. versicolor* for extended cathode lifetime is presented in chapter 5 of this thesis. The air-breathing cathode design obviates the need for energy-intensive active aeration. In a corresponding long-term experiment at a constant current density of 50 µA cm^{-2}, an increased cathode lifetime of 33 days (cathode potential above 0.430 V vs. SCE), independent of the enzyme degradation could be demonstrated. In a control experiment without continuous enzyme supply, the cathode potential dropped immediately upon applying the current. This indicates that the continuous supply is crucial to increase the number of enzymes which can adsorb to the electrode to sustain the current density of 50 µA cm^{-2}. The obtained data suggest that theoretically a longer lifetime than 33 days is feasible. However, further engineering effort is required to prevent clogging and fouling of the supply tubes to further increase the operation time of the cathode. These results represent an important step towards the realization of a hybrid microbial-enzymatic biofuel cell with extended lifetime and enhanced performance.

Zusammenfassung

Mikrobielle Brennstoffzellen sind eine aufstrebende ökologische und nachhaltige Technologie zur Stromerzeugung aus reichlich verfügbaren organischen Reststoffen oder aus Abwasser, die den Einsatz teurer Edelmetall-Katalysatoren überflüssig macht. Elektroaktive Mikroorganismen fungieren als Biokatalysatoren, indem sie organische Biomasse oxidieren und die frei werdenden Elektronen auf die Anodenelektrode als externen Elektronenakzeptor übertragen, um ihren bakteriellen Metabolismus aufrecht zu erhalten.

Ein Ziel dieser Arbeit ist es Anodenmaterialien zu identifizieren, die hohe Stromdichten liefern. Der Vergleich von Anodenmaterialien aus der Literatur ist schwierig, da sich die Studien in ihren Betriebsbedingungen, Messverfahren, Inokulationsstrategien und Brennstoffzellen-Konstruktionen unterscheiden. Daher werden hier systematische und umfangreiche Anodenmaterialuntersuchungen unter anwendungsrelevanten steady-state Bedingungen mit den beiden Stämmen *Shewanella oneidensis* und *Geobacter sulfurreducens* vorgestellt. Beide sind Modellorganismen für mikrobielle Brennstoffzellen, besitzen jedoch unterschiedliche Elektronentransport-Mechanismen: diffusiver indirekter Elektronentransfer über selbst-sekretierte Shuttle (*S. oneidensis*) und direkter Elektronentransfer über die äußeren Membran-Cytochrome von an der Elektrode anhaftenden Zellen (*G. sulfurreducens*). In diesem Zusammenhang ist es von großem Interesse herauszufinden, ob diese Modellorganismen aufgrund ihrer verschiedenen Elektronentransfer-Mechanismen eine unterschiedliche Performance mit den Anodenmaterialien zeigen.

In Kapitel 2 dieser Arbeit wird ein systematisches Screening von Kohlenstoff-basierten Anodenmaterialen für mikrobielle Brennstoffzellen mit *S. oneidensis* vorgestellt. Unter anoxischen Bedingungen ist nanoporöses Aktivkohlegewebe ein ausgezeichnetes Anodenmaterial, sowohl hinsichtlich der auf die Anodenfläche als auch auf das Anodenvolumen projizierten Stromdichte (24,0 ± 0,3 µA cm^{-2} bzw. 482 ± 7 µA cm^{-3} bei -0,2 V vs. SCE). Die gute Performance ist auf die hohe spezifische Oberfläche des Materials zurückzuführen, die für indirekten Elektrontransport über selbstsekretierte Flavine zur Verfügung steht. Unter aeroben Bedingungen erreicht *S. oneidensis* mit Aktivkohlegewebe eine etwa dreimal höhere Stromdichte (79 ± 5 µA cm^{-2} bei -0,2 V vs. SCE) und mit Graphitvlies eine etwa sechsfach höhere Stromdichte (78 ± 1 µA cm^{-2} bei -0,2 V vs. SCE),

jedoch auf Kosten der coulombschen Effizienz. Diese höheren Stromdichten im Vergleich zum anoxischen Betrieb könnten mit der Bildung eines dickeren Biofilms unter Luftzufuhr zusammenhängen. Interessanterweise wurde unter aeroben Bedingungen kein Einfluss der spezifischen Oberfläche hinsichtlich der erreichten Stromdichten beobachtet, was auf eine Verschiebung des primär indirekten Elektronentransfers über Mediatoren zu direktem Elektronentransfer über adhärente Zellen zurückzuführen ist. Darüber hinaus konnte mit Aktivkohlegewebe gezeigt werden, dass eine aerobe initiale Wachstumsphase die Stromdichte unter nachfolgenden anoxischen Bedingungen um das Fünffache erhöht, im Vergleich zu einem ähnlichen Experiment, das dauerhaft unter anoxischen Bedingungen durchgeführt wurde.

Kapitel 3 dieser Arbeit zeigt einen Vergleich der beiden Modellorganismen *G. sulfurreducens* und *S. oneidensis* mit zwei ausgewählten Anodenmaterialien. Aktivkohle mit großer spezifischer Oberfläche und Graphitvlies mit geringer spezifischer Oberfläche wurden hinsichtlich der Polarisationskurven unter quasi-steady-state Bedingungen verglichen. Unerwarteterweise zeigt *G. sulfurreducens* unabhängig vom Anodenmaterial ähnliche Stromdichten von bis zu 700 µA cm^{-2}. Das ist ∼50% höher als zuvor veröffentlichte steady-state Werte. Der vernachlässigbare Einfluss des Elektrodenmaterials auf die elektrische Performance von *G. sulfurreducens* wird darauf zurückgeführt, dass dieser nur direkten Elektronentransport ausübt, aber dicke Biofilme ausbildet. Im Gegensatz dazu verwendet *S. oneidensis* hauptsächlich indirekten Elektrontransport und kann offenbar die große spezifische Oberfläche der Aktivkohle besser ausnützen und erzielt damit höhere Stromdichten als mit Graphitvlies. Dies unterstreicht die Wichtigkeit die Anodenmaterialien an die verwendeten Mikroorganismen anzupassen.

Um den Einfluss des Anodenmaterials auf die erreichbare Stromdichte mit *G. sulfurreducens* weiter zu untersuchen, wurde in Kapitel 4 dieser Arbeit eine systematische Untersuchung verschiedener Kohlenstoff- und Metall-basierter Anodenmaterialien mit einer Reinkultur des Modellorganismus *G. sulfurreducens* durchgeführt. Die höchste limitierende Stromdichte von 756 ± 15 µA cm^{-2} bei -0,253 V vs. SCE wurde mit Graphitfolie unter Verwendung einer schrittweisen galvanostatische Technik erzielt. Aber auch die Verwendung völlig anderer Anodenmaterialien wie Aktivkohlegewebe, Edelstahl und Graphitvlies führte zu ähnlich hohen limitierenden Stromdichten, was darauf hindeutet, dass *G. sulfurreducens* in der Lage ist, eine große Bandbreite an wesentlich unterschiedlichen Anodenmaterialien als externen Elektronenakzeptor zu verwenden. Außerdem konnte für die untersuchten Kohlenstoff-basierten Materialien gezeigt werden, dass eine schrittweise galvanostatische Polarisation zur Aufnahme von Polarisationskurven ähnliche Stromdichten liefert wie die potentiostatische Steuerung bei -0,400 V vs. SCE. Im Falle von Edelstahl wurde

jedoch mit der schrittweisen galvanostatischen Polarisation eine deutlich geringere Stromdichte erreicht als mit der potentiostatischen Steuerung bei -0.400 V vs. SCE, was auf eine starke Polarisierung von Edelstahl insbesondere im Bereich der geringen Stromdichten in der Polarisationskurve zurückzuführen ist. Dieser Effekt hängt vermutlich mit der Bildung einer Oxidschicht mit erhöhtem elektrischen Widerstand auf der Metalloberfläche zusammen, wie zuvor berichtet wurde.

Zusammenfassend konnte gezeigt werden, dass für *S. oneidensis* die erreichbare Stromdichte signifikant von der spezifischen Oberfläche des Materials abhängt, die vermutlich für die als Elektronen-Shuttle fungierenden selbstsekretierten Flavine zugänglich ist. Dieses Ergebnis ist vorteilhaft für Anwendungen, bei denen Reinkulturen von *S. oneidensis* eingesetzt werden, wie z.B. bei der Bioproduktion von Plattformchemikalien durch „unbalanced fermentation“ oder in einem Biosensor. Im Gegensatz zu *S. oneidensis* erreicht *G. sulfurreducens* wesentlich höhere Stromdichten als *S. oneidensis* mit einer großen Bandbreite verschiedener Anodenmaterialien, ohne dass ein Einfluss der spezifischen Oberfläche der Materialien beobachtet wurde. Dieses Ergebnis eröffnet die Möglichkeit eine Vielzahl an Anodenmaterialien zu verwenden und sich auf robuste und kostengünstige Materialien zu konzentrieren, die alle Kriterien für ein zukünftiges Scale-up erfüllen. Im Zusammenhang neuerer Literatur, die über Verstopfen und Zusetzen von teuren, komplexen dreidimensionalen Anoden berichtet, die gleichhohe oder sogar geringere Stromdichten wie 2-dimensionale Anoden liefern, sind die in dieser Arbeit untersuchten flachen Anodenmaterialien im Hinblick auf die zukünftige praktische Anwendung vielversprechend. Diese Ergebnisse deuten darauf hin, dass das Anodenmaterial entsprechend dem verwendeten elektroaktiven Mikroorganismus ausgewählt werden muss.

Auf der Kathodenseite einer mikrobiellen Brennstoffzelle findet typischerweise die Sauerstoffreduktionsreaktion statt. Um den Einsatz teurer Edelmetall-Katalysatoren zu vermeiden, rückt der Einsatz von Enzymen als Biokatalysatoren immer mehr in den Fokus. Dennoch sind die zeitaufwendige und kostenintensive Enzymaufreinigung sowie die begrenzte Enzymlebensdauer durch intrinsische Proteindegradation gravierende Nachteile dieser Technologie. In diesem Zusammenhang haben frühere Untersuchungen gezeigt, dass die Lebensdauer einer eingetauchten Laccase-Kathode durch die periodische Zufuhr von unaufgereinigtem enzymhaltigen Überstand des Pilzes *T. versicolor* verlängert werden kann. Ein weiteres Ziel dieser Arbeit ist es daher, diesen vielversprechenden Ansatz auf ein anwendungsrelevantes luftatmendes Kathodendesign zu übertragen.

Ein neuartiges Konzept einer luftatmenden enzymatischen Kathode in Kombination mit der kontinuierlichen Zufuhr von unaufgereinigtem Laccase-haltigen Überstand von

T. versicolor für eine verlängerte Kathodenlebensdauer, wird in Kapitel 5 dieser Arbeit vorgestellt. Das luftatmende Kathodendesign macht eine Energie-intensive aktive Luftzufuhr überflüssig. In einem entsprechenden Langzeitversuch konnte bei einer konstanten Stromdichte von 50 µA cm^{-2} eine verlängerte Kathodenlebensdauer von 33 Tagen (Kathodenpotential über 0,430 V vs. SCE), unabhängig von der Enzymdegradation gezeigt werden. In einem Kontrollversuch ohne kontinuierliche Enzymzufuhr sank das Kathodenpotential unmittelbar nach Anlegen des Stroms ab. Dies zeigt, dass die kontinuierliche Zufuhr entscheidend ist, um die Anzahl der Enzyme zu erhöhen, die an die Elektrode adsorbieren können, um die Stromdichte von 50 µA cm^{-2} aufrechtzuerhalten. Die erhaltenen Daten deuten darauf hin, dass theoretisch eine längere Lebensdauer als 33 Tage möglich ist. Allerdings ist weiterer technischer Aufwand erforderlich, um ein Verstopfen und Zusetzen der Zufuhrschläuche zu verhindern, um die Betriebsdauer der Kathode weiter zu erhöhen. Diese Ergebnisse sind ein wichtiger Schritt zur Realisierung einer hybriden mikrobiellen-enzymatischen Brennstoffzelle mit verlängerter Lebensdauer und verbesserter Performance.

List of publications

Publications in peer reviewed journals

- E. Kipf, S. Sané, D. Morse, T. Messinger, R. Zengerle, S. Kerzenmacher: *An air-breathing enzymatic cathode with extended lifetime by continuous laccase supply*. Bioresource Technology 264 (2018) 306–310.

- E. Kipf, J. Erben, R. Zengerle, J. Gescher, S. Kerzenmacher: *Systematic investigation of anode materials for microbial fuel cells with the model organism G. sulfurreducens*. Bioresource Technology Reports 2 (2018) 29–37.

- K. Sturm-Richter, F. Golitsch, G. Sturm, E. Kipf, A. Dittrich, S. Kerzenmacher, J. Gescher: *Unbalanced fermentation in Escherichia coli via heterologous production of an electron transport chain and connection to anodes in microbial fuel cells.* Bioresource Technology 186 (2015) 89–96.

- E. Kipf, R. Zengerle, J. Gescher, S. Kerzenmacher**:** *How does the choice of anode material influence electrical performance? A comparison of two microbial fuel cell model organisms*. Chem. Electro. Chem. 1 (2014) 1849–1853.

- E. Kipf, J. Koch, B. Geiger, J. Erben, K. Richter, J. Gescher, R. Zengerle, S. Kerzenmacher: *Systematic screening of carbon-based anode materials for microbial fuel cells with Shewanella oneidensis MR-1.* Bioresource Technology 146 (2013) 386–392.

Publications at national and international conferences

- E. Kipf, D. Morse, T. Messinger, S. Sané, S. Kerzenmacher: *An air-breathing enzymatic cathode with extended lifetime by continuous laccase supply.* 2015 European Fuel Cell Technology & Applications Conference, Naples, Italy, 2015.

- E. Kipf, T. Messinger, S. Sané, S. Kerzenmacher: *An air-breathing cathode based on buckypaper electrodes with reversibly adsorbed laccase.* 2nd European International Society for Microbial Electrochemistry and Technology Meeting, Alcalá, Spain, 2014.

- K. Richter, F. Golitsch, G. Sturm, E. Kipf, A. Dittrich, S. Kerzenmacher, J. Gescher: *Unbalanced fermentation in Escherichia coli by heterologous production of an electron transport chain and electrode-interaction in microbial electrochemical cells.* 2nd European International Society for Microbial Electrochemistry and Technology Meeting, Alcalá, Spain, 2014.

- K. Richter, F. Golitsch, G. Sturm, E. Kipf, A. Dittrich, S. Kerzenmacher, J. Gescher: *Heterologous production of an electron transport chain and electrode-interaction in microbial electrochemical cells enables Escherichia coli to perform unbalanced fermentation.* Jahrestagung der Vereinigung für allgemeine und angewandte Mikrobiologie (VAAM) 2014, Dresden, Germany, 2014.

- E. Kipf, D. Thissen, S. Kerzenmacher: *Air-breathing cathodes for microbial fuel cells based on activated carbon cloth and spin-coated PDMS membranes as hydrophobic diffusion layer.* 4th International Microbial Fuel Cells Conference, Cairns, Australia, 2013.

- J. Erben, A. Sido, E. Kipf, S. Thiele, S. Kerzenmacher: *Improving current production of Shewanella oneidensis MR-1 with electrospun anode materials.* 4th International Microbial Fuel Cell Conference, Cairns, Australia 2013.

- S. Kerzenmacher, J. Danzer, J. Erben, E. Kipf, A. Kloke, C. Köhler, S. Sané, R. Zengerle: *Neue Materialien und Konzepte für Biobrennstoffzellen.* MikroSystemTechnik-Kongress 2013, Aachen, Germany, 2013.

- E. Kipf, J. Koch, B. Geiger, S. Kerzenmacher: *Systematic Comparison of Anode Materials for Microbial Fuel Cells*. Meeting of the European International Society for Microbial Electrochemical Technologies, Ghent, Belgium, 2012.

- E. Kipf, J. Koch, S. Kerzenmacher: *Systematic comparison of anode materials for microbial fuel cells.* 1st International Conference on Marine Resources and Beyond, Bremerhaven, Germany, 2011.

- S. Kerzenmacher, J. Danzer, E. Kipf, A. Kloke, C. Köhler, S. Rubenwolf, S. Sané, R. Zengerle, J. Gescher: Biobrennstoffzellen zur Energieversorgung von Mikrosystemen: *Vom energieautarken Implantat hin zum dezentralen Umwelt-Monitoring.* MikroSystemTechnik-Kongress 2011, Darmstadt, Germany, 2011.

Table of Contents

1 Introduction

Microbial fuel cells are defined as bioelectrochemical systems that convert chemical energy stored in organic matter directly into electricity. At the anode, the electrochemical reactions are catalyzed by electroactive microorganisms which function as biocatalysts for the anodic oxidation reaction [1]. In detail, to maintain their metabolism the bacteria oxidize organic substrates and transfer the gained electrons by different means of electron transfer mechanisms via their outer membrane to a solid external electron acceptor - in this case the anode electrode. At the cathode of a microbial fuel cell, typically the oxygen reduction reaction takes place, which is an either abiotic or biotic (using enzymes or microorganisms as biocatalysts) electrochemical reaction.

In contrast to conventional fuel cells, microbial fuel cells work at ambient temperatures (15 °C – 45 °C), neutral pH values and are able to utilize complex biomass as fuel such as wastewater or other renewable resources. In the upcoming depletion of fossil fuels and the thread of global warming, the possibility to generate electricity out of waste products has gained more and more interest. Especially with the fact, that up-to-date >86% of the energy is derived from the combustion of fossil fuels such as oil, coal, and natural gas, which leads to the emission of greenhouse gases such as CO_2 into the environment with the drastic consequence of global warming and environmental pollution [2, 3]. In that context, microbial fuel cells are regarded as a promising and sustainable wastewater treatment technology which does not generate any toxic by-products and at the same delivers clean water and green energy [1, 4].

One of the main applications of microbial fuel cells is electricity generation. Especially in poor areas without an urban energy infrastructure, microbial fuel cells are of interest as power source from waste products [5]. Furthermore, in remote areas where battery replacement is difficult microbial fuel cells are attractive for low power applications such as wireless sensor networks or environmental sensors, such as in a meteorological buoy [1, 5].

Another important application is wastewater treatment since industrial (e.g. brewery, food industry, or animal wastewater) and domestic wastewater contain high amounts of carbon compounds which can be oxidized by the electroactive microorganisms leading to electricity generation and at the same time treatment of the wastewater [6]. In this context,

it was demonstrated that cost-intensive existing wastewater treatment plants can be complemented with the microbial fuel cell technology which can lead to an autonomous self-sustainable treatment plant [1, 7]. Also related with this topic is the application of microbial fuel cells for bioremediation which can recycle water that is highly polluted and contains toxic compounds [6]. Therein, the reactions usually take place at the cathode where the toxic components are reduced either for removal or to a less toxic form and simultaneously generate electricity [6].

Besides the typical microbial fuel cell which converts chemical energy into electricity which is the most studied application, further bioelectrochemical systems have been developed. These include microbial electrolysis cells in which hydrogen is formed at the abiotic cathode by applying additional voltage [2], or microbial electrosynthesis cells in which CO_2 is reduced by bacteria to multi-carbon compounds using an external electrical circuit [1]. Another development is the microbial desalination cell which combines electricity generation and water desalination by inserting a seawater desalination chamber, separated by an anion-exchange and cation-exchange membrane from the anode and cathode electrode [1].

Nevertheless, microbial fuel cells are not a new technology as they were already invented by Potter et al. [8] in the year 1911 who was able to achieve current from yeasts and bacteria. However, as the results showed only minor advances, it took several years until microbial fuel cells gained interest again. In the 1960s biological fuel cells became more popular when NASA was interested in the technology to turn waste into electricity for their space missions [1]. But as the citation analysis on the keyword “microbial fuel cell” (Figure 1.1) indicates, only in the late 90s the attention of microbial fuel cells began to rise and is still increasing until today.

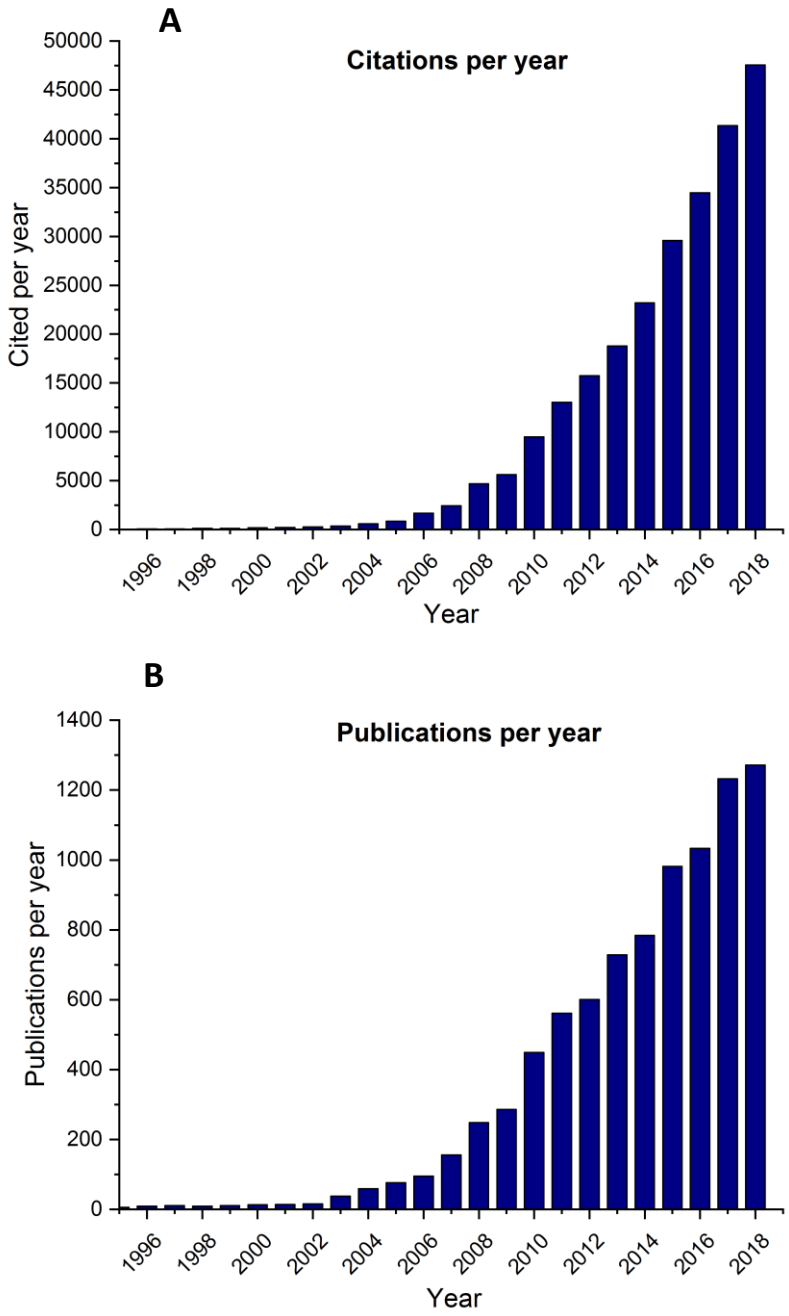

Figure 1.1: Citation analysis**. A** Number of citations per year and **B** number of publications per year on the keyword "microbial fuel cell" in the last 20 years (Web of Science, Basic search for Topic: microbial fuel cell, data collected on September 2nd, 2019).

However, there still exist limitations which hinder practical fuel cell application at a large scale, which are challenges in the scale-up process, the orders of magnitude lower power output compared to chemical fuel cells, and the cost of the materials used [1]. The power density reported for microbial fuel cells remains usually in the range 1-2 W m^{-2} (normalized to the cathode area) [9]. Typically, the electrodes are made of cost-efficient carbonaceous

materials, but especially at an abiotic cathode expensive noble metals such as platinum are typically used to catalyze the oxygen reduction reaction [5].

1.1 Microbial fuel cells

1.1.1 The principle of microbial fuel cells

The working principle of a microbial fuel cell is shown in Figure 1.2. The oxidation and reduction reaction take place in two separated compartments. In the anode compartment electroactive microorganisms oxidize organic matter and transfer the electrons resulting from the bacterial metabolism to an external electron acceptor: the anode. The detailed mechanism of the electron transfer depends on the applied anode microorganism and is discussed in detail in chapter 1.1.3. The electrons flow from the anode through an external electrical load (as depicted in Figure 1.2) to the cathode electrode. The driving force for the electrons to travel from the anode to the cathode is based on the thermodynamic potential difference between the oxidation (anode) and reduction (cathode) reaction. In a microbial fuel cell the cathode is either abiotic or biotic applying enzymes or microorganisms as biocatalysts. At the cathode, typically an oxygen reduction reaction takes place in which oxygen is reduced together with protons to water. In addition, in the anodic oxidation reaction protons are formed which travel through the electrolyte to the cathode electrode maintaining a closed electrical circuit, often via an ion-conductive membrane which separates the anode and cathode compartment.

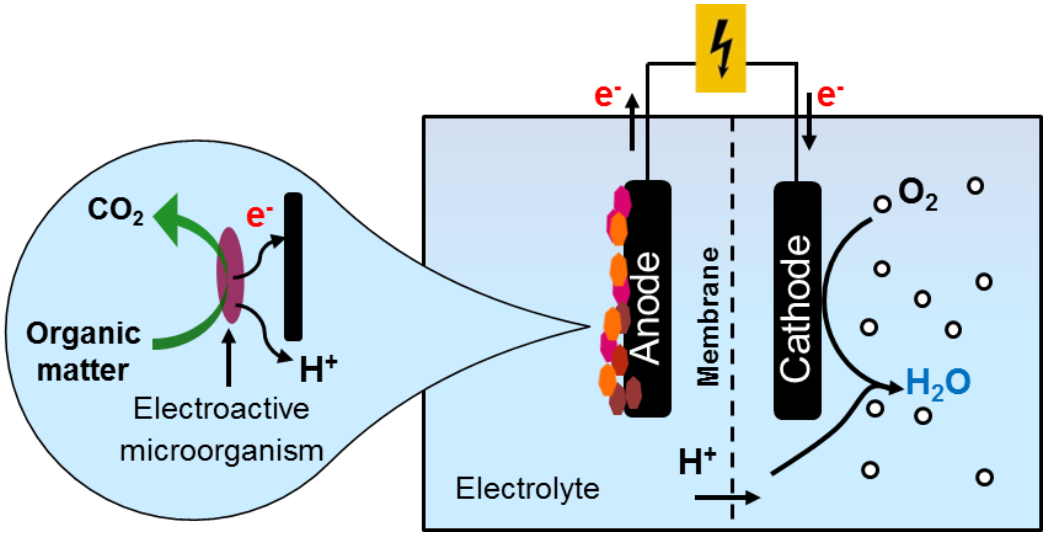

Figure 1.2: Schematic of a microbial fuel cell with a microbial anode and an abiotic cathode.

1.1.2 Microorganisms as biocatalysts

In nature, there exists a great diversity of electroactive bacteria [10], but the gram-negative proteobacteria *Shewanella oneidensis* and *Geobacter sulfurreducens* are the most frequently investigated electroactive organisms, especially as model organisms for microbial fuel cells, and for the investigation of the different underlying electron transfer mechanisms for extracellular respiration.

1.1.2.1 *Shewanella oneidensis*

Originally, *S. oneidensis* was isolated from anaerobic sediments of the Oneida Lake in the state New York [11]. It is a facultative anaerobic gram-negative γ-proteobacterium which has diverse respiratory abilities [12, 13]. In an aerobic environment *S. oneidensis* uses oxygen as terminal electron acceptor, but under anaerobic conditions it shows an outstanding ability to use a large range of insoluble and soluble terminal electron acceptors such as Mn(III) and (IV), Fe(III), Cr(VI), U(VI)), fumarate, nitrate, etc. [11, 14]. As carbon source, *S. oneidensis* oxidizes a variety of mainly fermentation end products (lactate, formate, and H_2) but only to the level of acetate under anoxic conditions [13].

S. oneidensis belongs to the electroactive microorganisms as it is able to transfer electrons via an extended respiratory chain to its cell surface [15]. The respiratory electrons travel from the cytoplasmic membrane through the periplasm and over the outer membrane which is facilitated by mainly multiheme c-type cytochromes, which are electron-transferring proteins [15]. The final reduction step of the external electron acceptor, e.g. metal oxide or the anode electrode is catalyzed by outer membrane cytochromes. For *S. oneidensis,* it was demonstrated that two of these outer membrane cytochromes are of high importance for the anodic respiration: OmcA (outer membrane cytochrome A) and MtrC (metal reducing protein C) [16, 17]. Genetic analysis of the *S. oneidensis* genome revealed up to 42 possible genes for c-type cytochromes [18]. This indicates that a multitude of c-type cytochromes is involved in the periplasmic electron transfer process and further research is still required to identify their role in the complex cascade of extracellular respiration. The fact that the whole genome of *S. oneidensis* has been sequenced allows for further characterization of the extracellular electron transfer on a genetic level [12].

Different electron transfer mechanisms for *S. oneidensis* were proposed in literature (explained in detail in chapter 1.1.3) including direct contact of the outer membrane cytochromes of the cells with the solid terminal electron acceptor, as well as the usage of self-secreted electron shuttles such as flavins, and direct contact via conductive pili (nanowires) [19]. However, it was demonstrated that mediated electron transfer via flavins

accounts for ~75% of the extracellular electron transfer and thus seems to be the dominant electron transfer pathway of *S. oneidensis* under anaerobic conditions [20].

1.1.2.2 *Geobacter sulfurreducens*

The *Geobacter* species was first isolated from anoxic freshwater sediments, and was later enriched and isolated from wastewater around the world [10]. In these anoxic regions hardly any oxygen is available as final electron acceptor. Thus, electroactive microorganisms have evolved the respiratory ability to transfer the electrons via their outer membrane to insoluble external electron acceptors outside the cell, such as Fe(III) or Mn(IV) [21].

G. sulfurreducens is one of the most promising electroactive model organisms due to its ability to completely oxidize the typical fermentation end products acetate or hydrogen (with a strong preference for acetate) to carbon dioxide with a high coulombic efficiency. Moreover, it produces among the highest current densities compared to other electroactive microorganisms [22, 23]. This is in contrast to *S. oneidensis* that uses under anaerobic conditions mainly lactate as sole substrate for current generation, not in a complete oxidation reaction but only to acetate, carbon dioxide and four electrons [24]. Thus, the energy yield gained by *S. oneidensis* in its respiratory chain is not completely exploited [13].

Literature studies have shown that *G. sulfurreducens* does not secrete - unlike *S. oneidensis* - soluble compounds for mediated electron transfer [25, 26]. Instead, direct electron transfer via the outer membrane cytochromes of cells attached to the electrode, or via conductive pili is proposed as the main electron transfer mechanism [27]. In contrast to *S. oneidensis* which forms only a very thin biofilm under anaerobic conditions [28], *G. sulfurreducens* is able to form structured, multilayer biofilms up to 50 µm thickness [29]. In this biofilm also the cells which are not in direct contact with the anode electrode can contribute to the current generation [29]. More precisely, these cells are presumably connected in a biofilm network via conductive pili which have been shown to be up to 20 µm long [29].

So far it is unknown how the detailed electron transfer process over the periplasm and the outer membrane works in *G. sulfurreducens* [15]. In its genome 110 genes encoding for putative c-type cytochromes were identified [30]. In comparison to *S. oneidensis* the network of cytochromes involved in the electron transfer to the external electron acceptor seems to be more branched [21]. In that context, the outer membrane cytochrome OmcZ which was found in the extracellular matrix of the cells is highly concentrated at the biofilm-anode interface, and seems to play a crucial role, besides the formation of conductive pili, for the generation of high current densities in *G. sulfurreducens* [21, 23]. In addition,

Rollefson et al. demonstrated that the secretion of extracellular polysaccharides is important for anchoring of cytochromes (in particular OmcZ) in the extracellular matrix and hence for the electron transport and cell attachment [31]. However, the electron transfer mechanisms underlie complex pathways that are not yet completely elucidated and require further research.

The current production of the *Geobacter* species is especially of interest since this model organism was found to be the dominant microorganism at the anode of microbial fuel cells working with aquatic sediments or complex wastewaters [32, 33].

1.1.2.3 Inoculation with mixed consortia derived from wastewater

Besides the inoculation of microbial fuel cells with pure cultures of e.g. model organisms such as *S. oneidensis* or *G. sulfurreducens,* also real wastewater, activated sludge, or anaerobic sewage sludge collected in a wastewater treatment plant can be used. These types of inoculum contain a great microbial diversity which leads to different microbial communities at the anode [34]. Additionally, this microbial composition differs depending on the type of wastewater that is used (e.g. domestic or industrial wastewater), since they vary in their organic substrate contents [35]. This fact renders the evaluation of microbial fuel cell experiments inoculated with different sources of wastewater rather difficult.

Nevertheless, the microbial consortium is also advantageous since it leads to synergistic effects in the multistep degradation of the complex substrate mixture in wastewater, such as long-chained hydrocarbons and fermentation end products [36]. The majority of the bacteria in anaerobic sludge consists typically of non-electrogenic bacteria such as fermentative bacteria, methanogens and sulfate reducers, which consume organic substrates and occupy space on the anode which leads to a diminished power output of the microbial fuel cell [37]. Thus, different strategies for the enrichment of the electroactive strains on the anode have been developed. These include the inoculation with a pre-acclimated consortium of an already operating microbial fuel cell [37]. Using this technique of transferring an anode-grown biofilm to a new anode electrode is in literature often described as a “secondary biofilm”. In this technique, typically acetate instead of complex wastewater is used as carbon source, as it is an easy to metabolize electron donor and leads to the further enrichment of the electroactive strains [37]. Studies have shown that the bacterial community which has developed at the anode originating from domestic and winery wastewater are dominated by *Geobacter* species [38].

The composition of the enriched bacteria can also be controlled by the applied anode potential. In literature it was demonstrated that on the one hand the start-up time of a

microbial fuel cell can be decreased by applying a poised anode potential [39]. On the other hand, the bacterial composition varies dependent on the anode potential: Torres et al. showed that by applying a relatively high anode potential (+0.37 V vs. SHE) at graphite anode electrodes, the bacterial community stays diverse and achieves only low current densities. In contrast, at lower anode potentials (-0.15 V and -0.09 V vs. SHE) the largest bacteria fraction of the biofilm belongs to the electroactive genus *Geobacter* leading to significantly higher current densities [40].

1.1.3 Anodic electron transfer mechanisms

Dissimilatory iron-reducing microorganisms use respiration with extracellular electron acceptors to yield energy in the form of ATP (adenosine triphosphate) [41]. First, the substrate (electron donor) is oxidized by the bacteria and intracellular reducing power is produced and stored in the form of NADPH as intermediate electron carrier [42]. Then, energy is generated by re-oxidizing of NADPH by cell-membrane bound dehydrogenases and by transferring the electrons into a quinone/menaquinone pool located in the cytoplasmic membrane [41]. During the electron transfer protons are pumped over the cell membrane to establish a proton gradient which is used for subsequent ATP generation via the enzyme ATP synthase [41, 43]. In the next step, the electrons originating from the quinone/menaquinone pool travel from the cytoplasm through the periplasm and over the outer membrane to an external electron acceptor, e.g. metal oxide or an anode electrode [15]. Therein, heme-containing c-type cytochromes located in the periplasm and the outer membrane are responsible for the transport across the cell barrier. These participating cytochromes have each a specific redox potential and the electrons flow sequentially from low to higher thermodynamic potential [21]. Nevertheless, the external electron transfer pathway is not yet completely elucidated and several pathways are discussed in literature [41].

Three different electron transfer mechanisms for the final reduction step, i.e. the electron transfer from the outer membrane cytochromes to an external electron acceptor, e.g. metal oxide or an anode electrode, are proposed in literature [42] and are depicted in Figure 1.3.

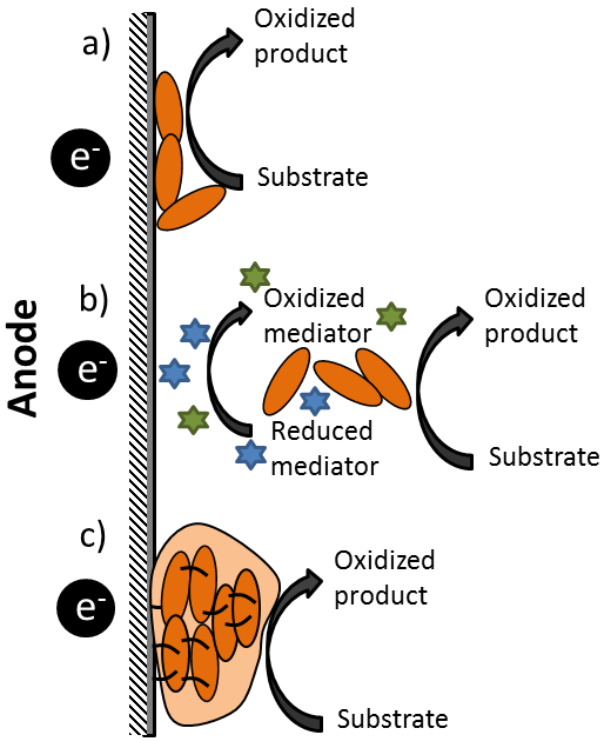

Figure 1.3: Extracellular electron transfer mechanisms: a) direct electron transfer b) mediated electron transfer via electron shuttles and c) a solid conductive matrix and conductive nanowires

The first mechanism described is the direct electron transfer via the outer-membrane c-type cytochromes that interact directly with the solid surface of the anode [44, 45], as shown in Figure 1.3a. Direct contact with the electrode leads to the lowest extracellular potential loss, since the electrons do not need to overcome long distances to reach the anode electrode. However, one limiting factor is that the microorganisms need direct contact with the electrode, making the electrode area the bottleneck of the achievable current density. With this assumption only a monolayer biofilm would be actively connected to the electrode [42].

The second mechanism proposes an indirect, diffusion-based electron transport using soluble, self-secreted electron shuttles (also called mediators), as depicted in Figure 1.3b. Members of the genus *Shewanella, Pseudomonas,* and *Escherichia* are known to produce electron shuttles [42]. These shuttles are reduced by the bacteria and diffuse to the surface of the electrode where they are oxidized. These oxidized mediators can be re-used by the microorganisms until the mediators degrade. Typically, these self-secreted electron shuttles are composed of flavins and quinones [46, 47]. In some studies [48, 49] artificial mediators such as neutral red or methylene blue are added to the anode compartment of the microbial fuel cell, however this is an expensive and not sustainable approach, especially for microbial fuel cells operating with continuous flow. Using electron shuttles allows for connecting more

bacteria cells to the electrode than in a monolayer biofilm attached to the electrode. However, as the main transport mechanism of mediators is diffusion, the distance to the anode as well as the mediator concentration gradient become diffusion limiting according to Fick's first law, which is described in the following:

$$j = -D \cdot \frac{dc}{dx} \quad (1.1)$$

with j the diffusion flux, D the diffusion coefficient, and dc/dx the concentration gradient. However, electron transport via electron shuttles results in an inherent potential loss at the anode due to the concentration gradient needed for the diffusive transport [42]. This potential loss can be calculated by the Nernst equation (see equation 1.2).

The third electron transfer mechanism suggests an external solid conductive matrix which contains components such as e.g. conductive nanowires, also called pili, which transfer electrons in a long-range transport over the biofilm [27, 50], shown in Figure 1.3c. Thus, this solid conductive matrix allows for connecting more electroactive bacterial cells to the electrode compared to a monolayer biofilm. However, it is still unknown how the solid conductive matrix is exactly composed, but it is proposed that conductive nanowires and other conductive components in the matrix, such as bound cytochromes play an important role [42]. In contrast to soluble electron shuttles, the electron transfer is not restricted by diffusion limitations according to Fick's first law, but on the conductivity of the conductive matrix which can assumedly be described by Ohm's law [42]. As long as the conductivity of the solid conductive matrix is high enough, high current densities with low anode potential losses can be achieved [42]. Studies have calculated that this combination of high current densities combined with low anode potential losses is only possible if the electroactive bacteria use a solid conductive matrix for the external electron transfer [42]. *G. sulfurreducens,* known to form multilayer biofilms and to produce conductive pili, is able to achieve these high current densities, which strongly indicates the presence of a solid conductive matrix [42].

In this context, more research studies investigating the complex mechanisms of electron transfer were published. Regarding the conductive pili, it was reported that c-type cytochromes are localized on the nanowire surface which allows for multistep electron hopping as physical mechanism of the long-range electron transfer [51]. In addition, it was suggested that *G. sulfurreducens* requires cytochromes localized beyond the cell membrane, e.g. anchored in the extracellular polysaccharide matrix, in a 3-dimensional network between the cells, which allows for electron hopping through the biofilm [31]. Another study suggests that self-secreted flavins do not act as free electron shuttles for the mediated

electron transfer, but bind as co-factors to the outer-membrane cytochromes which enhances the direct electron transfer rate [52].

Although a number of cytochromes and electron transfer mechanisms were already characterized, further research is still required to identify all involved components and their individual roles in the complex electron transfer pathways.

1.1.4 Electrochemical characterization of microbial fuel cells

Polarization curves are an electrochemical tool to characterize microbial fuel cells. Typical polarization curves of the anode and the cathode electrode are depicted in Figure 1.4. A polarization curve plots the electrode potential as a function of the current density. It can be recorded either separately for the individual electrodes in a half-cell setup against a reference electrode (as shown in Figure 1.4), or for the complete cell voltage of a microbial fuel cell. The advantage of a half-cell setup is the possibility to identify which electrode is limiting the fuel cell performance, e.g. performance loss at the anode or cathode electrode [53]. Polarization curves are commonly recorded with a potentiostat which is typically used in a three-electrode setup consisting of a working electrode (anode or cathode), a reference electrode, and a counter electrode [53]. With this rather expensive and sophisticated device either the potential (potentiostatic control) or the current (galvanostatic control) of an electrode can be controlled. Theoretically, both approaches should deliver equivalent results, when steady-state conditions are reached [54]. If such an expensive device is not available in the laboratory, a variable resistor box combined with a multimeter is often used to set different external loads for galvanostatic control [53]. In this context, Kerzenmacher et al. developed an inexpensive, highly parallelized testing equipment which allows for the step-wise recording of galvanostatic polarization curves for the characterization of microbial fuel cells [55].

The theoretical thermodynamic electrode potential of an electrochemical reaction at non-standard conditions, which is the case in most biological systems (e.g. pH= 7), can be calculated using the Nernst equation (see equation 1.2). The Nernst equation relates the redox potential to the activity of the oxidized and reduced species including the pH value of the solution and the temperature [56, 57]. Therein, E^0 is the electrode potential at standard conditions (pH= 0, T =298 K, concentration of liquids 1 mol L^{-1} and of gases 1 bar), R the gas constant, T the absolute temperature in K, n the number of transferred electrons, and F the Faraday constant. The quotient describes the ratio of the activities of the products and educts to the power of their respective stoichiometric coefficients [57].

$$E^{0\prime} = E^{0} - \frac{RT}{nF} ln \frac{[products]^{p}}{[educts]^{e}} \quad (1.2)$$

During electrochemical characterization of an electrode, the potential is measured against a reference electrode in a half-cell setup. The measured potential differs to the theoretical value calculated with the Nernst equation due to a number of losses. At open circuit conditions when the current flow is zero, a potential closest to the theoretical value calculated with the Nernst equation is reached. The occurring losses, also called overpotentials, are typically divided into three categories: Activation losses, ohmic losses, and mass transfer losses [58] as depicted in Figure 1.4.

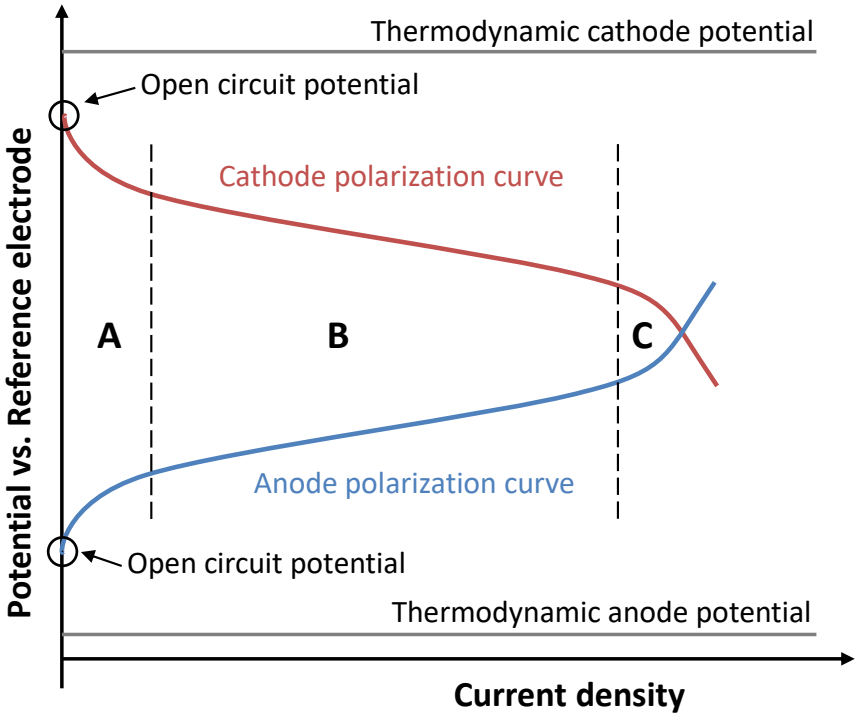

Figure 1.4: Typical anode and cathode polarization curves showing the three different types of potential losses: **A)** Activation losses, **B)** Ohmic losses, and **C)** mass transfer losses. The open circuit potential describes the electrode potential at zero current.

Activation losses (Figure 1.4A) mainly occur due to slow electron transfer kinetics [58] and are especially apparent at low current densities. Decreasing the activation losses can be achieved by using more effective catalysts (e.g. change of the anode bacteria strain), by increasing the electrode surface area, or by increasing the reaction temperature which is however of only limited applicability for bioelectrochemical systems [53, 58, 59].

The region of higher current densities is governed by ohmic losses, as depicted in Figure 1.4B. This linear potential loss obeys Ohm's law (see equation 1.3) and occurs due to the resistance of electron flow through the electrode material, and the ion flow through the electrolyte and the separator membrane, respectively [58].

$$\eta_{ohm} = I \cdot R \quad (1.3)$$

Here, η_{ohm} represents the ohmic overpotential, I the current flow and R the total cell resistance, comprising electronic, ionic and contact resistances [58]. Decreasing the ohmic losses is the main focus of microbial fuel cell design and scale-up [59]. Possibilities to limit these ohmic losses are e.g. minimizing the electrode spacing, increasing the solution conductivity (which is however of only limited applicability for low conductive wastewater operated in continuous flow), and the usage of current collectors [53, 58].

At high current densities mass transfer limitations are the main reason for potential losses (shown in Figure 1.4C). These limitations occur when the transfer rate of a component to or from the electrode limits current production [53]. These mass transfer limitations can occur in different transfer processes of a microbial fuel cell: mass transfer providing substrate to the catalyst (e.g. microorganisms) and removing by-products, mass transfer of ions through the electrolyte, and mass transfer of electrons from the bacterial metabolism to the external electron acceptor via outer membrane cytochromes, nanowires or diffusive electron shuttles [58]. Substrate transport to the bacteria can be limited due to diffusion limitations into thick biofilms because of a decreased diffusion coefficient [58]. In submerged oxygen reduction cathodes, the oxygen supply can be mass transfer limited as a result of the finite oxygen solubility in aqueous solutions [58].

Additionally, at the anode proton flow from the anode into the electrolyte solution can be mass transfer rate limited which results in a decrease of the pH value. Due to the low proton concentration at the anode at neutral pH, compared to other cations present in the solution (Na^+, K^+, NH_4^+, Ca^{2+}, and Mg^{2+}), mostly other cations migrate towards the cathode for charge balance [60]. Since for every transferred electron a proton is generated at the anode, this leads to an accumulation and a decrease of the pH value [61]. The resulting pH drop at the anode electrode can on the one hand inhibit bacterial metabolism due to biofilm acidification, and on the other hand affects the anode electrode potential according to the Nernst equation (see equation 1.2), leading to an unfavorable positive shift of the anode potential [58]. The same is true for the cathode where limited proton flow from the anode to cathode leads to an increase of the pH value, and according to the Nernst equation results in a decrease of the cathode potential which eventually leads to a reduced microbial fuel cell performance [60]. As it can be calculated by the Nernst equation, the difference of one pH unit leads to a change of the electrode potential of 59 mV (potential increases by a decrease of the pH value and vice versa) [62]. Only sufficient buffer capacity of the electrolyte can overcome the change of the pH value, which would however require additional cost-

intensive chemicals which is not applicable under scaled-up conditions or continuous flow operation [35].

Another solution to overcome the mass transfer limitation in a microbial fuel cell is active mixing of the electrolyte solution. However, mixing comes at the cost of additional energy input to the system [58], and even under mixed conditions, there still exists a diffusive boundary layer of tens to hundreds of microns in which only diffusive transport of e.g. nutrients occurs [61, 63].

1.1.5 Microbial fuel cell designs

There exists a huge variety of different microbial fuel cell reactor designs, each coming with distinct advantages and disadvantages. The classical inexpensive microbial fuel cell setup which is widely used in research laboratories is a 2-compartment reactor design. It consists of an anode compartment containing the exoelectrogenic bacteria and a cathode compartment with a usually submersed oxygen reduction cathode [64]. In order to separate the anode and cathode compartment, an ion conductive membrane (typically a proton exchange membrane, e.g. Nafion) is applied which allows for the charge transfer of protons (and other cations present in the electrolyte in microbial fuel cells [60]), and which prevents substrate and oxygen cross-over. A schematic of a 2-compartment microbial fuel cell is shown in Figure 1.2. However, this inexpensive design is limited in the power production due to the high internal resistance as a result of the large electrode spacing. Thus, it is mostly used in research laboratories aiming not at high power densities but at fundamental research on microbial strains, electrode materials, or separator membranes [53].

The reactor design is an important aspect for the operation of microbial fuel cells, since it affects several parameters such as power output, Coulombic efficiency, stability and longevity [64]. In that regard, new concepts such as flat-plate configurations with minimized electrode spacing and therewith decreased internal resistance were developed for optimal power production [53]. Flat-plate reactors typically consist of an anode chamber and a separator material (e.g. a membrane or other separators) which is sandwiched between the anode and cathode electrode [35]. The flat-plate design usually involves an air-breathing gas-diffusion cathode which makes the cathode chamber redundant, and enables the construction of this favorable 1-compartment fuel cell. The air-breathing cathode design allows for the passive oxygen diffusion directly to the catalyst particles which overcomes the issue of limited current densities due to the finite oxygen solubility in aqueous solution, as it is the case in submerged oxygen cathodes. In addition, due to the passive oxygen supply

from ambient air, no active energy-intensive aeration is required [53]. The detailed structure and principle of an air-breathing cathode is explained in chapter 1.2.2.

Besides the flat-plate configurations, an increasing variety of other microbial fuel cell designs in order to increase the power density has been developed, either in batch mode or with a continuous flow through the anode compartment [53]. These include for example cylindrical, tube shaped configurations with either the cathode on the outside and the anode on the inside separated with an insulating membrane, or vice versa [53]. Or for instance an upflow fixed-bed reactor featuring a continuous flow through the porous anode [53]. Most of the reported tubular and flat-plate designs were operated in continuous flow mode [35].

A major concern in microbial fuel cell application is the low cell voltage that is produced [65]. In order to increase the overall voltage of the system, microbial fuel cells can be stacked in series [53], or to increase the current of the system the fuel cells can be stacked in parallel [35]. However, the former is impeded when the microbial fuel cells are operated in a common electrolyte due to ionic short circuiting between the cells, which can result in a drastic loss of the power production [65].

For future practical application it has to be considered that the microbial fuel cell design should be transferable from the laboratory to the pilot plant scale. Moreover, also the anode and separator materials need to be available on a large scale preferably manufactured with inexpensive mass production methods. This is important since scale-up is an essential step for microbial fuel cells to become an economical technology used in an application-relevant environment [64]. Until now, the successful long-term operation of a scaled-up microbial fuel pilot plant still needs to be demonstrated [35].

1.2 Electrode materials for microbial fuel cells

Among the key components for microbial fuel cells are the electrodes. The electrode materials should meet some basic requirements, i.e. they should be inexpensive, durable, long-term stable and biocompatible. For economic reasons and in order to enable scaling-up, the electrode materials should preferably be produced using low-cost mass fabrication techniques. Moreover, the materials should comprise a high conductivity to decrease the internal resistance which can eliminate the need for current collectors. For abiotic cathodes, a high catalytic activity for the oxygen reduction reaction without the use of precious noble metal catalysts is desirable. For electrodes using biocatalysts such as electroactive microorganisms or enzymes, an optimized biocatalyst-electrode interaction and thus an optimal electron transfer between the biocatalyst and the electrode material is targeted. In addition, diffusion limitations regarding e.g. the substrate supply and the removal of by-products through the material's pores should be minimized.

1.2.1 Anode materials

In literature, a lot of different anode materials have been investigated. Among these, carbon-based materials fulfil the above mentioned basic requirements and were tested in various forms: in planar form such as carbon cloth, carbon paper, graphite granules, graphite rods or in 3-dimensional form such as carbon felt, carbon foam, reticulated vitreous carbon or carbon fiber brush [63, 66, 67].

In order to increase the microbe-electrode interaction and to improve the kinetics of the electron transfer, the electrodes were often treated using different chemical or physical surface modification methods. As bacteria are negatively charged on their surface, it has been shown that positively charged electrodes promote the adhesion of the bacterium at the electrode surface leading to a more favored biofilm formation [67]. The positive charge can be introduced on the electrodes by chemical treatment, e.g. with 5% ammonia gas at a temperature of 700 °C. This treatment resulted in a shortened acclimatization time of the bacteria and an increased power density of an acetate-fed microbial fuel cell [68]. Alternatively, electrochemically controlled reduction of positively charged aryl diazonium salts on the electrode surface could increase the power output in an acetate-fed microbial fuel cell compared to an unmodified anode. On the contrary, the presence of negative charged groups on the anode surface led to a reduced power density [69].

Guo et al. investigated the effect of surface charge and hydrophobicity of the anode electrode on biofilm formation in acetate-fed microbial fuel cells [70]. By introducing different functional groups on glassy carbon electrodes using electrochemical reduction, they demonstrated that positively charged hydrophilic anode surfaces are best suited for the selection of electroactive microorganisms such as *Geobacter* species, and at the same time lead to a more conductive biofilm. Interestingly, hydrophobicity seems to play a greater role than the charge of the electrode [70]. But according to Santoro et al. the influence of the hydrophobicity or hydrophilicity of the anode disappears after two weeks of fuel cell operation [71], indicating that electrode surface modification might only play a minor role for practical long-term operation.

In addition to the commercially available carbon-based materials, novel carbon-based anodes were fabricated by carbonization of various precursor materials. These comprise naturally available raw materials such as mushrooms, corn stem, the crop plant kenaf (*Hibiscus cannabinus)* and polyaniline-modified natural loofah sponge [72–74]. These materials possess an open 3-dimensional macroporous structure which is advantageous for the mass transfer processes in microbial fuel cell anodes. The carbonization step converts the precursor materials into conductive electrodes. Also layered corrugated carbon material made by carbonization of the packing material corrugated cardboard was proposed as macrostructured anode material [75]. In addition, the novel process of electrospinning of synthetic polymers such as polyacrylonitrile with subsequent carbonization was shown to be a promising method to fabricate 3-dimensional carbon fiber mats as anode material [76].

Typically, carbon-based materials show an average electrical conductivity only sufficient for the laboratory scale, but regarding scale-up of the fuel cell with increasing electrode areas the application of a current collector should be considered [77]. Otherwise, the electrical resistance translates directly into ohmic losses and therewith leads to a decreased power density of the microbial fuel cell.

Metal-based anode materials are employed when the focus lies on mechanically robust, long-term stable, commercially available and highly conductive materials which make a current collector redundant. In that context, Baudler et al. demonstrated with an acetate-fed secondary biofilm the successful use of various metal-based anode materials such as gold, silver, copper, nickel and stainless steel [78]. In addition, stainless steel was identified as promising anode material in further studies [79, 80], either as plane electrode or as 3-dimensional stainless steel foam [81]. However, at high potentials the naturally present oxide layer of stainless steel converts from conductive p-type to semi-conductive n-type

properties which leads to an additional resistance of the electrode and can hamper efficient electron transfer [78, 82].

In addition, the disadvantage of using non-noble metals as anode material in general is the fact that they are prone to oxidative dissolution when operated at higher potentials. Whereas, stainless steel and nickel are passivated materials whose metal oxide layer protects the metal from oxidation, copper and silver in contrast undergo an oxidative dissolution which starts in the case of copper at a potential of around +0.1 V vs. Ag/AgCl [78]. But also copper and silver can be operated as anodes in microbial fuel cells as long as the working potential stays below this boundary [78]. Additionally, silver and copper are known to have antimicrobial effects on microorganisms. This effect is called an oligodymanic effect which has a damaging influence on microorganisms as a result of the released metal ions from the metal surface upon oxidation [78]. It was proposed that e.g. silver ions irreversibly damage the key enzymes in the cell membrane of the microorganisms. However this effect could not be confirmed in the setup of a microbial fuel cell [78]. Whether the missing antimicrobial effect is related to a tolerance of the electroactive biofilm against copper and silver ions, or due to the relatively negative redox potentials in anaerobic environments and the comparatively noble standard potentials of copper and silver ($E^0_{Cu/Cu2+}$= +0.34 V vs. SHE and $E^0_{Ag/Ag+}$= +0.80 V vs. SHE), could not be answered and requires further investigation [78].

Composite materials are new developments for the fabrication of anode materials. Typically, they combine the advantages of several materials such as the electrical conductivity and the increased microbe-electrode interaction. Baudler et al. introduced a novel 3-dimensional composite anode consisting of a metal-polymer hybrid material made of copper-plated melamine foams [83]. This hybrid material combines the polymers' mechanical flexibility and the conductivity of metals like copper. In the work of Xie et al. [84] they combined the porous and open 3-dimensional architecture of a sponge made of polyurethane with the conductivity of carbon nanotubes. Carbon nanotubes (CNTs) are also a promising material for anodes in microbial fuel cells, since they provide high electrical conductivity, chemical stability, a high specific surface area, biocompatibility and high catalytic properties [66]. Erbay et al. showed that CNTs grown on stainless steel resulted in a composite anode with excellent charge transfer characteristics which are related to the $\pi-\pi$ stacking between the graphite carbon rings and the pili of the microorganisms [85].

In summary, composite materials are a promising new development for anode materials as they combine the advantages of different material types. However, the fabrication of these materials can be laborious and expensive, which has to be further improved for large-

scale applications [63]. In addition, the long-term stability and functionality of the complex composite anode materials under application-relevant conditions still need to be demonstrated. In that context, robust and inexpensive materials such as metal anodes seem to be advantageous for practical application.

Furthermore, the size and volume of the anode electrodes are of high relevance, since the electrode spacing determines among other factors the ohmic resistance of the fuel cell. Large, 3-dimensional electrodes such as e.g. graphite fiber brushes [86] can thus diminish the volumetric performance of a microbial fuel cell in comparison to planar electrodes which enable the favorable flat-plate construction with diminished internal resistance. The efficiency of how the anode space is used by the bacteria can be evaluated by calculating the volume-based current density which is an important parameter regarding size and cost of the overall fuel cell system [63].

The comparison of anode materials presented in literature is rather difficult due to the fact that most studies vary significantly in their operating conditions, the applied microorganisms (pure strains or mixed consortium), the organic substrate (acetate or real wastewater), the applied anode potential, the reactor setup, and the operation temperature as well as the operation time. Sometimes even only the cell voltage of the complete fuel cell is reported which severely impedes the evaluation of the individual electrodes. In addition, the normalization of the current density is not standardized and varies between the normalization based on the anode area, the cathode area, the volume of the electrode, and the volume of the reactor. In that regard, it is highly relevant to conduct systematic anode material screenings under comparable and application-relevant conditions which allow for the material evaluation.

Nevertheless, in Table 1.1 an overview of selected anode materials from literature relevant for practical application, including the achieved current densities and the used inoculum is presented. As can be seen from this table, microbial fuel cells fed with acetate tend to deliver higher current densities compared to microbial fuel cells fed with lactate. The reason for this is that acetate-fed microbial fuel cells usually contain high amounts of the high-performance anode microorganism *G. sulfurreducens*. This demonstrates that the achievable current density depends not only on the anode material but also on the organic substrate and the evolved microbial biofilm composition [63].

Table 1.1: Selected anode materials and the corresponding current densities (based on the anode area, if not mentioned otherwise) relevant for practical application in acetate- and lactate-fed microbial fuel cells (modified table, based on [63]). In addition, the used inoculum, the operating conditions and the operation time until the current densities are achieved, are listed.

Anode material	Type	Inoculum	Operating conditions	Current density	Operation time	Ref.
Acetate-fed						
Stainless steel (smooth, micro- and macro structured)	Flat	Garden compost optimized with acetate	-0.2 V vs. SCE, 40 °C	**17 - 25 A m^{-2}**	7 days	[80]
Stainless steel mesh coated with carbon black	Flat	Secondary biofilm based on wastewater	+0.2 V vs. Ag/AgCl, 35 °C	**15 A m^{-2}**	4 days	[87]
Graphite	Flat	Secondary biofilm based on wastewater	+0.2 V vs. Ag/AgCl, 35 °C	**10 A m^{-2}**	Not reported	[78]
Silver	Flat	Secondary biofilm based on wastewater	+0.2 V vs. Ag/AgCl, 35 °C	**11 A m^{-2}**	Not reported	[78]
Gold	Flat	Secondary biofilm based on wastewater	+0.2 V vs. Ag/AgCl, 35 °C	**12 A m^{-2}**	Not reported	[78]
Copper	Flat	Secondary biofilm based on wastewater	-0.2 V vs. Ag/AgCl, 35 °C	**15 A m^{-2}**	7 days	[78]
Nickel	Flat	Secondary biofilm based on wastewater	-0.2 V vs. Ag/AgCl, 35 °C	**4 A m^{-2}**	Not reported	[78]
Stainless steel	Flat	Secondary biofilm based on wastewater	-0.2 V vs. Ag/AgCl, 35 °C	**7 A m^{-2}**	Not reported	[78]
Carbon cloth	3-D	Garden compost optimized with acetate	-0.2 V vs. SCE, 40 °C	**32 - 36 A m^{-2}**	7 days	[80]
Stainless steel foam	3-D	Garden compost optimized with acetate	-0.2 V vs. SCE, 40 °C	**63 - 82 A m^{-2}**	20 days	[81]

Copper-plated melamine foam	3-D	Secondary biofilm based on wastewater	-0.2 V vs. Ag/AgCl, 35 °C	**23 A m^{-2}** based on six sides of the cubic electrode	8 days	[83]
Electrospun carbon fiber mat	3-D	Secondary biofilm based on wastewater	+0.2 V vs. Ag/AgCl, 35 °C	**30 A m^{-2}**	3 days	[76]
Carbon fiber brush anode	3-D	Secondary biofilm based on wastewater	-0.4 V vs. Ag/AgCl, 30 °C	**~10 A m^{-2}** projected to cathode area, extracted from polarization curve	Not reported	[88]
Lactate-fed						
Carbon paper	Flat	*S. oneidensis*	+0.4 V vs. SHE, 30 °C	**0.22 A m^{-2}**	13 days	[24]
Carbon-fiber-fabric	Flat	*S. oneidensis*	+0.4 V vs. SHE, 30 °C	**0.45 A m^{-2}** (under aerated conditions)	7 days	[28]
Glassy carbon modified with carbon nanotubes	Flat	*S. oneidensis*	0 V vs. SCE, 25 °C	**0.09 A m^{-2}**	15 hours	[89]
Carbon nanofiber mat	Flat	*S. oneidensis*	+0.043 V vs. Ag/AgCl	**0.36 A m^{-2}**	15 days	[90]
Carbon microfiber paper (Toray carbon paper)	Flat	*S. oneidensis*	+0.043 V vs. Ag/AgCl	**0.04 A m^{-2}**	15 days	[90]
Carbon cloth	Flat	*S. oneidensis*	+0.2 V vs. Ag/AgCl, 30 °C	**0.5 A m^{-2}** (batch, anaerobic) **0.85 A m^{-2}** (continuous, aerobic)	7 days	[91]
Hydroxylated/ aminated polyaniline nanowire network on a carbon plate	Flat	*Shewanella loihica*	+0.2 V vs. Ag/AgCl, 30 °C	**2.5 A m^{-2}**	33 hours	[92]
Polyaniline nanowire network on a carbon plate	Flat	*Shewanella loihica*	+0.2 V vs. Ag/AgCl, 30 °C	**0.9 A m^{-2}**	33 hours	[92]

The comparison of the achieved current densities in literature (Table 1.1) showed the tendency that with 3-dimensional porous anode materials higher current densities were achieved compared to flat anodes. This can be related to the fact that with the porous anode structure more bacteria can be connected to the electrode per projected anode area. However, it was described that during long-term operation the pores of a 3-dimensional anode were clogged due to overgrowing biofilm, which resulted in mass transfer limitations and led to current densities similar or even lower than 2-dimensional anodes [83, 93]. On this account, Blanchet et al. proposed that for long-term operation in industrially-scalable conditions 2-dimensional electrodes are a worthwhile alternative to complex 3-dimensional anodes [93]. This highlights the use of flat anode materials for long-term fuel cell operation in application-relevant environments.

1.2.2 Abiotic cathodes

Oxygen is the most preferred oxidant on the cathode side of a microbial fuel cell due to its wide availability and its high oxidation potential. In addition, compared to other reducible compounds used in microbial fuel cell cathodes it does not need to be regenerated or replaced, as it is the case with e.g. ferricyanide [94]. The oxygen reduction reaction (ORR) takes place in a three-phase interaction: oxygen from the air, protons from the electrolyte, and electrons from the electrical circuit. The oxygen reduction reaction can follow two pathways, either via the direct 4-electron pathway (see equation 1.4) or via the 2-electron pathway (equations 1.5a and 1.5b) with hydrogen peroxide as intermediate product, which is subsequently reduced to water. Theoretically both pathways should result in an identical electrode potential (in case of the 2-electron pathway due to the mixed potential of eq. 1.5a + 1.5b). However, in the 2-electron pathway, H_2O_2 is produced as intermediate product, and since the subsequent reduction reaction to water is quite slow (1.5b) parts of the hydrogen peroxide are released into the electrolyte solution [94]. This does not only decrease the cathode potential, but H_2O_2 can furthermore act as aggressive oxidizing agent reducing the long-term stability of the cathode electrode [94].

$O_2 + 4H^+ + 4e^- \rightarrow 2H_2O$	$E^{0\prime}_{O2/H2O}$	= 0.816 V vs. SHE (pH= 7)	(1.4)
$O_2 + 2H^+ + 2e^- \rightarrow H_2O_2$	$E^{0\prime}_{O2/H2O2}$	= 0.257 V vs. SHE (pH= 7)	(1.5a)
$H_2O_2 + 2H^+ + 2e^- \rightarrow 2H_2O$	$E^{0\prime}_{H2O2/H2O}$	= 1.375 V vs. SHE (pH= 7)	(1.5b)

Due to the slow oxygen reduction kinetics which result from the high activation energy of 498 kJ mol^{-1} required to break the O=O bond [95], different catalyst materials are investigated in literature. The use of a catalyst decreases the activation energy barrier and improves the oxygen reduction kinetics [96]. State-of-the-art is the use of platinum as catalyst material due to its high catalytic activity for the oxygen reduction reaction [97]. However, the conditions for the oxygen reduction reaction in microbial fuel cells are not as ideal as in conventional fuel cells due to the ambient temperature, the neutral pH value and the diluted electrolyte concentrations which constrain the cathode performance [98]. Although microbial fuel cell cathodes require only low platinum loadings compared to polymer electrolyte fuel cells - due to their comparatively lower current densities and the different operating conditions [99], the focus lies on the identification of noble-metal free and inexpensive catalyst materials. This can on the one hand be attributed to the still high cost of platinum and on the other hand to the fact that platinum is prone to irreversible poisoning with H_2S which is present in wastewater – an application-relevant fuel for microbial fuel cells [100]. The usage of bare carbon at the cathode resulted in a high

overpotential and only low current densities, thus further modifications such as increasing the surface area (e.g. activated carbon) or chemical modifications have been proposed [94]. Instead of platinum noble-metal free cathode materials based on iron(II) phthalocyanine (FePc), manganese oxides (MnO_x) or CoTMPP (cobalt tetramethylphenylporphyrin) are used with a however slightly diminished cathode performance (open circuit potential, maximum current density, see Table 1.2) compared to platinum [94]. Nevertheless, in this context additional studies regarding loadings and long-term stability of these alternative catalyst materials are required [99].

Table 1.2: Performance (open circuit potential (OCP) and maximum current densities) of selected abiotic oxygen reduction catalysts in microbial fuel cell cathodes (modified table, based on [94]).

ORR catalyst	Electrolyte solution	OCP_{cat}	Current density	Ref.
Abiotic catalysts				
Platinum loading: 0.5 mg cm^{-2}	0.05 M phosphate buffer, pH 7	307 mV vs. Ag/AgCl	~0.36 mA cm^{-2} @0 V vs. Ag/AgCl	[99]
CoTMPP loading: 0.6 mg cm^{-2}	0.05 M phosphate buffer, pH 7	~230 mV vs. Ag/AgCl	~0.27 mA cm^{-2} @0 V vs. Ag/AgCl	[99]
Plain carbon cathode	0.05 M phosphate buffer, pH 7	~260 mV vs. Ag/AgCl	~0.03 mA cm^{-2} @0 V vs. Ag/AgCl	[99]
Platinum (Pt/C) loading 0.82 mg cm^{-2}	0.25 M phosphate buffer, pH 7	~380 mV vs. Ag/AgCl	~0.104 mA cm^{-2} @340 mV vs. Ag/AgCl	[101]
MnO_x/C loading 0.82 mg cm^{-2}	0.25 M phosphate buffer, pH 7	~310 mV vs. Ag/AgCl	~0.088 mA cm^{-2} @255 mV vs. Ag/AgCl	[101]
FePc loading: 1 mg cm^{-2}	0.05 M phosphate buffer, pH 7	300 mV vs. Ag/AgCl	~0.11 mA cm^{-2} @90 mV vs. Ag/AgCl	[98]

Cathodic overpotentials are among the main limitations of the microbial fuel cell performance [35, 96]. Thus, optimization of the cathode is of major importance. Regarding the construction of the oxygen reduction cathode, it can typically be distinguished between a submersed and an air-breathing cathode design. In the submersed cathode configuration the electrode is completely immersed in the electrolyte solution. However, increasing the dissolved oxygen concentration is limited by its solubility in water, which constrains the current density and power output of the microbial fuel cell [96]. In addition, active purging with air or oxygen requires additional energy which adversely affects the energy balance.

The use of air-breathing gas-diffusion cathodes can significantly increase the oxygen availability due to the direct oxygen diffusion from the ambient air to the catalyst particles

which obviates the issue of limited oxygen solubility in aqueous solutions [58]. As a result, mass transfer limitations are reduced which leads to increased limiting current densities [96]. In gas-diffusion electrodes the electrochemical reactions take place at the three-phase boundary which is formed at the interface of the electrolyte (liquid or solid), the gaseous air phase and the solid electrode, typically located in the catalyst layer (see Figure 1.5) [102]. The total length of the three-phase boundary within the electrode material is important as it is the only region where the oxygen reduction reaction can take place [103]. Hence, it is of high relevance to engineer porous electrodes with an increased length of the three-phase boundary by optimizing the interactions between the microstructure, the electrical properties and the electrocatalytic activity [103].

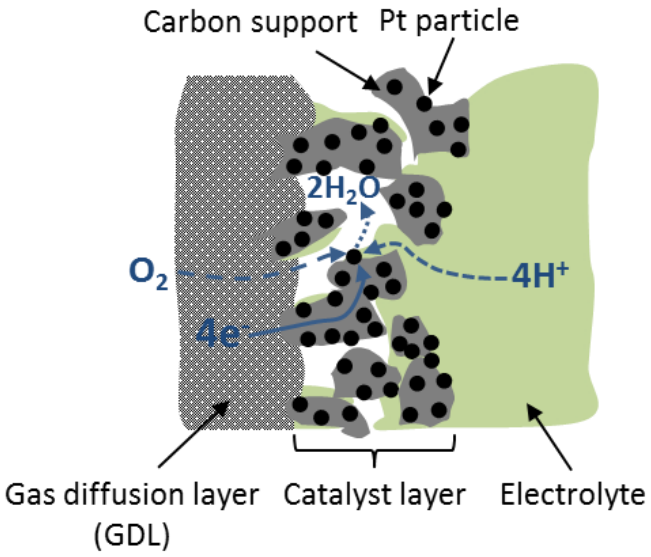

Figure 1.5: Schematic view of the cross-section of a conventional air-breathing gas-diffusion cathode (adapted from [103]). The three-phase boundary is depicted in the center of the catalyst layer, at the interface between the electrolyte, the gaseous air, and the solid electrode. Only in this region the oxygen reduction reaction can take place.

In Figure 1.5 the cross-section of a conventional air-breathing gas-diffusion cathode is depicted. In the following the different layers of this composite electrode are explained:

Gas diffusion layer (GDL): A hydrophobic porous layer of electronically conducting material which provides on the one hand the gaseous air phase and on the other hand conducts electrons to the catalyst layer. In addition, it serves as a mechanical support for the gas-diffusion cathode. Typically, it consists of porous carbon-fiber paper treated with PTFE to increase its hydrophobicity which is essential to prevent water leakage and flooding of the electrode pores which results in severe mass transport limitations [103]. Flooding and water leakage typically occur due to the formation of liquid water during the electrochemical

oxygen reduction reaction at the three-phase boundary, or due to the leakage of liquid electrolyte as a result of the water pressure [104, 105].

Catalyst layer: This porous layer contains graphitic carbon support particles (e.g. carbon black) with the deposited catalyst such as platinum particles. The three-phase boundary between the electrolyte, the gaseous and the solid phase is located in this catalyst layer. In order to bind the catalyst particles to the carbon support, binders such as PTFE or Nafion are employed. The application of Nafion - a proton conductive perfluorinated polymer, which functions as electrolyte additionally increases the length of the three-phase boundary [103]. However, the structure of the catalyst layer must be carefully tailored in order to achieve a mechanically stable structure with an optimized ratio of support particles, catalyst particles and binder for an optimal ionic and electrical connection without clogging of the pores for sufficient air supply [103].

Electrolyte: It is an ionically conducting phase which transports ions between the electrodes along the electric field, but is not conductive to electrons [106]. In conventional PEM fuel cells, typically a solid electrolyte, e.g. Nafion is used. In microbial fuel cells on the contrary only aqueous electrolytes are employed (i.e. the anolyte in the favorable 1-compartment fuel cell design with an air-breathing cathode) [1]. Thus, for this application the air-breathing cathode must especially be designed in a way that water leakage and flooding of the porous cathode structure are prevented [105]. In that context, Luo et al. demonstrated that in microbial fuel cells the number of hydrophobic layers (made of the hydrophobic polymers PDMS or PTFE) applied onto the outside of the air-breathing cathodes needs to be optimized to achieve a trade-off between maximized oxygen permeability and water impermeability [107].

Moreover, a single chamber microbial fuel cell with an air-breathing cathode can be either operated with a separating membrane (e.g. Nafion) or in a membrane-less configuration in which the membrane is completely excluded [96]. The latter configuration has the advantage of an enhanced power density due to the diminished internal ohmic resistance. However, this setup can also lead to unwanted substrate and bacteria cross-over from the anode to the cathode which might result in unwanted biofilm formation on the cathode, and lead to a decreased cathode potential caused by the formation of mixed potentials [96, 108]. In addition, in the membrane-less configuration oxygen cross-over from the cathode to the anode can occur and result in a substantial decrease of the coulombic efficiency [96]. These issues can be overcome by the use of a separating membrane. Nevertheless, in microbial fuel cells also cations other than protons, which are present in a significantly higher concentration, can cross the Nafion membrane from the anode to the

cathode, resulting in a pH gradient across the membrane which decreases the fuel cell performance [96]. Furthermore, the cross-over of cations and anions over the membrane leads on the one hand to salt accumulation at the three-phase boundary which reduces the activity of the catalyst particles, and on the other hand can result in salt precipitation outside of the gas diffusion layer leading to clogged pores of the microstructure [96, 105, 107].

1.2.3 Biocatalysts for the oxygen reduction reaction

Besides the use of abiotic cathode catalysts for the oxygen reduction reaction, also biotic catalysts such as electrochemically active microorganisms or enzymes are of great interest for the application in microbial fuel cells, since they provide an inexpensive alternative with high catalytic activity and specificity.

Under non-sterile conditions microbial growth on the cathode surface could be observed [96], which indicated an electrochemical activity of these microorganisms. This finding was confirmed by several studies which demonstrated that some microorganisms are able to use the cathode as electron donor and transfer the electrons to a final electron acceptor, such as oxygen. In that context, an increased performance of an oxygen reduction cathode was reported which was related to the formation of a biocatalytic biofilm on the electrode [109, 110]. However, the underlying cathodic electron transfer mechanisms are still not yet completely understood [96]. For instance, it is still unknown whether the cathode bacteria obtain the electrons required for their energy metabolism from a carbon source or solely from the cathode electrode [96]. Besides the use of the electrode as electron donor, the cathode bacteria are also able to re-oxidize mediators incorporated into the cathode electrode such as manganese oxide (MnO_2/Mn^{2+}) which leads to high current densities (see Table 1.3) [96, 111].

In Table 1.3 the cathode performance (open circuit potential, maximum current density) of selected microbial and enzymatic oxygen reduction catalysts is shown. In comparison to the abiotic catalysts depicted in Table 1.2, the microbial catalysts in Table 1.3 perform less (except the study employing manganese oxide electron shuttles [111]), as they achieve comparably lower current densities accompanied by high overpotentials indicating large biological activation losses [94]. Nevertheless, an advantage of using microorganisms as biocatalysts is, besides the low catalyst costs, the fact that they are self-regenerating which would theoretically lead to an unlimited catalyst lifetime [94]. However, using microorganisms as cathode catalysts is still in its infancy and requires further research to elucidate the complete reaction mechanisms [96]. Moreover, a detailed investigation on a fundamental level is necessary regarding the cathodic electron transfer mechanisms (e.g.

electron uptake by the microorganisms and electron transfer to an electron acceptor), the long-term stability of the biocathode, as well as the optimal selection and cultivation conditions of the cathodic microorganisms in order to overcome the accompanying high overpotentials [96].

Table 1.3: Performance (open circuit potential (OCP) and maximum current densities) of selected microbial and enzymatic oxygen reduction catalysts in microbial fuel cell cathodes (modified table, based on [94]).

ORR catalyst	Electrolyte solution	OCPcat	Current density	Ref.
Microbial biofilms				
Mixed consortium from environmental samples	Modified M9 medium, pH 6.5	-99 mV vs. Ag/AgCl	0.05 mA cm^{-2} @MPP	[112]
Manganese-oxidizing biofilm (*Lepthothrix discophora*)	Bacterial growth medium, pH 7.2	545 mV vs. Ag/AgCl	0.1 mA cm^{-2} @245 mV vs. Ag/AgCl	[111]
Electroactive biofilm	Natural sea water, pH ~8	Not reported	0.06 mA cm^{-2} @-200 mV vs. Ag/AgCl	[113]
Enzyme-based ORR cathodes				
Laccase from *Trametes versicolor*	0.1 M citrate buffer, pH 5	680 mV vs. Ag/AgCl	0.15 mA cm^{-2} @545 mV vs. Ag/AgCl	[114]
Laccase in supernatant secreted by *Trametes versicolor*	Supernatant of growth medium, pH 5	657 mV vs. Ag/AgCl	0.13 mA cm^{-2} @445 mV vs. Ag/AgCl	[115]
Laccase from *Trametes versicolor* with 2 mM ABTS as mediators	0.1 M acetate buffer, pH 5	Not reported	0.009 mA cm^{-2} @MPP	[116]

MPP: Maximum Power Point

More common is the application of enzymes as biocatalysts for the oxygen reduction reaction. In this context, a broad range of redox enzymes such as laccases, oxidases (e.g. bilirubin oxidase), and peroxidases (e.g. horseradish peroxidase) has been studied [117]. The advantage of enzymatic cathodes lies in the high specificity of the redox enzymes that can eliminate the need for a separator membrane to prevent substrate cross-over [118]. Due to their specificity enzymatic cathodes are hardly prone to poisoning and fuel cross-over which would result in an unwanted mixed potential, as it is the case with e.g. abiotic cathode catalysts [94, 119]. Enzymatic catalysts typically lead to higher current densities compared to microbial catalysts due to a faster electron transport since no cell wall hampers the electron transfer [120]. This tendency can also be confirmed in Table 1.3, in which the selected microbial and enzymatic oxygen reduction catalysts are compared. Furthermore, isolated enzymes are smaller than whole bacterial cells and can thus more efficiently access the

electrode surface in a higher loading leading to a higher volumetric catalytic activity compared to microorganisms [120]. Moreover, it should be noted that enzymatic cathodes are usually operated at acidic pH values (pH 4-5), which are necessary for an optimal electrocatalytic activity of the typically used fungal enzymes. This is in contrast to microbial cathodes that typically operate at neutral pH 7. The more acidic pH value of the enzymatic cathode positively affects the thermodynamic cathode potential according to Nernst, but it can also influence the proton migration between microbial anode and enzymatic cathode.

The electron transfer between the enzyme and the cathode electrode can be conducted via direct electron transfer (DET). For that mechanism the distance between the active center of the redox enzyme and the cathode surface must be maximum 1.5 nm which allows for electron tunneling [121]. Therefor the protein orientation of the enzyme and the location of the redox center (typically deep inside the protein shell) are important. Efficient direct electron transfer is only achieved when the active center is close to the protein surface and the enzyme is oriented with its active redox site towards the electrode [122]. Here, the redox potential of the cathode depends on the redox potential of the active site of the enzyme.

Another electron transfer mechanism in enzymatic cathodes is the mediated electron transfer via redox shuttles (mediators) that transport electrons from the cathode electrode to the active site of the enzyme. Mediators are mostly employed when the active center of the enzyme is deeply buried within the insulating protein shell with a long distance to the electrode surface. One of the most common mediators in enzymatic cathodes is ABTS (2,2'-azino-bis(3-ethylbenzothiazoline-6-sulphonic acid)), either dissolved in solution or immobilized on the electrode [122]. Mediated electron transfer typically increases the current density in the oxygen reduction reaction due to the relatively fast reduction rate of the mediators compared to that of oxygen, which enhances the kinetics of the cathode reaction [96]. However, a drawback is the thermodynamic loss as a result of the decreased redox potential of the applied mediators in comparison to the redox potential of the oxygen reduction reaction [94]. In addition, employing mediators is considered unsustainable due to the need for regular replacement which is also not suitable for practical long-term applications of microbial fuel cells [96].

A major weakness of enzymatic cathodes is the limited long-term stability of the redox enzymes since they cannot self-regenerate, in contrast to microorganisms. Due to the irreversible denaturation of the enzyme's fragile 3-dimensional protein structure which is essential for the catalytic activity, only enzyme lifetimes in the range of days or weeks have been demonstrated [118]. In order to increase the enzyme lifetime strategies to stabilize the

enzyme by immobilization on the electrode surface have been reported. These include adsorption, microencapsulation, entrapment, crosslinking, and covalent binding [118, 122]. However, the still limited long-term performance of only several weeks in combination with high enzyme purification costs remain critical aspects. Especially practical application in bioelectrochemical systems such as in a hybrid microbial-enzymatic fuel cell is limited, since microbial anodes can show operation times of up to several years [123].

A first step towards a self-regenerating enzymatic cathode with extended lifetime was introduced by Rubenwolf et al. [114]. In their study purified laccase from the fungus *Trametes versicolor* was periodically re-supplied to a submersed oxygen reduction cathode. With this approach the electrode lifetime could be increased about 2.5 times. This concept was further developed by Sané et al. [115] who demonstrated that crude supernatant of *T. versicolor* without purification and periodically re-supplied to an immersed cathode leads to a 5 times enhanced cathode lifetime of up to 120 days, at a constant current density of 50 µA cm^{-2}. This approach demonstrates that the electrode lifetime can be successfully decoupled from the limited enzyme lifetime.

Nevertheless, in both studies [114, 115] an immersed oxygen reduction cathode was employed which requires a separate cathode chamber preventing the construction of a favorable 1-compartment fuel cell with minimized internal resistance. Thus, for practical fuel cell application the transfer of this promising approach to an air-breathing cathode design is of major importance. Moreover, with an air-breathing cathode additional energy input for active aeration can be omitted. At the same time, it enables an increased oxygen concentration at the cathode catalysts which is limited in immersed cathodes as a result of the finite oxygen solubility in water. Furthermore, Rubenwolf et al. [114] and Sané et al. [115] presented both a periodic and manual supply of the laccase solution, which is not suitable for long-term fuel cell operation in an application-relevant environment. Hence, a continuous supply system with appropriate periphery for the enzyme-containing solution needs to be developed.

1.3 Motivation and aims of this thesis

This thesis aims at the characterization and evaluation of anode and cathode electrodes for microbial fuel cells. In the first part of this thesis the anode of a microbial fuel cell is addressed. As discussed in chapter 1.2.1, the evaluation of anode materials from literature is relatively complicated as the materials are investigated under operation conditions which vary severely between the respective studies, including different measurement techniques, fuel cell constructions, and inoculation and feeding strategies. This renders a direct comparison of the material's performance rather difficult.

Hence, the first goal of this thesis is to systematically investigate a broad range of anode materials under comparable and application-relevant steady-state conditions. For this purpose, two different microbial fuel cell model organisms, *S. oneidensis* and *G. sulfurreducens* are used which are representative for two different electron transfer mechanisms: mainly direct electron transfer via outer membrane cytochromes and the formation of thick conductive biofilms (*G. sulfurreducens*), and mainly diffusive electron transfer via self-secreted electron shuttles (*S. oneidensis*). In that context, the research question arises whether these two model organisms which rely on substantially different electron transfer mechanisms perform differently due to different microbe-electrode interactions.

The second part of this thesis addresses the enzymatic oxygen reduction cathode. As described in chapter 1.2.3, enzymatic biocatalysts are characterized by their high specificity and high electrocatalytic activity. However, enzymatic cathodes have the intrinsic drawback of a limited lifetime due to enzyme denaturation, accompanied by high costs for the enzyme purification. In order to extend the electrode lifetime Sané et al. [115] presented a novel approach towards a self-regenerating cathode in which unpurified laccase-containing supernatant of the fungus *Trametes versicolor* was periodically re-supplied to the cathode. With this new approach the cathode lifetime could be successfully extended independently of the limited enzyme lifetime. Nevertheless, in their work a submerged cathode was used which requires a separate cathode chamber that prevents the construction of an advantageous 1-compartment fuel cell with diminished internal resistance.

Thus, the second aim of this thesis is to transfer this promising approach to a novel air-breathing cathode concept, which combines the advantage of an extended cathode lifetime by enzyme renewal with the benefits of an air-breathing cathode that obviates the need for energy-intensive aeration and enables high oxygen concentrations at the cathode catalyst site. Moreover, a continuous supply system for the enzyme-containing supernatant needs to

be developed to overcome the manual and periodic enzyme supply which is not suitable for practical operation.

1.4 Structure of this thesis

This doctoral thesis comprises 4 research articles published in peer-reviewed journals (chapters 2-5). In the beginning of the corresponding chapters, information is provided about the bibliography of the publication and the contribution of the co-authors to the respective research article. A preface is given at the start of each chapter 2-5 in order to link the work to the context and the overall aims of this thesis.

In the following an overview of the content of each chapter of this thesis is provided:

Chapter 1: Introduction explains the fundamentals and relevant theoretical background of microbial fuel cells. In particular, it presents a review of the state-of-the art of microbial anode materials and oxygen reduction cathodes.

Chapter 2 presents a systematic anode material screening of carbon based-anode materials using the microbial fuel cell model organism *Shewanella oneidensis* MR-1 under application-relevant conditions. In addition, the influence of aeration on the performance of *S. oneidensis* is investigated.

Chapter 3 presents the comparison of the two model organisms *Geobacter sulfurreducens* and *Shewanella oneidensis* with two selected anode materials: high-surface area activated carbon cloth and low-surface area graphite felt. Both model organisms differ substantially in their electron transfer mechanisms. *G. sulfurreducens* uses primarily direct electron transfer and forms typically thick conductive biofilms, whereas *S. oneidensis* is known to rely on mainly diffusive mediated electron transfer via self-secreted flavins. In this study, the influence of the surface area of the anode materials on the achieved current density with the respective model organism is investigated.

Chapter 4 demonstrates a systematic investigation of anode materials with the high performance model organism *G. sulfurreducens*. In this work, a broad range of carbon-based and metal-based anode materials are investigated under application-relevant steady-state conditions. In addition, highly parallelized and inexpensive galvanostatic polarization is compared with state-of-the-art but cost-intensive potentiostatic control.

Chapter 5 presents a novel concept of an air-breathing laccase cathode which combines the advantage of using unpurified laccase-containing supernatant of the fungus *Trametes*

versicolor for extended cathode lifetime, with the benefits of an air-breathing cathode which obviates the need for energy-intensive active aeration.

Chapter 6: Overall conclusions and outlook summarizes the main outcomes of this thesis and gives the overall conclusions of this work. In addition, an outlook for future research within this topic is presented.

The following chapters are *Glossary, Abbreviations,* and *Physical measures* providing definitions for terms, abbreviations and measures used in this thesis. These chapters are followed by the chapter *Appendix* providing supporting information of the journal publications, the chapter *Acknowledgements,* and the final chapter which lists the *References* of this thesis.

2 Systematic screening of carbon-based anode materials for microbial fuel cells with *Shewanella oneidensis* MR-1

This chapter has been published as original research article as follows (reprinted with permission from Elsevier):

E. Kipf, J. Koch, B. Geiger, J. Erben, K. Richter, J. Gescher, R. Zengerle, S. Kerzenmacher: *Systematic screening of carbon-based anode materials for microbial fuel cells with Shewanella oneidensis MR-1*. Bioresource Technology 146 (2013) 386–392.

DOI: https://doi.org/10.1016/j.biortech.2013.07.076,

Compared to the published manuscript, the numbering of sections, figures, tables and references was adapted to the overall numbering of this dissertation. The section *Methods* was renamed to *Materials and methods* to obtain the same structure as the other chapters of this dissertation. Minor improvements due to additional proof reading were implemented.

Contributions to this publication:

- Elena Kipf: Idea, literature search and analysis, experimental work (except the experiments of Julia Koch and Bettina Geiger as listed below), planning and analysis of all experiments, manuscript preparation, supervision of Julia Koch and Bettina Geiger.

- Julia Koch: Experimental assistance during anode material screening, experiments with buckypaper under anoxic conditions, as well as with C-Tex 13 and graphite felt using an aerated initial growth phase and an anoxic polarization curve (part of her Bachelor thesis).

- Bettina Geiger: Experiments with the anode materials C-Tex 27, V1 felt, 4-layer composite of C-Tex 13 and C-Tex 20 under anoxic conditions (part of her Bachelor thesis).
- Johannes Erben: Taking SEM pictures of the anode materials and scientific advice during manuscript preparation.
- Katrin Richter: Performing HPLC analysis and scientific advice during manuscript preparation.
- Johannes Gescher, Roland Zengerle, Sven Kerzenmacher: Scientific advice during experiments and manuscript preparation.

Preface to chapter 2

As discussed in chapter 1, the comparison and evaluation of anode materials from literature is rather complicated, since the literature studies vary significantly in their operation conditions. This can comprise different inoculation methods, e.g. pure strains or a mixed consortium, or different feeding strategies with e.g. easily degradable organic substrates or complex long-chained carbon compounds. Moreover, also the measurement techniques such as the applied anode potential and the microbial fuel cell constructions can differ substantially between different research groups. In addition, often only the polarization curves of the complete fuel cell and not of the individual electrodes are given which impedes the evaluation of the single electrodes (anode and cathode) severely. All these facts render the comparison and evaluation of anode materials from literature rather difficult.

Thus, in chapter 2 a systematic screening of carbon-based anode materials is conducted under application-relevant steady-state conditions in a half-cell setup, using the microbial fuel cell model organism *Shewanella oneidensis* MR-1. This approach allows for the evaluation and characterization of carbon-based anode materials regarding practical microbial fuel cell application. In addition, the influence of different operation modes such as anoxic and/or aerated conditions on the anode performance of the oxygen-tolerant *S. oneidensis* strain is examined.

2.1 Abstract

We present a systematic screening of carbon-based anode materials for microbial fuel cells with *Shewanella oneidensis* MR-1. Under anoxic conditions nanoporous activated carbon cloth is a superior anode material in terms of current density normalized to the projected anode area and anode volume (24.0 ± 0.3 µA cm^{-2} and 482 ± 7 µA cm^{-3} at −0.2 V vs. SCE, respectively). The good performance can be attributed to the high specific surface area of the material, which is available for mediated electron transfer through self-secreted flavins. Under aerated conditions no influence of the specific surface area is observed, which we attribute to a shift from primary indirect electron transfer by mediators to direct electron transfer via adherent cells. Furthermore, we show that an aerated initial growth phase enhances the current density under subsequent anoxic conditions fivefold when compared to a similar experiment that was conducted under permanently anoxic conditions.

2.2 Introduction

Microbial fuel cells are an emerging technology to directly generate electricity from e.g. wastewater or other biomass resources. The practical applicability of microbial fuel cells is closely linked to the discovery of exoelectrogenic bacteria [7]. In nature, these bacteria occur in an ecological niche where only little or no oxygen is present as terminal electron acceptor. Consequently, these bacteria developed the capability to transfer metabolic electrons via proteins across their outer cell membrane to reduce a number of other substances instead of oxygen [15]. For instance, *Shewanella oneidensis* MR-1 can use a wide range of soluble and insoluble compounds including oxygen, iron III, manganese oxide, nitrate, nitrite, thiosulfate, trimethylamine oxide and fumarate as electron acceptors [11]. In the context of microbial fuel cells, this electron transfer capability obviates the need for potentially toxic and costly mediators to shuttle electrons from the bacterial metabolism to an anode as external electron acceptor.

S. oneidensis MR-1 was originally isolated from sediments of Oneida Lake, New York [11] and is capable of direct electron transfer via outer membrane cytochromes that are either localized directly to the cell surface or to pilus like cell appendages called nanowires [50, 124]. In addition, studies have shown that electrons can also be transferred via a mediated pathway involving self-secreted flavins [20, 125]. Recently, Okamoto et al. (2013) proposed a different mechanism in which flavins enhance the electron transport over the outer

membrane cytochromes as bound cofactors, but not as free-form flavins [52]. The genome of *S. oneidensis* MR-1 is fully sequenced which makes it an ideal model organism for genomic analysis of the electron transport mechanisms.

Under anoxic conditions *S. oneidensis* MR-1 is able to metabolize only a limited group of carbon compounds as electron donors, such as amino acids and hydrogen or fermentation end products like lactate, formate, pyruvate [126]. Under aerated conditions fuel diversity is increased and as shown by Biffinger et al. (2008), *S. oneidensis* DSP10 is then also able to consume glucose, fructose and ascorbic acid to produce electric current in a fuel cell [127]. This capability is presumably linked to the expression of certain key proteins in higher amounts compared to anoxic conditions [127].

For the construction of a microbial fuel cell also the choice of the electrode material is of great importance. In literature, a number of different anode materials have been investigated with different exoelectrogenic bacteria. These comprise mostly carbon materials such as carbon paper [128], cloth [68], mesh [129] and reticulated vitreous carbon (RVC) [130]. Also graphite based materials in the form of sticks [131], felts [130] and fiber brushes [128] have been used. In addition, chemical [68], physical [132] and electrochemical [69] surface modification methods of carbon materials were demonstrated as a promising approach to improve microbial fuel cell performance. Furthermore, metal based materials such as stainless steel [80], gold and gold-sputtered carbon paper [133] were investigated.

Despite numerous publications in this field, the available data are not sufficient to benchmark the different materials from an application-oriented point of view. One reason is that often different microbial fuel cell constructions and varying operating conditions (pH, temperature, inoculum source, and operation time, etc.) are used [53]. This renders the evaluation and comparison of literature data difficult. In addition, polarization data were recorded with different measurement methods and often the microbial fuel cell is only investigated as complete fuel cell [134]. This impedes a comparison as it is not evident if the anode or cathode is the limiting component of the system.

In this work, we therefore report for the first time a systematic anode material screening with *S. oneidensis* MR-1 based on a half-cell setup using a galvanostatic technique in order to evaluate different carbon-based anode materials under quasi-steady-state conditions. Since Biffinger et al. (2009) and Rosenbaum et al. (2010) reported enhanced current production of *S. oneidensis* in the presence of oxygen [28, 135], we consider both anoxic and aerated operation, as well as the influence of an aerated initial growth phase followed by anoxic operation in our experiments.

2.3 Materials and methods

2.3.1 Media, growth conditions and inoculation

S. oneidensis MR-1 (obtained from Johannes Gescher, Institute of Applied Biosciences, KIT, Karlsruhe, Germany) was grown aerobically at 30 °C in LB medium or under anoxic conditions in PBS buffered growth medium, pH 7.4 containing 50 mM Na-D/L-lactate as carbon source and 100 mM fumarate as terminal electron acceptor. As growth medium a modified PBS buffered medium (conductivity: 20.2 mS/cm; the uncompensated resistance amounts to ~10 Ω per electrode, corresponding to a negligible potential deviation of 3 mV at the maximum tested absolute current of 300 µA) as described elsewhere was used [16]. In short, the medium (containing 137 mM NaCl, 2.7 mM KCl, 10 mM Na_2HPO_4, 1.76 mM KH_2PO_4, and 9 mM $(NH_4)_2SO_4$) was supplemented with 1 mM $MgSO_4$, 0.1 mM $CaCl_2$, 1 g L^{-1} casein hydrolysate, and trace elements. Cells were centrifuged at 9511*g* for 4 min and washed 3 times in growth medium lacking lactate and fumarate before inoculation. The electrochemical test reactor contained growth medium without the electron acceptor fumarate. All aqueous solutions were prepared using deionized water. Chemicals used were obtained from Sigma–Aldrich (Taufkirchen, Germany), Carl Roth (Karlsruhe, Germany), and Merck (Darmstadt, Germany). The electrochemical test reactor was inoculated with an optical density (OD_{600}) of ~0.06 [Abs].

2.3.2 Anode materials

Different commercially available carbon-based materials, as listed in Table 2.1, were investigated as anode electrodes. In addition, buckypaper electrodes made from multi-walled carbon nanotubes (MWCNTs) were characterized. These electrodes were self-produced similarly to the procedure described by Hussein et al. (2011) [136], the detailed manufacturing protocol of which is given in the Appendix A2.

Table 2.1: Overview of the tested anode materials.

Material name	Description	Supplier
Graphite foil	Graphite foil	Alfa Aesar (Karlsruhe, Germany)
Toray Paper (TP-120)	Carbon paper	QuinTech (Goeppingen, Germany)
Graphite felt (Sigratherm GFD 2)	Graphite felt	SGL Carbon (Wiesbaden, Germany)
V1-Felt	Activated carbon felt	MAST Carbon (Basingstoke, UK)
C-Tex 13	Activated carbon cloth (knitted)	MAST Carbon (Basingstoke, UK)
C-Tex 20	Activated carbon cloth (knitted)	MAST Carbon (Basingstoke, UK)
C-Tex 27	Activated carbon cloth (woven)	MAST Carbon (Basingstoke, UK)
Buckypaper	Thin film of MWCNTs on a supporting filter	Self-produced (see Appendix A2)

The area-specific mass of the electrode materials was gravimetrically determined. Thicknesses were provided by the suppliers, except for buckypaper for which it was determined by analyzing its cross-section with a scanning electron microscope (SEM; see Appendix A2). Scanning electron microscope images of the materials were acquired with a Zeiss DSM 962 scanning electron microscope. For the enlarged SEM image of the buckypaper a Zeiss 40ESB was used.

The specific surface areas of the anode materials were determined by Andreas Warmbold at the Freiburg Materials Research Center (FMF, University of Freiburg) using the BET (Brunauer–Emmett–Teller) multi-point adsorption method. The measured nitrogen adsorption/desorption data were fitted with a linearized two parameter BET model in the region of 0.05–0.3 p/p0. BET measurements were performed on a Sorptomatic 1990 device (CE Instruments, Milan, Italy) and for data analysis the software Advanced Data Processing from the same manufacturer was used. Prior to the nitrogen adsorption, the samples were heated at 100 °C for 5 h under high vacuum conditions.

2.3.3 Electrochemical test reactor and measurement setup

The aseptic electrochemical reactor used in this work is already described in detail elsewhere [55]. In short, it consists of a modified plastic desiccator (1008.1, Carl Roth, Karlsruhe, Germany) which enables the parallel characterization of six half-cell anode electrodes in 1 L cell suspension. The anode materials were assembled into electrode

holders made from polycarbonate and silicon rubber gaskets, exposing one side of the electrode with a projected (geometric) area of 2.25 cm^2 to the solution.

All materials except the activated carbon materials were wetted with isopropanol and rinsed with deionized water prior to assembly. Each anode material was tested as triplicates. Values are reported in the text and in the tables as mean value ± sample standard deviation. In the graphs the values are shown as mean value ± maximum and minimum value of the triplicates. Platinum mesh units (Goodfellow, Bad Nauheim, Germany) were used as counter electrodes and a saturated calomel electrode (SCE, +0.244 V vs. SHE, KE 11, Sensortechnik Meinsberg, Ziegra-Knobelsdorf, Germany) was used as the reference electrode. All anodes were connected with two platinum wires (0.1 mm, Chempur, Karlsruhe, Germany) for separate current and potential measurements.

Prior to cell inoculation, the test reactor was filled with 990 mL growth medium (described above) and then autoclaved at 121 °C to provide sterile conditions. For the anoxic conditions the test reactor was continuously purged with humidified nitrogen (flow rate 458 mL min^{-1}). To obtain aerated conditions the reactor was purged with a humidified mixture of air and nitrogen (flow rate: 38 mL min^{-1} air, 373 mL min^{-1} nitrogen), containing 2% oxygen.

For recording half-cell anode polarization curves, the electrical testing environment described elsewhere was used [55]. It consists of an electronic load (STG 2008 stimulus generator, Multichannel Systems, Reutlingen, Germany) to apply load current to the anode half-cell, and a data acquisition unit (Keithley 2700, Keithley, Germering, Germany) to simultaneously record the anode potentials against a reference electrode. All measurements were conducted at a constant temperature of 30 °C.

2.3.4 Anode polarization curves

The measurement protocol used in this work is divided in two phases (shown in Figure 2.1). First an initial growth phase at a constant current density of 4.4 µA cm^{-2} was applied for one week to allow for the stabilization of the anode potential at about −0.4 V vs. SCE. After this initial growth phase a polarization curve with step-wise increase in load current (22.2 µA cm^{-2} every 48 h) was recorded. This approach enables a quasi-steady-state anode potential at each end of a load-curve step and prevents erroneous performance estimation by too fast a current sweep rate.

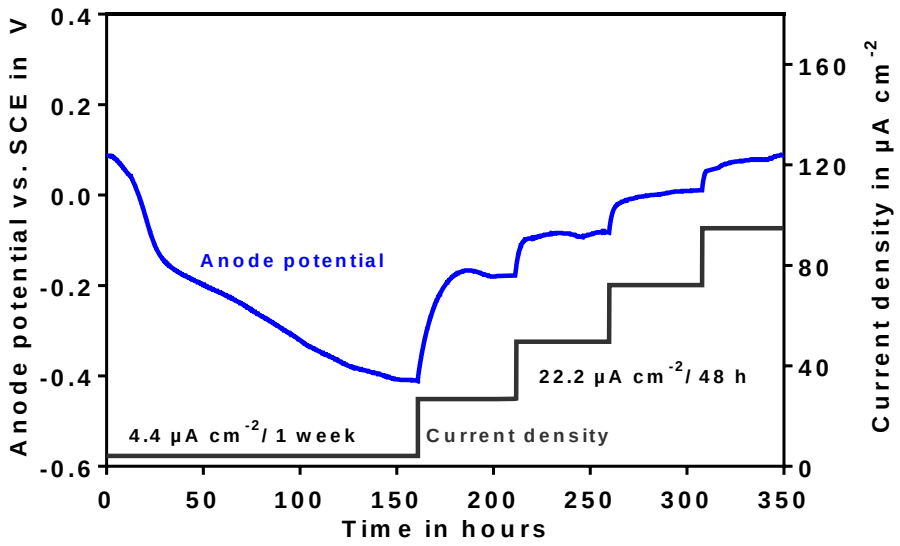

Figure 2.1: Measurement protocol exemplarily shown for the activated carbon cloth C-Tex 13 with *S. oneidensis*: after a one week initial growth phase at 4.4 µA cm^{-2}, the galvanostatic polarization curve with steps of 22.2 µA cm^{-2} every 48 h was started.

The polarization curves shown in Section 2.4.2 were recorded under completely anoxic conditions. Only for the investigation of the different aeration modes in Section 2.4.4 additional polarization curves under fully aerated conditions (solution purged with 2% oxygen in nitrogen), and under anoxic conditions but after a fully aerated initial growth phase were recorded.

In order to compare the electrode performance in terms of current density at −0.2 V vs. SCE, each polarization curve was linearly fitted in the region of −0.2 V vs. SCE. With the obtained linear fit, the current density at −0.2 V vs. SCE was interpolated. The value is given as mean value ± sample standard deviation of the triplicate experiments with each anode material.

2.3.5 Sample analysis and calculation of the coulombic efficiency

Medium samples from the test reactor were collected every other day to determine pH, OD_{600} and L-lactate concentration (Accutrend Plus Lactate Analyzer, Roche Diagnostics, Mannheim, Germany). Na-D/L-lactate was replenished to 50 mM once the measured L-lactate concentration was below 15 mmol L^{-1}. The pH value was re-adjusted with 1 M NaOH or 1 M HCl once the pH shift was larger than 0.5 pH units (starting pH: 7.4).

In order to compare the coulombic efficiency of aerated operation with anoxic operation, the total lactate content of selected samples from the experiment with the

aerated initial growth phase followed by an anoxic polarization curve was analyzed by high performance liquid chromatography (HPLC). In detail, HPLC analysis was performed on a Hitachi LaCrom Elite equipped with a 300 × 7.8 mm Aminex HPX-87H column (Bio-Rad) and 5 mM H_2SO_4 as solvent with a flow rate of 0.6 mL/min. Hundred microlitre of each sample were mixed with 10 µL 0.5 M H_2SO_4 and of that 90 µL were loaded into the column. The column temperature was 60 °C. The signal was detected at 210 nm with a Hitachi L-2455 diode array detector. Calculation of the coulombic efficiency (CE) was performed as described by Logan et al. (2006) according to the following equation [53]:

$$CE = \frac{\int I dt}{F \cdot b \cdot \Delta n} \quad (2.1)$$

with I the current density (A), t the time of the polarization curve (s), F the Faraday's constant (96,485 C/mol electrons), b the number of mol electrons available from one mol lactate (anaerobic metabolism: 4 mol electrons since lactate is oxidized to acetate, formate was detected only in negligible quantities; aerobic metabolism: 12 mol electrons since lactate is oxidized to CO_2) and Δn for the amount of lactate used by *S. oneidensis*.

2.4 Results and discussion

2.4.1 Material characteristics

The SEM images which illustrate the different surface properties of the anode materials investigated in this study are shown in the Appendix A2.

The hydrophobic surface of the graphitic materials is comprised of a graphite crystal lattice consisting of several stacks of parallel layers with sp^2-hybridized carbon atoms which are bonded in hexagonal rings [137]. Among these materials, the graphite foil exhibits a relatively smooth, dense surface without pores. At lower magnification also the buckypaper electrode shows a relatively smooth surface, but at higher magnification the entangled network of carbon nanotubes (nanotube diameter: ~13 nm) with pores in the range of 110 nm is visible. In contrast, graphite felt and carbon paper consist of fibers with diameters in the range of 8 µm. The randomly ordered fibers of the graphite felt are loosely connected providing larger pores in the range of 150 µm compared to the more tightly pressed fibers of the carbon paper that also contains a hydrophobic binding agent.

Compared to graphite, the materials based on activated carbon exhibit a hydrophilic surface chemistry with oxygen functionalities, such as carboxylic or phenolic groups [138]. They come as knitted (C-Tex 13 and C-Tex 20) or woven (C-Tex 27) textile-like cloth materials, or in the form of felt with loosely connected fibers (V1). A common characteristic is the nanoporosity of the activated carbon fibers, induced by steam activation at elevated temperatures (nanopores not visible in the SEM images). This is also reflected in the values for the specific surface area of the electrode materials shown in Table 2.2, determined by the BET method and expressed as real (interior) surface area per weight unit. The activated carbon materials show specific surface areas between approx. 700 and 1200 $m^2 g^{-1}$. The graphitic electrodes show an order of magnitude lower values between 10 $m^2 g^{-1}$ (carbon paper) and 70 $m^2 g^{-1}$ (buckypaper). The specific surface area of graphite foil is not listed in Table 2.2, since due to its low surface area the results of the BET measurements were inaccurate and hence unreliable.

Table 2.2: Characteristics of the tested anode materials. Specific surface areas were determined with the multi-point nitrogen adsorption BET-method. Thicknesses of the materials were provided by the suppliers, except the one of buckypaper which was determined by analyzing the cross-section with the SEM. Area densities were determined gravimetrically, roughness factors were calculated.

Materials	Thickness in mm	Specific surface area (BET) in $m^2 g^{-1}$	Area-specific mass in $g m^{-2}$	Roughness factor
Graphite foil	0.254	-	305	-
Carbon paper	0.37	10	169	~2,000
Graphite felt	2.0	60	182	~11,000
V1-Felt	1.8	1180	137	~162,000
C-Tex 13	0.5	800	165	~132,000
C-Tex 20	1.0	660	252	~166,000
C-Tex 27	0.5	770	135	~104,000
Buckypaper	~0.16 (with supporting filter) ~0.04 (without supporting filter)	70	68	~5,000

Table 2.2 lists a summary of the thickness and the area-specific mass of all materials. As can be seen, the thicknesses differ significantly, ranging from ~40 µm (Buckypaper without the supporting filter) to 2 mm (graphite felt). The roughness factor (the ratio between the real surface area and the geometric surface area) describes how much of real (interior) surface area is available per geometric (projected) electrode area. This factor is also listed in Table 2.2, and was calculated for each material as the product of the specific surface area

and the area-specific mass. As can be seen the activated carbon materials have roughness factors in the range of up to 162,000, which is two orders of magnitude above the other materials.

2.4.2 Comparison of anode polarization curves under anoxic conditions

Figure 2.2 compares the half-cell polarization curves of all tested anode materials, with the current densities normalized to the projected anode area. As can be seen, the tested materials differ substantially in their polarization behavior. The activated carbon materials show significantly better anode performance as they reach higher current densities than buckypaper, graphite felt, and carbon paper, at a given potential. For a quantitative assessment of the anode performance we choose to compare the different materials in terms of the current densities at a potential of −0.2 V vs. SCE. The potential of −0.2 V vs. SCE was chosen since it corresponds to a reasonable anode potential. In combination with a typical cathode potential of about +0.2 V vs. SCE [107] this enables a useful cell voltage of 0.4 V, that can be further stepped up to higher levels by means of a DC–DC converter. The corresponding values are listed in Table 2.3 and were calculated by linear interpolation between the data points. The highest current density at −0.2 V vs. SCE was obtained with the activated carbon cloth C-Tex 20 (29 ± 2 µA cm^{-2}), followed by C-Tex 13 (24.0 ± 0.3 µA cm^{-2}). In comparison, graphite felt and carbon paper, which are often used anode materials in microbial fuel cells show only half the current densities with 12.0 ± 0.2 µA cm^{-2} and 12 ± 2 µA cm^{-2} at −0.2 V vs. SCE, respectively [128, 130].

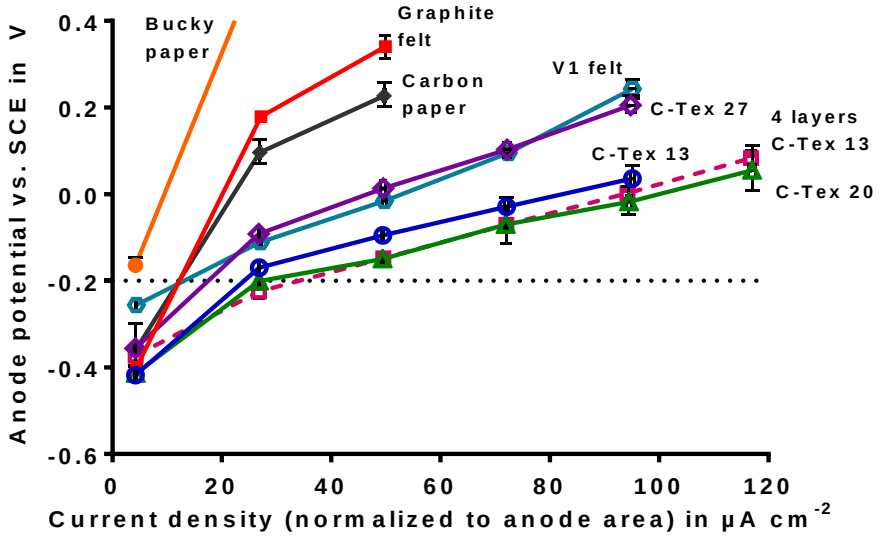

Figure 2.2: Anode polarization curves recorded with *S. oneidensis*. Current densities are normalized to the projected anode area. Anode materials tested are: Buckypaper, Carbon paper, Graphite felt, and the activated carbon materials: C-Tex 27, V1 felt, C-Tex 13, 4-layer composite of C-Tex 13 and C-Tex 20. Each data point depicts the mean value; bars indicate the minimum and maximum values of the triplicates.

Table 2.3: Current densities normalized to the anode area, anode volume and the specific surface area achieved with the tested anode materials with *S. oneidensis*, interpolated at -0.2 V vs. SCE and given as mean ± sample standard deviation.

Anode materials	Bucky paper	Graphite felt	Carbon paper	V1felt	C-Tex 27	C-Tex 13	C-Tex 20	4-layer C-Tex 13
Area based current density at -0.2 V vs. SCE in µA cm^{-2}	4.00 ± 0.05[a]	12.0 ± 0.2	12 ± 2	14 ± 1	18.0 ± 0.4	24.0 ± 0.3	29 ± 2	34 ± 3
Volumetric current density at -0.2 V vs. SCE in µA cm^{-3}	262 ± 3[a,b] 1049 ± 13[a,c]	61 ± 1	327 ± 60	76 ± 6	353 ± 7	482 ± 7	288 ± 23	172 ± 14
BET based current density at -0.2 V vs. SCE in µA m^{-2}	8.8 ± 0.1[a]	12.1 ± 0.2	67.5 ± 12.3	0.8 ± 0.1	1.70 ± 0.04	1.80 ± 0.03	1.7 ± 0.1	-

[a] at -0.164 V vs. SCE.
[b] with supporting filter.
[c] without supporting filter.

The buckypaper electrode shows heavy polarization at already small current densities. Even after the one week initial growth phase at 4.4 µA cm^{-2} the potential did not drop below −0.164 V vs. SCE. Our results are in agreement with the results of Peng et al. (2010) who achieved 9.70 ± 0.40 µA cm^{-2} at 0 V vs. SCE with *S. oneidensis* using a multi-walled carbon nanotube modified glassy carbon anode [89].

No useful electrode performance was obtained with graphite foil, which is not listed in Table 2.3 as it showed too high a polarization. At the beginning of the polarization curve (at 4.4 µA cm^{-2}) the graphite foil had already reached a potential of 0.88 ± 0.15 V vs. SCE. Apparently the load steps of our screening procedure are too large for this smooth material. Already at low current densities, the anode potential appears to reach a range where water electrolysis occurs, and the associated oxygen evolution perhaps hinders electron transfer through self-secreted mediators or the biofilm formation of *S. oneidensis*.

2.4.3 Influence of material characteristics

The differences between the materials can be explained by their different specific surface area. Expressed as roughness factor (ratio of real electrode surface area to the projected geometric area), the activated carbon materials show roughness factors above 100,000, whereas the graphitic materials show roughness factors below 10,000 (see Table 2.2). *S. oneidensis* can more efficiently transfer electrons to anode materials that offer more surface area for the electrochemical electron transfer reaction. Taking into account that the activated carbon fibers exhibit mostly nanoporosity and that the size of *S. oneidensis* cells is in the µm-range, our results suggest that mediated electron transfer via small molecules is playing a key role. This explanation is in agreement with previous studies, which demonstrated that in case of *S. oneidensis* the majority of the electrons (>70%) are transferred to the anode via self-secreted mediators such as flavins [20, 125].

A more detailed analysis of this can be undertaken when normalizing the current densities on the basis of the electrode's BET surface, as shown in Table 2.3. The corresponding graph is shown in the Appendix A2. Here, the materials with low specific surface area but larger pores (graphite felt, carbon paper, buckypaper) exhibit BET-based current densities between 8.8 and 67.5 µA m^{-2}. In contrast, the nanoporous activated carbon materials exhibit BET-based current densities below 2 µA m^{-2}. Thus, the large specific surface area of the nanoporous activated carbon cloth leads to higher overall current densities when normalized to the projected anode area, but when normalized to the BET surface it is evident that to a great extent the large area seems to be unused by bacteria and mediators. We attribute this difference to a limitation of mediator diffusion into the

nanoporous structure as well as of bacterial migration into the macroporous structure of the activated carbon materials.

From an application-oriented point of view the volumetric current density of an electrode material is of particular interest. It directly influences the volumetric power density and size of the microbial fuel cell, which is also related to the overall investment cost of the device. Anode materials that enable high volumetric current densities are thus highly desirable. Therefore Table 2.3 also shows the current densities at −0.2 V vs. SCE normalized to the electrode volume. The corresponding graph can be found in the Appendix A2. Here, a single 500 µm thin layer of activated carbon cloth C-Tex 13 exhibits the highest volumetric current density of 482 ± 7 µA cm^{-3} at −0.2 V vs. SCE. Lower volumetric current densities are obtained when a composite electrode is formed by stacking 4 layers of C-Tex 13. Although formed from the same material, the now 2 mm thick material exhibits a volumetric current density of only 172 ± 14 µA cm^{-3} at −0.2 V vs. SCE. This is attributed to diffusive and convective transport limitations inside the thicker layer, which hinders the supply of mediators and substrate, or the removal of by-products out of the material. Similar low volumetric current densities (presumably also resulting from transport limitations) were observed with the activated carbon felt V1 and the graphite felt, both ∼2 mm thick, which exhibit 76 ± 6 µA cm^{-3} and 61 ± 1 µA cm^{-3} at −0.2 V vs. SCE, respectively.

Although buckypaper does not show potentials below −0.164 V vs. SCE, it exhibits a remarkably high volumetric current density of 1.05 mA cm^{-3} due to its low thickness of only 40 µm (disregarding the volume of the supporting filter). This is higher by a factor of approximately 2, compared to C-Tex 13 at the same potential.

Regarding previous results from literature, our results are consistent with the little data available for comparison. In terms of current density normalized to the geometric electrode area Bretschger et al. (2007) obtained a maximum current density of 13.8 µA cm^{-2} using *S. oneidensis* MR-1 with a graphite felt anode, which is comparable to our results [139]. In terms of volumetric current density a remarkably high value of 1.04 mA cm^{-3} (at the maximum power density) was obtained with graphite felt and *S. oneidensis* DSP10 in a miniature MFC by Ringeisen et al. (2006) [130]. However, as already discussed by Nevin et al. (2008) [22], the high current densities Ringeisen et al. (2006) [130] achieved might be attributed to oxygen available in the reservoir which could have served as electron acceptor and thereby promoting cell growth. Using *S. oneidensis* MR-1, Watson and Logan (2010) reported a current density of as much as 116 µA cm^{-2} (at maximum power density) [128], but this value was normalized to the projected cathode area and can thus not be directly compared to our results. Nevertheless, calculating the corresponding volumetric current

density based on the volume of their ammonia treated carbon fiber brush anode (137 cm^3) yields only ~4 µA cm^{-3}, which is less than 1% of the 482 ± 6 µA cm^{-3} at −0.2 V vs. SCE obtained with activated carbon cloth C-Tex 13 in our study.

Huang et al. (2011) investigated graphene oxide nanoribbons deposited on carbon paper as anode material with *S. oneidensis* and achieved remarkable 190 µA cm^{-2} in a potentiostatic experiment at +0.08 V vs. SCE [140]. This result is higher than in our experiment, as the activated carbon cloth C-Tex 20 shows about 120 µA cm^{-2} interpolated at +0.08 V vs. SCE. However, it is unclear whether their experiment was conducted under anoxic or aerated conditions and what amount of inoculum was used, which may explain the differences.

Our results related to the BET surface area show that the degree to which the available electrode surface is used for electron transfer differs drastically between the electrode materials. In the case of the activated carbon materials we attribute this behavior to limited mediator access to the nanopores of the material. But also the macro-scale porosity of the electrode has an influence on bacterial migration and transport characteristics. Torres et al. (2008), for instance, have shown that the current density of flat anodes is limited by substrate transfer and proton transport out of the biofilm [141]. Our observations thus underline the need to develop hierarchically ordered materials with optimized transport characteristics. For instance, Flexer et al. (2013) proposed an ideal electrode with multidirectional pores in the macroporous scale for a maximized fluid flow towards and out of the pores [142]. A high macroporosity also increases the surface area for the biofilm attachment and therefore the biofilm/liquid interface, allowing for better transport characteristics and higher current densities. In addition, the electron transfer on the nanoporous scale can be improved, for example by modifying the carbon nanostructure of a reticulated vitreous carbon (RVC) anode with carbon nanotubes [142].

In summary, the activated carbon cloth anodes presented in this study are very promising anode materials for microbial fuel cells based on *S. oneidensis* MR-1, both in terms of volumetric and geometric current density at relevant anode potentials.

A prime candidate for further optimization is the buckypaper electrode. Its geometric current density (4.00 ± 0.05 µA cm^{-2} at −0.164 V vs. SCE) is about 6-times below the value for activated carbon cloth C-Tex 13. However, due to its low thickness it exhibits the highest volumetric current density among the investigated materials in our study.

2.4.4 *Influence of different aeration modes on the polarization curves*

Figure 2.3 shows the polarization curves of the two materials graphite felt and activated carbon cloth C-Tex 13 recorded under anoxic and aerated conditions compared to a polarization curve recorded under anoxic conditions but after an aerated initial growth phase. The related current densities at a potential of −0.2 V vs. SCE are listed in Table 2.4.

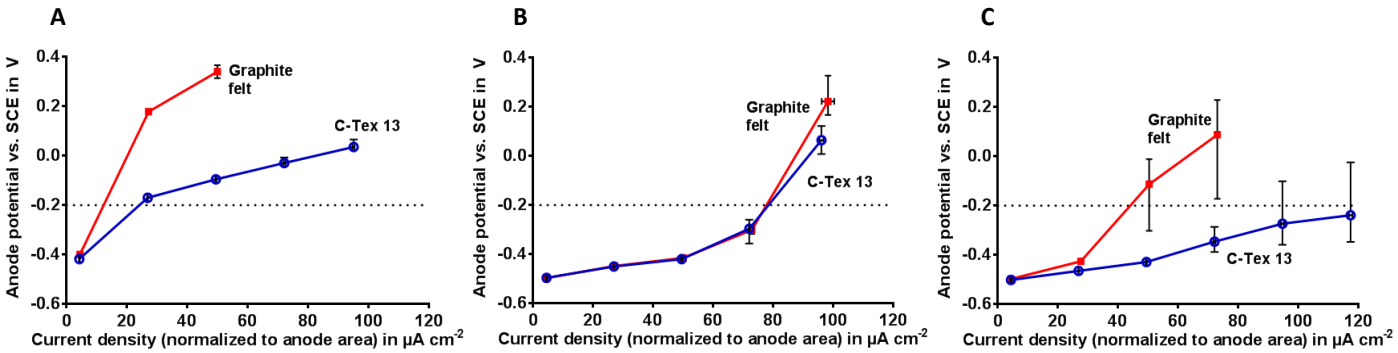

Figure 2.3: Anode polarization curves of the activated carbon cloth C-Tex 13 and graphite felt, achieved with *S. oneidensis* under (A) anoxic conditions, (B) aerated conditions and (C) with an aerated initial growth phase and an anoxic polarization curve. Current densities are normalized to the projected anode area. Each data point depicts the mean value of 3 measurements; bars indicate the minimum and maximum values of the triplicates.

Table 2.4: Current densities normalized to the anode area, achieved with graphite felt and activated carbon cloth C-Tex 13 with *S. oneidensis* under anoxic, aerated and divided (aerated/ anoxic) conditions. Values are interpolated at -0.2 V vs. SCE from the measurement triplets, given as mean ± sample standard deviation.

Aeration mode	**Area based current densities at -0.2 V vs. SCE in µA cm^{-2}**	
	Graphite felt	**C-Tex 13**
Anoxic	12.0 ± 0.2	24.0 ± 0.3
Aerated	78 ± 1	79 ± 5
Aerated/ anoxic	50 ± 17	126 ± 37

As can be seen, under aerated conditions both materials exhibit less polarization with more negative anode potentials under load (Figure 2.3B). The current density of the activated carbon cloth C-Tex 13 increases by about three times from 24.0 ± 0.3 µA cm^{-2} (anoxic conditions) to 79 ± 5 µA cm^{-2} at −0.2 V vs. SCE (aerated conditions). The same tendency can be observed with graphite felt which reaches even six times higher current densities under aeration (12.0 ± 0.2 µA cm^{-2} (anoxic conditions) compared to 78 ± 1 µA cm^{-2} (aerated conditions) at −0.2 V vs. SCE). At the same time the optical density (OD_{600})

increased fivefold (data no shown) compared to anoxic conditions which indicates an expected elevated ratio of anabolism over catabolism under aerated growth conditions.

Remarkably, the polarization curves of graphite felt and activated carbon cloth C-Tex 13 coincide under aerated conditions, and the larger specific surface area of the activated carbon material is no longer essential for a good anode performance. It could be argued that the high cell growth and large number of planktonic cells under aerated conditions lead to a higher mediator concentration, which in turn leads to a better anode performance since more cells can be electrically connected to the anode. However, this hypothesis cannot explain the similar performance of graphite felt and activated carbon cloth. A more satisfying explanation is the formation of thicker biofilms under aerated conditions as observed by Biffinger et al. (2009) [135] and Rosenbaum et al. (2010) [28], suggesting that under aerated conditions the electrons are not primarily transferred by mediators but rather by the attached cells of the biofilm. This hypothesis is further supported by the lower electrode potential under aerated conditions at low current densities, which is indicative of direct electron transfer not involving mediators and without their associated potential loss. Clearly, further research (e.g. including quantification of mediator concentration and biofilm thickness) beyond the scope of the present work is necessary to clarify the exact mechanism of the improved performance under aerated conditions.

Although aeration leads to a better electrocatalytic performance of the anode, this comes at the expense of a drastically lower coulombic efficiency since the majority of electrons released upon oxidation of the substrate by planktonic cells is directly transferred to oxygen and thus cannot contribute to the electric current at the anode. Obviously, the continuous aeration of a microbial fuel cell anode is not useful for efficient electricity generation. Nevertheless, an aerated initial growth phase to promote biofilm formation on the anode followed by anoxic operation for electricity generation may be interesting from a practical implementation point of view. The corresponding polarization curves recorded under anoxic conditions with a previous aerated initial growth phase are shown in Figure 2.3C. As expected, the coulombic efficiency during the one week initial growth phase under aerated conditions is very low (∼0.1%). During the subsequent recording of the polarization curve under anoxic conditions the coulombic efficiency reaches ∼17%. This value is in the range of the 15–35% reported by Watson and Logan (2010) for different reactor configurations with *S. oneidensis* MR-1 [128]. The corresponding current density of C-Tex 13 amounts to 126 ± 37 μA cm^{-2} at −0.2 V vs. SCE, which is about five times larger than under anoxic and nearly two times larger than under aerated conditions. Similarly, the graphite felt shows an increase in the current density of about four times compared to the anoxic mode,

but compared to fully aerated conditions the achieved current density is about 1.5 times less.

Remarkably, the polarization curve of both anode materials are initially comparable to those from aerated operation, but tend to more positive potentials at higher current densities. Furthermore, the differences between the triplicate electrodes (all operated simultaneously in the same bioreactor) become abnormally large. Here it has to be considered that the underlying effect may not be so much related to the operational current density but to the operation time, since the polarization curve was recorded at extremely slow steps of 22.2 µA cm^{-2} every 48 h. The results thus suggest that initially direct electron transfer occurs, but after some time the mediated electron transfer pathway becomes increasingly dominant. This may be attributed to a successive decrease of the biofilm which was previously formed during the aerated initial growth phase. Further work is thus needed to fully investigate this phenomenon and to evaluate, whether the increased anode performance due to an aerated initial growth phase is sustainable in the long-run.

2.5 Conclusions

To our knowledge, the present work is the first systematic screening of carbon-based anode materials with *S. oneidensis* MR-1 performed under quasi-steady-state conditions. We show that the electrode material has a significant effect on the performance of the corresponding fuel cell anode, which underlines the need to develop hierarchically structured materials with optimized transport characteristics. Under anoxic conditions the high surface area activated carbon cloth outperforms the state of the art of graphite felt and fiber brush, which is attributed to the high surface area available for mediated electron transfer through self-secreted flavins.

3 How does the choice of anode material influence electrical performance? A comparison of two microbial fuel cell model organisms

This chapter has been published as communication paper as follows (reprinted with permission from John Wiley & Sons):

E. Kipf, R. Zengerle, J. Gescher, S. Kerzenmacher**:** *How does the choice of anode material influence electrical performance? A comparison of two microbial fuel cell model organisms.* Chem. Electro. Chem. 1 (2014) 1849–1853.

Special Issue: Biofuel Cells

DOI: https://doi.org/10.1002/celc.201402036

Compared to the published manuscript, the section headlines *Introduction, Results and discussion* and *Conclusions* were added to the text. The E*xperimental section* was renamed to *Materials and methods* and moved between the *Introduction* and *Results and discussion* section to obtain the same structure as the other chapters of this dissertation. Moreover, the numbering of sections, figures, tables and references was adapted to the overall numbering of this dissertation. Minor improvements due to additional proof reading were implemented.

Contributions to this publication:

- Elena Kipf: Idea, literature search and analysis, experimental work, planning and analysis of all experiments, manuscript preparation.
- Roland Zengerle, Johannes Gescher, Sven Kerzenmacher: Scientific advice during experiments and manuscript preparation.

Preface to chapter 3

In the systematic anode material screening in chapter 2, it was demonstrated that the model organism *S. oneidensis* achieves significantly higher current densities with activated carbon cloth than with the other tested carbon-based materials. This could be related to the high specific surface area of activated carbon cloth which is presumably available for the mediated electron transfer of *S. oneidensis* via self-secreted flavins.

In chapter 3 another model organism for microbial fuel cells, the high performance strain *G. sulfurreducens* which is known to produce high current densities via direct electron transfer and to form thick conductive biofilms, is employed and the electrical performance is compared with *S. oneidensis.* In this study, the two anode materials high surface area activated carbon cloth and low surface area graphite felt are used. The aim of this study is on the one hand to investigate the maximum current densities obtained with *G. sulfurreducens*. On the other hand, it is of major interest to examine if the specific surface area of the material has an influence on the current generation with *G. sulfurreducens,* as it was observed with *S. oneidensis.*

3.1 Abstract

The influence of the anode material on the electrical performance of the two microbial fuel cell model organisms *Geobacter sulfurreducens* and *Shewanella oneidensis* is investigated. High-surface-area activated carbon and low-surface-area graphite felt are compared in terms of polarization curves under quasi-steady-state conditions. Unexpectedly, *G. sulfurreducens* exhibits similar current densities up to 700 µA cm^{-2} independent of the anode material. This is ∼50 % higher than steady-state values reported previously. The negligible influence of the electrode material on the electrical performance of *G. sulfurreducens* is attributed to the fact that it performs only direct electron transfer, but forms thick biofilms. In contrast, *S. oneidensis*, relying mainly on mediated electron transfer, apparently makes better use of high-surface-area activated carbon and achieves higher current densities compared to graphite felt. This underlines the importance of tailoring anode materials according to the used organisms.

3.2 Introduction

Bioelectrochemical systems are an evolving technology to convert biogenic matter such as organic residues and wastewater into useful electricity or valuable chemical compounds [143–145]. A key component of these systems is the anode, to which electroactive microorganisms transfer electrons from anaerobic respiration. In this context, three different extracellular electron transfer mechanisms can be distinguished, as, for example, described by Borole et al. [146]. In the case of indirect (mediated) electron transfer, a soluble redox mediator shuttles the electrons via diffusive transport to the electrode. In contrast, direct electron transfer relies on outer membrane cytochromes to exchange electrons with an external electron acceptor. Furthermore, some organisms form conductive nanowires which are thought to contribute to a long-range electron transfer through biofilms [29]. However, due to their complexity the mechanisms of electron transfer are not yet completely elucidated.

Prominent electroactive model organisms are *Shewanella oneidensis* and *Geobacter sulfurreducens* [15]. Originally discovered in the sediments of Oneida Lake, and previously named *Alteromonas putrefaciens* [11], *S. oneidensis* is capable of using a broad range of soluble and insoluble electron acceptors [11], including the anode of a microbial fuel cell [139]. Besides exhibiting direct electron transfer via outer membrane cytochromes,

S. oneidensis is able to transfer>70 % of its electrons via self-secreted flavins as mediators under batch conditions [20, 125]. As facultative anaerobic microorganism, *S. oneidensis* can tolerate high levels of oxygen as terminal electron acceptor. This is of particular advantage in applications where oxygen intrusion into the anode compartment cannot be excluded [147], or in biosensors where oxygen may be required as alternative electron acceptor in the absence of analytes [91]. The genomes of *S. oneidensis* as well as of several other members of the genus have been sequenced [12, 148]. Moreover, the phylogenetic resemblance to *Escherichia coli* (both are γ-proteobacteria) is also mirrored in the multitude of tools for genetic engineering that work equally well in both organisms [13].

The genome of the second model organism, *G. sulfurreducens*, has also been fully sequenced and a genetic system for the organism was introduced [30]. Members of the genus *Geobacter* are among the prevailing electroactive organisms colonizing anodes in microbial fuel cells operated on wastewater [38]. *G. sulfurreducens* is known for direct electron transfer via both, outer membrane cytochromes and long-range electrically conductive pili [29]. In contrast to *S. oneidensis*, *Geobacter* sp. is able to form multilayer biofilms with up to 50 µm thickness [29], but does not secrete mediators for electron transfer via soluble shuttles [25, 26]. The members of *Geobacteraceae* are able to completely oxidize acetate to carbon dioxide [149] which leads to a theoretical maximum yield of eight electrons, compared to only four electrons for *S. oneidensis* in anaerobic respiration (oxidation of lactate to acetate and carbon dioxide) [24]. *G. sulfurreducens* was originally considered to be a strict anaerobic microorganism [150], but later studies showed that when pregrown on the soluble electron acceptor fumarate it can also grow under low dissolved oxygen conditions (max. 10 % in the headspace) [151].

Despite the frequent application of these two model organisms in microbial fuel cells [22, 25, 29, 139, 152], both microorganisms have so far only been compared under non-steady-state conditions. In these studies, almost exclusively a single electrode material has been considered [125, 153–155]. In a comparison of high-surface-area activated carbon cloth and low-surface-area graphite felt Dolch et al. [156] recently reported that for both microorganisms activated carbon shows higher current densities and more sessile cells than graphite felt. A limitation of this previous study is that it was performed using a rapid galvanodynamic method that does not represent quasi-steady-state conditions.

In the case of *S. oneidensis* we could already show that also under quasi-steady-state conditions the high surface area activated carbon cloth enables two times higher current densities ((24.0±0.3) µA cm^{-2} at −0.200 V vs. SCE, normalized to the projected anode area) compared to graphite felt [152]. The aim of the present study is to clarify whether with

G. sulfurreducens a similar dependency of the anode performance on the electrode material exists, which is of prime interest for the systematic development of anode materials. Furthermore, we compare both model organisms with respect to their current production capability in a comparable setup and under quasi-steady-state conditions—which refer to a stabilization of the anode potential at the end of each current density step of the polarization curves—relevant for technical application. Both microorganisms were tested in identical reactor setups and at the same temperature and with the same length of the initial growth phase. Only the medium composition and the length of current density steps to record steady-state polarization curves were adjusted with respect to the microorganisms' characteristics (see Appendix A3 for details).

3.3 Materials and methods

3.3.1 Media and growth conditions

Geobacter sulfurreducens PCA and *Shewanella oneidensis* MR-1 were obtained from Johannes Gescher (Institute of Applied Biosciences, KIT, Karlsruhe, Germany). The anaerobic growth medium for *G. sulfurreducens* was used as described elsewhere [157] but modified by omitting resazurin. In short, it contained 15 mM acetate as the electron donor, 40 mM fumarate as the electron acceptor, and the following amounts of salt per liter of deionized water: 0.42 g of KH_2PO_4, 0.22 g of K_2HPO_4, 0.2 g of NH_4Cl, 0.38 g of KCl, 0.36 g of NaCl, 0.04 g of $CaCl_2 \cdot 2H_2O$, 0.1 g of $MgSO_4 \cdot 7H_2O$, 1.8 g of $NaHCO_3$, 0.5 g of Na_2CO_3, 1 mL of 100 mM Na_2SeO_4, and 10 mL of NB trace mineral solution [157]. After autoclaving, the medium was complemented with 10 mL sterile filtered vitamin solution [158] and anoxic, sterile filtered solutions of yeast extract and cysteine to achieve final concentrations of 0.1 % (wt/vol) and 1 mM, respectively [157]. For cultivation, a 1 mL cryo culture was inoculated into a Hungate tube with a butyl rubber septum containing 10 mL anaerobic growth medium. After three days' incubation, 5 mL each were transferred into two 100 mL bottles with butyl rubber stoppers containing 80 mL anaerobic growth medium, respectively. After two days' incubation, the cells were centrifuged at 9511 *g* for 4 min and washed three times with anaerobic growth medium lacking acetate and fumarate. The transfer of the cryo culture into the Hungate tube as well as the washing step of the cells was conducted in a glove bag (1937.1, Carl Roth, Karlsruhe, Germany), which was continuously flushed with nitrogen in order to achieve anoxic conditions. For electrochemical experiments with *G. sulfurreducens* at the anode, the electron acceptor fumarate was omitted from the anaerobic growth

medium (conductivity: 6.0 mS cm^{-1}, which amounts to an uncompensated resistance of ~15 Ω corresponding to a potential loss of 24 mV at the maximum absolute current of 1600 µA), and the reactor was inoculated with an optical density (OD_{600}) of ~0.06.

Regarding comparison to *S. oneidensis*, the previously reported polarization curves cited from Kipf et al. [152] are presented. In that work *S. oneidensis* MR-1 was cultivated in a deaerated (nitrogen purged) phosphate buffered growth medium containing 50 mM Na-D/L-lactate as electron donor and 100 mM fumarate as terminal electron acceptor [16]. These experiments were conducted in an identical reactor setup as the investigations with *G. sulfurreducens* presented in this study. Furthermore, the experimental conditions temperature and length of the initial growth phase were controlled to be the same. Also during experiments with *S. oneidensis* in the electrochemical reactor, the electron acceptor fumarate was omitted from the medium, and the reactor was inoculated with an optical density (OD_{600}) of ~0.06. All solutions were prepared with deionized water and all incubations were conducted at a temperature of 30 °C.

3.3.2 Electrochemical test reactor and measurement setup

The electrochemical test reactor was previously described [55]. In short, it consists of a 1 L modified plastic desiccator (1008.1, Carl Roth, Karlsruhe, Germany) which enables the investigation of six anode half-cell electrodes at a time. The detailed setup and anode assembly has been described elsewhere [152]. A saturated calomel electrode (SCE, +0.244 V vs. SHE, KE 11, Sensortechnik Meinsberg, Ziegra-Knobelsdorf, Germany) was used as reference electrode. A previously described electrochemical testing environment was used to record the half-cell polarization curves under stepwise galvanostatic control [55, 152]. All measurements were conducted at 30 °C. Prior to cell inoculation, the growth medium was filled inside the electrochemical test reactor and autoclaved at 121 °C to provide sterile conditions. In the case of *G. sulfurreducens* the medium was afterwards complemented with the heat-sensitive sterile filtered components described in the section above. To obtain anoxic conditions in the test reactor, the growth medium was continuously purged with humidified nitrogen (flow rate 458 mL min^{-1}) in the case of *S. oneidensis*, and with a mixture of 80 % N_2-20 % CO_2 (84 mL min^{-1} N_2, 21 mL min^{-1} CO_2) in the case of *G. sulfurreducens*, resulting in a pH of ~7.2.

3.3.3 Anode materials

As anode materials graphite felt and activated carbon cloth were used (see Table 3.1). Graphite felt has a relatively low surface area (determined by nitrogen adsorption using the multi-point BET (Brunauer-Emmett-Teller)-method) [159] of 60 $m^2 g^{-1}$ compared to the one order of magnitude higher value of the activated carbon cloth with 800 $m^2 g^{-1}$ [152]. Each anode material was assembled in polycarbonate frames exposing a projected anode area of 1.5 cm×1.5 cm, corresponding to 2.25 cm^2, to the solution. Prior to assembly, the graphite felt was wetted with isopropanol and afterwards rinsed with deionized water due to its hydrophobicity. Each of the two materials was tested as triplicates.

Table 3.1: Description and characteristics of the investigated anode materials. Data cited from Kipf et al. [152].

Anode materials	Description	Supplier	Thickness [mm]	Specific (BET) surface area [$m^2 g^{-1}$]
Graphite felt	Sigratherm GFD 2	SGL Carbon (Wiesbaden, Germany)	2.0	60
Activated carbon cloth	C-Tex 13	MAST Carbon (Basingstoke, UK)	0.5	800

3.3.4 Anode polarization curves

Prior to recording half-cell polarization curves, the inoculated electrodes were subject to an initial growth phase of one week at a constant current density of 4.4 µA cm^{-2}. During this period, the anode potentials stabilized at about −0.4 V vs. SCE (*S. oneidensis*) and about −0.5 V vs. SCE (*G. sulfurreducens*). For comparability, the same time for the initial growth phase was chosen for both model organisms. Subsequently, polarization curves were recorded by a step-wise increase of the current density, which prevents performance overestimation due to a too fast current sweep rate and non-steady-state conditions [55]. This was conducted in a way that the anode potential achieves a quasi-steady-state at the end of each current density step. In the case of *S. oneidensis* this resulted in steps of 22.2 µA cm^{-2} every 48 h [152], whereas for *G. sulfurreducens* shorter steps of 22.2 µA cm^{-2} every 6 h were conducted.

In order to compare the anode performances, the current densities of each polarization curve were compared at −0.400 V vs. SCE. Thereto, the distinct data points obtained by the step-wise increase in current density were linearly interpolated to yield the exact value at

−0.400 V vs. SCE. In the text and in Table 3.2 the values of the current densities at −0.400 V vs. SCE are given as the mean values ± sample standard deviation of the triplicates of each material. In the graphs the anode potentials are shown as mean values ± maximum and minimum value of the triplicates.

3.3.5 Sample analysis

Every other day, samples were taken from the electrochemical test reactor in order to monitor the pH value and the substrate consumption (lactate for *S. oneidensis* and acetate for *G. sulfurreducens*). For *S. oneidensis*, the detailed procedure is described elsewhere [152]. In the case of *G. sulfurreducens*, acetate was assumed to be the only organic acid present, and its amount was determined using an organic acids cuvette test (LCK365, Organic Acids Cuvette Test 50–2500 mg L^{-1}, Hach Lange, Düsseldorf, Germany). Acetate was replenished to 15 mM when the concentration reached a value below ∼11 mM. In all cases substrate replenishing did not lead to a change of the anode potential for *S. oneidensis* and *G. sulfurreducens*, which indicates that during the experiments no substrate limitation occurred.

3.4 Results and discussion

In Figure 3.1 the polarization curves (normalized to the projected anode area) of graphite felt and activated carbon cloth recorded with *G. sulfurreducens* and *S. oneidensis* are compared. Obviously *G. sulfurreducens* enables much higher current densities than *S. oneidensis*. For quantitative analysis we chose to compare current densities at an electrode potential of −0.400 V vs. SCE. The corresponding current densities normalized to the projected anode area, the anode volume, and the specific surface area (determined by the multi-point nitrogen adsorption BET method) [159] of the anodes are listed in Table 3.2. Normalized to the projected anode area, *G. sulfurreducens* yields current densities of (412±19) µA cm^{-2} and (400±35) µA cm^{-2} at −0.400 V vs. SCE using activated carbon cloth and graphite felt, respectively. In the case of *S. oneidensis*, the corresponding current densities at −0.400 V vs. SCE amount to only 1.5 % (activated carbon cloth) and 1.1 % (graphite felt) of the values with *G. sulfurreducens.* For comparison, even at the more positive and thus more favorable anode potential for current generation of −0.200 V vs. SCE, *S. oneidensis* yields

only 6 % and 3 % of the current densities exhibited by *G. sulfurreducens* at −0.400 V vs. SCE, respectively [152].

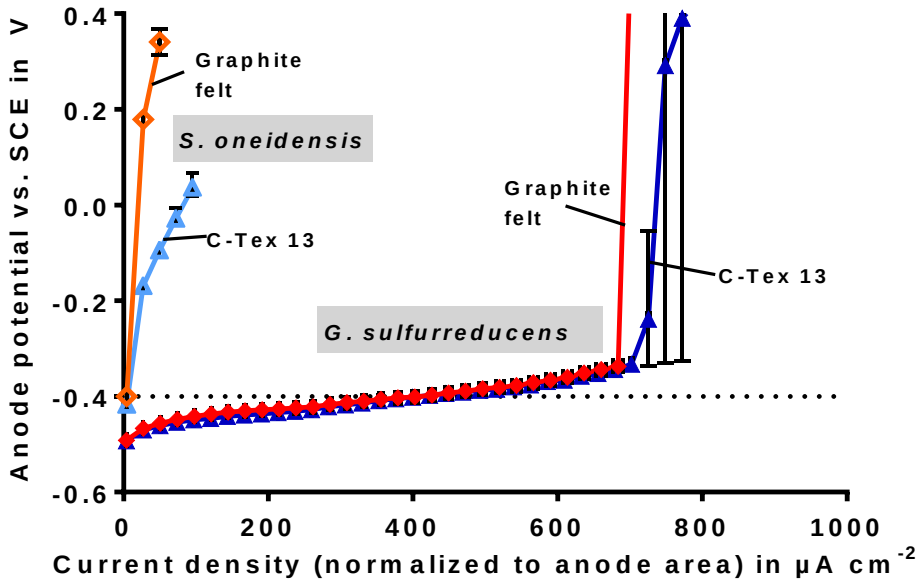

Figure 3.1: Anode polarization curves recorded with *S. oneidensis* and *G. sulfurreducens*. Current densities are normalized to the projected anode area. Tested anode materials are graphite felt and activated carbon cloth C-Tex 13. Each data point depicts the mean value; bars indicate the minimum and maximum values of the triplicates. Data for *S. oneidensis* cited from Kipf et al. [152].

Table 3.2: Current densities normalized to the projected anode area exposed to the solution (1.5 cm x 1.5 cm=2.25 cm²), anode volume and the specific surface area (determined by multi-point nitrogen adsorption BET method) achieved with graphite felt and activated carbon cloth C-Tex 13 with *G. sulfurreducens* and *S. oneidensis*, interpolated at −0.400 V vs. SCE and given as mean values ± sample standard deviation of the triplicates. Data for *S. oneidensis* cited from Kipf et al. [152].

	G. sulfurreducens		***S. oneidensis***	
Current density	Graphite felt	C-Tex 13	Graphite felt	C-Tex 13
Area-based current density at -0.400 V vs. SCE in µA cm^{-2}	400 ± 35	412 ± 19	4.4 ± 0.4	6 ± 1
Volume-based current density at -0.400 V vs. SCE in mA cm^{-3}	2.0 ± 0.2	8.2 ± 0.4	0.022 ± 0.002	0.12 ± 0.01
BET-based current density at -0.400 V vs. SCE in µA m^{-2}	397 ± 35	32 ± 1	4.3 ± 0.4	0.4 ± 0.1

For both materials, the maximum current density with *G. sulfurreducens* is in the range of 700 µA cm^{-2}. This value is about 50 % higher than the maximum quasi-steady-state current densities reported for similar materials of planar shape. Using glassy carbon and

carbon fiber materials current densities of ~400 µA cm^{-2} [155] and of 456 µA cm^{-2} [22] were achieved, respectively. The higher maximum current densities with graphite electrodes reported by Soussan et al. [160] (1600 µA cm^{-2} at +0.2 V vs. SCE) were normalized only to the projected anode area. However, in their work the edges and back of the anode were exposed to the solution as well (personal communication), as opposed to our study, where only the front of the anode is exposed to medium. Normalized to the total geometric electrode area exposed to the solution (8.5 cm^2) the current density recorded in their work is thus closer to 470 µA cm^{-2} at +0.2 V vs. SCE.

Our results show that at higher current densities the anode potential increases drastically, indicating that a reaction-limiting step such as limited metabolic rate or mass transfer of for example, the substrate has been reached. The high current density sustained by *G. sulfurreducens* can be explained by its capability to form thick, multilayer biofilms with conductive long-range pili, allowing for the linkage of many bacteria and large colonization of the anode [29]. In contrast, *S. oneidensis* forms only thin monolayer biofilms under anaerobic conditions [28], but it can transfer a majority (>70 %) of the liberated electrons by shuttling via self-secreted mediators such as flavins [20, 125]. In the case of mediated electron transfer thus additional losses occur due to the mediator gradient required for diffusive transport and the diffusion limitation of the mediators [42]. Furthermore, a potential loss occurs due to the redox cascade between the electrode and the biocatalyst by using mediators [94].

Moreover, by setting up the equations of the catalyzed reactions starting from lactate and acetate, respectively and by using sulfate as surrogate for an electron acceptor with a similar redox potential as an anode, it becomes evident that *S. oneidensis* is able to gain about three times more energy per transferred electron than *G. sulfurreducens* (20 kJ mol^{-1} versus 6.0 kJ mol^{-1} per transferred electron, calculated from tabulated thermodynamic data [161] as described in the Appendix A3). Hence, *G. sulfurreducens* has to maintain a higher metabolic turnover in order to provide sufficient energy for ATP synthesis. This situation becomes even more accentuated if the buildup of biomass is also considered. Acetate has to be converted to acetyl-CoA in an ATP consuming reaction before it can be converted to pyruvate and thereby funneled into gluconeogenesis [162]. However, lactate is been converted to pyruvate in comparatively simple oxidation reaction. Therefore, the energy consuming buildup of biomass starting from acetate will most probably also contribute to higher turnover rates in *G. sulfurreducens*.

Remarkably, *S. oneidensis* yields significantly higher current densities with activated carbon cloth than with graphite felt [152], whereas *G. sulfurreducens* exhibits almost

identical current densities and polarization behavior with both materials. Again, this can be explained by the different electron transfer mechanisms of both organisms. Relying mainly on mediated electron transfer, *S. oneidensis* is apparently able to benefit from the higher specific surface area and the nanoporosity of the activated carbon cloth compared to graphite felt, as discussed elsewhere in detail [152]. In contrast, *G. sulfurreducens* exhibits only direct electron transfer. Since no mediator molecules are involved, the high specific surface area of the nanoporous activated carbon cloth appears to be of no advantage compared to the low surface area graphite felt. Remarkably, Dolch et al. [156] reported that *G. sulfurreducens* produced higher current densities on the activated carbon cloth C-Tex 13 compared to graphite felt. We attribute this difference to the development of a more mature biofilm under the quasi-steady-state conditions of the present work, which is also reflected in the about four times higher current densities with *G. sulfurreducens* as compared to Dolch et al. [156].

From the application point of view also the normalization of the current density to the anode volume is of relevance, in particular when it comes to cost and size of the reactor [53]. The corresponding values are listed in Table 3.2. With the 0.5 mm thick activated carbon cloth *G. sulfurreducens* exhibits a four times higher anode-volume-based current density of 8.2 ± 0.4 mA cm^{-3} at −0.400 V vs. SCE (see Table 3.2), compared to the 2 mm thick graphite felt (2.0 ± 0.2 mA cm^{-3} at −0.400 V vs. SCE). This suggests that not the entire volume of the graphite felt anode is involved in electron transfer. As *G. sulfurreducens* is known to form thick multilayer biofilms [29], presumably in our batch system with no flow through the electrode, only the outer layers of the electrode material are colonized, whereas further inside the porous electrode the biofilm limits substrate transport through the pores. Similarly, the anode-volume-normalized current density of *S. oneidensis* is higher with the thinner activated carbon cloth as with the thicker graphite felt. As described elsewhere, this cannot only be attributed to the limited accessibility of the thicker graphite electrode but also to the high surface area of the activated carbon cloth which is available for the secreted mediators of *S. oneidensis* [152].

Although activated carbon cloth yields the highest anode-volume-based current densities, relating the current density to the true (BET) surface of the electrodes (see Table 3.2) reveals that its large specific surface area is inefficiently used by *G. sulfurreducens* and *S. oneidensis*. For both organisms, the BET-based current density of the graphite felt electrode at −0.400 V vs. SCE is higher than with the activated carbon cloth by an order of magnitude. These results suggest that for both microorganisms the anode-area- and the anode-volume-based current densities can be further improved by carefully tailoring the three-dimensional nano- and macrostructure of the materials.

3.5 Conclusions

In summary, our investigation under comparable and application-oriented quasi-steady-state conditions yields the unexpected result that *G. sulfurreducens* exhibits similar current densities with both the high and the low surface area material. This might be related to the ability of *G. sulfurreducens* to form thick, multilayer biofilms and to perform direct electron transfer. In contrast, *S. oneidensis*, which relies mainly on mediated electron transfer, can make better use of the high surface area of the activated carbon cloth, and achieves higher current densities compared to the low surface area graphite felt. These findings underline that for the development of high-performance anode materials it is important to tailor the material in accordance to the employed anode organisms. Our results suggest that the electron transfer behavior of the anode organisms may play a major role for the choice of the anode material. However, to clarify the underlying mechanisms further research beyond the scope of the present study is required. In this context it should also be considered that some medium components may act as electron mediators. For instance, Habermann and Pommer [145] reported that sulfate can be reduced to sulfide by sulfate-reducing bacteria, which can then be re-oxidized to sulfate at an anode.

Furthermore, a direct comparison shows that *G. sulfurreducens* clearly outperforms *S. oneidensis* in terms of the achievable current densities. Consequently, *G. sulfurreducens* is the preferable anode organism for bioelectrochemical systems demanding high performance. Nevertheless, due to its high oxygen tolerance [11] *S. oneidensis* may be of advantage for applications where oxygen intrusion into the anode chamber, for example, from the cathode compartment or in membrane-less systems cannot be efficiently prevented. Oxygen can even enhance the anode performance of *S. oneidensis* [91, 152], in contrast to *G. sulfurreducens* which can be sensitive to the presence of oxygen [150, 151].

4 Systematic investigation of anode materials for microbial fuel cells with the model organism *G. sulfurreducens*

This chapter has been published as original research article as follows (reprinted with permission form Elsevier):

E. Kipf, J. Erben, R. Zengerle, J. Gescher, S. Kerzenmacher: *Systematic investigation of anode materials for microbial fuel cells with the model organism G. sulfurreducens*. Bioresource Technology Reports 2 (2018) 29–37.

DOI: https://doi.org/10.1016/j.biteb.2018.03.005

Compared to the manuscript, the numbering of sections, figures, tables and references was adapted to the overall numbering of this dissertation. Minor improvements due to additional proof reading were implemented.

Contributions to this publication:

- Elena Kipf: Idea, literature search and analysis, experimental work, planning and analysis of all experiments, manuscript preparation.
- Johannes Erben: Scientific advice during manuscript preparation, especially regarding the capacitance of the biofilm and the anode materials, as well as the electrical conductivity of the metal oxide layer.
- Roland Zengerle, Johannes Gescher, Sven Kerzenmacher: Scientific advice during experiments and manuscript preparation.

Preface to chapter 4

In chapter 3 it was demonstrated that the anode model organism *G. sulfurreducens* achieves similar high current densities with the two anode materials high surface area activated carbon cloth and low surface area graphite felt, however on a significantly higher level than *S. oneidensis*. Interestingly, the fact that *G. sulfurreducens,* which is known to perform direct electron transfer, achieves similar high current densities independently of the specific surface area of the anode material is in contrast to the results achieved with *S. oneidensis* in chapter 2. Therein, it was demonstrated that the specific surface area plays a major role in the current generation of *S. oneidensis,* presumably related to the mediated electron transfer via its self-secreted flavins. These results indicate that the anode materials may need to be selected according to the applied microorganisms.

In order to further evaluate the performance of *G. sulfurreducens* with different anode materials, an extensive and systematic investigation of substantially different carbon- and metal-based anode materials with *G. sulfurreducens* under application-relevant conditions is conducted in chapter 4. In addition, two electrochemical recording techniques are compared: state-of-the-art but costly potentiostatic control and inexpensive galvanostatic polarization which is available in a highly parallel fashion.

4.1 Abstract

Different carbon and metal-based anode materials for microbial fuel cells were systematically investigated with a pure culture of the model organism *G. sulfurreducens*. The highest limiting current density of 756 ± 15 µA cm^{-2} at −0.253 ± 0.037 V vs. SCE was achieved with graphite foil using a step-wise galvanostatic technique. But also the application of completely different anode materials such as activated carbon cloth, stainless steel and graphite felt led to similar high limiting current densities, suggesting that *G. sulfurreducens* is able to use a large range of substantially different anode materials as external electron acceptor. Additionally, we could show that a step-wise galvanostatic technique to record polarization curves yields similar current densities as potentiostatic control at −0.400 V vs. SCE with the investigated carbon-based materials. In case of stainless steel these techniques yield slightly different results, presumably due to an effect related to the material's surface properties.

4.2 Introduction

In microbial fuel cells electroactive microorganisms function as biocatalysts which directly convert chemical energy stored in organic waste to electricity. The principle of microbial fuel cells was first discovered by Potter (1911) [8] who described that microbial conversion of organic compounds leads to the release of electrical energy. However, not until the upcoming depletion of fossil fuels combined with global warming and at the same time an increasing energy demand, microbial fuel cells have come into focus as green technology working on renewable resources or wastewater [163].

The prominent model organism for microbial fuel cells is the Gram-negative δ-proteobacterium *Geobacter sulfurreducens*. This obligate respiratory organism is able to couple microbial respiration to external solid electron acceptors [15]. The complete mechanism of the extracellular electron transfer is however not yet completely elucidated. For instance, Rollefson et al. (2011) [31] showed that in *G. sulfurreducens* an extracellular polysaccharide matrix, in which c-type cytochromes such as OmcZ are anchored, is important for electron transfer, biofilm formation, and the attachment of the cells on the surface. Bond and Lovley (2003) [25] proposed that *Geobacter* sp. needs direct contact with the anode to transfer electrons suggesting direct electron transfer via outer membrane cytochromes. In a recent study, first evidence was provided that *Geobacter* sp. actually

secretes riboflavin but uses them as a bound co-factor in outer membrane c-type cytochromes instead of diffusive soluble redox molecules [164].

G. sulfurreducens forms thick, highly structured multilayer biofilms with up to 50 µm [29] and electrically conductive pili allowing for long-range electron transfer across the anode biofilm [27]. *Geobacter* species are the predominant microorganisms found in anode biofilms of microbial fuel cells working in winery and domestic wastewater [38]. In addition, they are among the most effective microorganisms regarding delivery of electrons originating from organic substrates to external solid electrodes as they are able to completely oxidize acetate to carbon dioxide and water, and at the same time accomplish very high coulombic efficiencies (>90%) [165, 166]. Therefore, it is one of the most frequent species used at the anode of microbial fuel cells.

In literature, a large number of different anode materials have been investigated including carbon based materials such as graphite felt, carbon paper, reticulated vitreous carbon (RVC), graphite fiber brushes, etc. together with varying surface treatment methods [1, 7]. In addition, metal-based anodes made of stainless steel, silver, copper or copper-melamine foams as alternative materials have been shown to be very promising [78, 80, 83]. Also new approaches such as electrospun, carbonized polymer fibers and metal-polymer hybrids as anodes have been introduced [76, 83]. However, all of these studies differ in inocula (e.g. wastewater or pure microbial strains), in fuel cell design, in the applied electrochemical measurement techniques, and the applied anode potential. This renders the systematic evaluation and comparison of anode materials difficult.

To the best of our knowledge, our previous study [167] with two very different carbon-based anode materials (high surface area activated carbon cloth and low surface area graphite felt) and the study of Dolch et al. (2014) [156] are the only systematic comparisons of anode materials under application-relevant conditions with a pure culture of *G. sulfurreducens*. In the more fundamental study of Dolch et al. (2014) [156] *G. sulfurreducens* was investigated with carbon-based anode materials with a focus on biofilm formation and the microbe-electrode interaction of mixed cultures. In our previous work [167] we could show that in the case of *S. oneidensis* the material with a high specific surface area shows significantly higher current densities, presumably due to the high surface area available for mediated electron transfer. In contrast, *G. sulfurreducens* yielded similar current densities with both materials, which were substantially higher compared to *S. oneidensis*. We proposed the hypothesis that *G. sulfurreducens*, a microorganism that forms relatively thick biofilms, is able to achieve similar current densities with various substantially different types of anode materials.

The aim of this work is to further investigate this hypothesis and to systematically evaluate the performance of a number of substantially different carbon and metal-based anode materials under application-relevant conditions (e.g. steady-state current densities) with a pure culture of *G*. *sulfurreducens* as model organism well represented also in wastewater-grown biofilms.

4.3 Materials and methods

4.3.1 Media and growth conditions

Geobacter sulfurreducens PCA was obtained from the group of Johannes Gescher (Institute of Applied Biosciences, KIT, Karlsruhe, Germany). Growth and anode medium are based on Coppi et al. (2001) [157] as described previously [167]. In short, it consists of a bicarbonate buffered medium (pH = 7.2) containing 15 mM acetate as electron donor and in case of the growth medium 40 mM fumarate as electron acceptor. *G*. *sulfurreducens* was cultivated using anaerobic cultivation methods and *G*. *sulfurreducens* cells were prepared for the inoculation as described elsewhere [167].

4.3.2 Electrochemical test reactor and measurement setup

The electrochemical test reactor was previously described [55]. In short, it consists of a 1 L modified plastic desiccator (1008.1, Carl Roth, Karlsruhe, Germany) that allows for the simultaneous operation of 6 anode half-cells at a time. The detailed assembly of the anodes was described elsewhere [152]. A saturated calomel electrode (SCE, +0.244 V vs. SHE, KE 11, Sensortechnik Meinsberg, Ziegra-Knobelsdorf, Germany) was used as reference electrode and platinum meshes (Goodfellow, Bad Nauheim, Germany) were used as counter electrodes.

For the galvanostatic measurements an electrochemical testing environment as previously described [55] was used in order to record galvanostatic half-cell polarization curves with a step-wise increase in current. A potentiostat (1470E, Solartron Analytical, Farnborough, England) was used for the potentiostatic measurements at +151 mV and −400 mV vs. SCE. The baseline current for all tested anode materials were recorded for 40 h at both anode potentials of +151 mV and −400 mV vs. SCE in a sterile test reactor containing

only the anode medium (for details the reader is referred to Appendix A4). The resulting current is insignificant compared to current production with *G*. *sulfurreducens*.

Prior to the measurements the electrochemical test reactor was autoclaved and prepared as described by Kipf et al. (2014) [167]. All measurements were conducted at 30 °C.

4.3.3 Anode polarization curves

In order to compare the electrical performance step-wise galvanostatic, quasi-steady state polarization curves were recorded. First an initial growth phase of one week at a constant current density of 4.4 µA cm^{-2} and afterwards a step-wise increase in the current density of 22.2 µA cm^{-2} every 6 h was performed as described previously [167]. For selected materials with a smooth surface this polarization curve was not applicable as the anode potential reaches a range in which water electrolysis occurs. For example, at an applied current density of 4.4 µA cm^{-2} graphite foil polarizes directly at the start of the initial growth phase toward a high potential corresponding to the potential of electrolytic oxygen evolution. Apparently, the applied current density could not be sustained by the growing culture of *G*. *sulfurreducens*. Thus, a polarization curve with smaller current density steps was applied. Therein the current density in the initial growth phase of one week was increased in very small increments until the current density of 4.4 µA cm^{-2} was reached. Afterwards, the current density was increased in small steps of 4.4 µA cm^{-2} every 6 h (for details the reader is referred to Appendix A4).

4.3.4 Anode materials

The tested carbon and metal-based anode materials are listed in Table 4.1. Each material was assembled in polycarbonate frames exposing a projected anode area of 2.25 cm^2 [152]. Prior to filling the reactor with medium, the anode materials graphite felt and buckypaper were wetted with isopropanol and deionized water due to their hydrophobicity.

For the glass bead blasted materials each metal electrode was blasted with glass beads in the range of 70–100 µm with a standard injector blast machine (TR 110, Sigg Strahltechnik, Jestetten, Germany). In order to remove the titanium oxide layer, the titanium was treated with abrasive paper (silicon carbide, grain size 2500).

Prior to assembly, all metal-based electrodes were treated in an ultrasonic bath, first in acetone, then isopropanol and at last in deionized water in order to remove particles and grease residues from the surface.

Table 4.1: Tested carbon-based and metal-based anode materials. BET-data cited from [152].

Anode materials	Detailed description	Supplier	Thickness in mm	Specific surface area (BET) in $m^2 g^{-1}$
Carbon-based				
Graphite felt	Sigratherm GFD 2	SGL Carbon (Wiesbaden, Germany)	2.0	60
Activated carbon cloth	C-Tex 13	MAST Carbon (Basingstoke, UK)	0.5	800
Graphite foil	-	Alfa Aesar (Karlsruhe, Germany)	0.25	-
Buckypaper	Thin film of MWCNTs on supporting filter	Self-produced based on [136, 152][a]	~0.16 (with supporting filter) ~0.04 (without supporting filter)	70
Metal-based				
Stainless steel	1.4301, V2A stainless steel, polished with grain 240 and cold-rolled	Metall Disch (Freiburg, Germany)	1.0	-
Titanium		Metall Disch (Freiburg, Germany)	0.5	-
Stainless steel glass bead blasted	see above	see above	1.0	-
Titanium glass bead blasted	see above	see above	0.5	-

[a] For the detailed fabrication procedure the reader is referred to the supplementary data of [152].

4.3.5 Sample analysis

Every other day, samples were taken and the optical density (OD_{600}), the pH value and the substrate consumption were monitored. Assuming that acetate was the only organic acid in the medium, its amount was determined with an organic acid cuvette test (LCK365, Organic Acids Cuvette Test 50–25,000 mg L^{-1}, Hach Lange, Düsseldorf, Germany). When the acetate concentration reached a value below ~11 mM, acetate was replenished to ~15 mM.

4.4 Results and discussion

4.4.1 Limiting current densities with different anode materials

4.4.1.1 Step-wise galvanostatic polarization

In Figure 4.1 the step-wise galvanostatic polarization curves of the carbon-based and metal-based anode materials tested with a pure culture of *G*. *sulfurreducens* are depicted. For the non-porous anode materials an adapted step-wise galvanostatic polarization curve with smaller current density steps (4.4 µA cm^{-2} every 6 h) as for the porous materials (22.2 µA cm^{-2} every 6 h) was recorded, allowing sufficient time to reach quasi-steady-state conditions. The corresponding limiting current densities are shown in Figure 4.2A. It is defined as the current density at which the anode potential rises steeply [17] to a potential where water electrolysis occurs (at potentials over 0.81 V vs. SHE at pH = 7 [168]). At this current density mass transfer limitations occur for instance due to limitations of the electron transfer rate of *G*. *sulfurreducens* or the acetate substrate consumption rate [169]. According to Popat and Torres (2016) [61] also the limited buffer capacity and the associated acidification of the biofilm may be limiting the current density. Since for every transferred electron one proton is generated this accumulation of protons can lead to a decrease of the pH value, especially when the buffer capacity is already exhausted. In the case of *G*. *sulfurreducens* growth is already inhibited at a pH below 5.8.

The highest limiting current density of 756 ± 15 µA cm^{-2} was achieved with graphite foil at an anode potential of −0.253 ± 0.037 V vs. SCE. Similar limiting current densities were reached with activated carbon cloth, graphite felt, and untreated stainless steel, whereas the buckypaper anode showed slightly lower values of 590 ± 43 µA cm^{-2} at −0.273 ± 0.025 V vs. SCE.

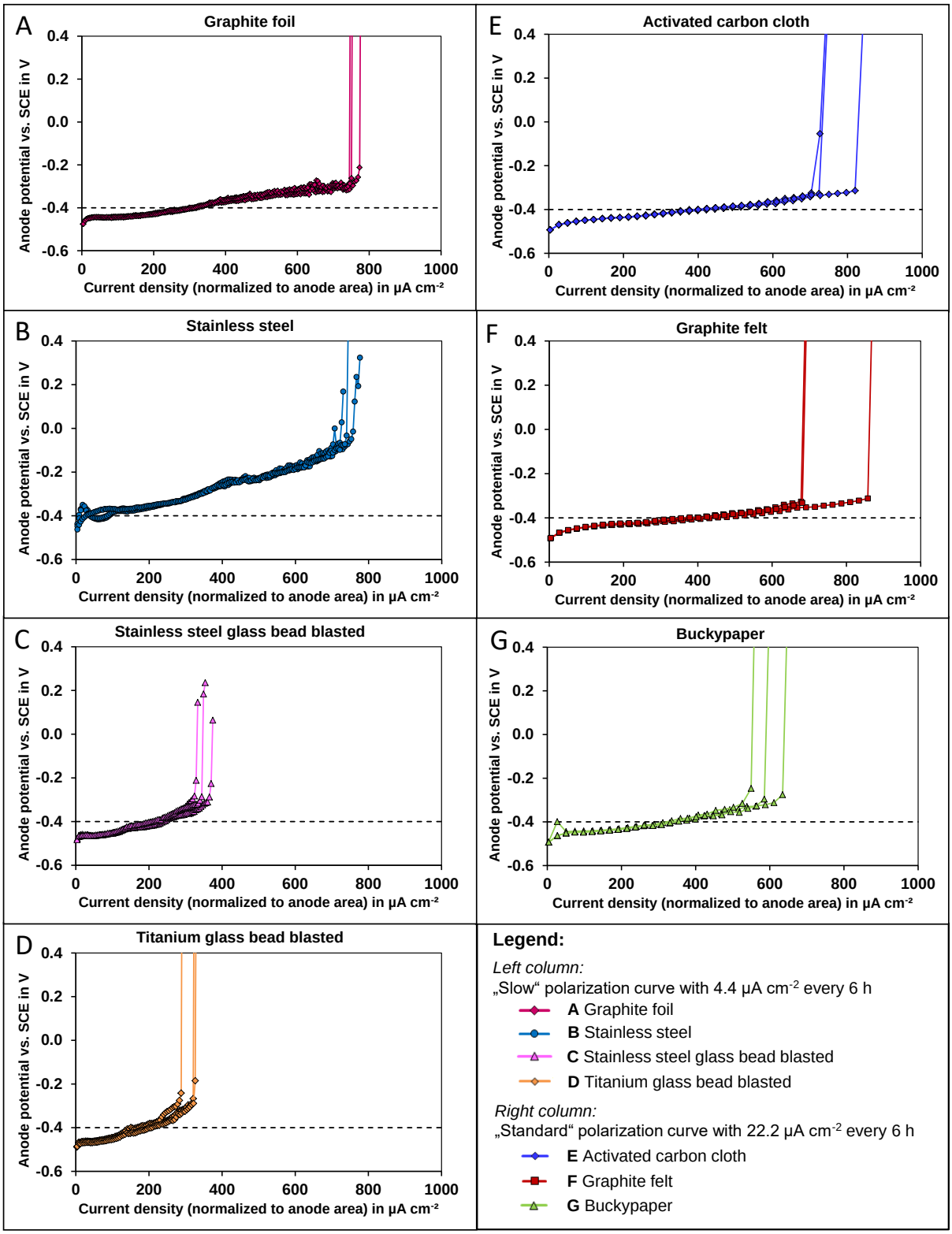

Figure 4.1: Step-wise galvanostatic polarization curves of carbon and metal-based anode materials recorded with *G. sulfurreducens*. Current densities are normalized to the projected anode area. Anode materials tested are: A Graphite foil, B Untreated stainless steel, C Stainless steel glass bead blasted, D Titanium glass bead blasted, E Activated carbon cloth, F Graphite felt and G Buckypaper. Each material is tested as triplicate. Data for activated carbon cloth and graphite felt are cited from [167].

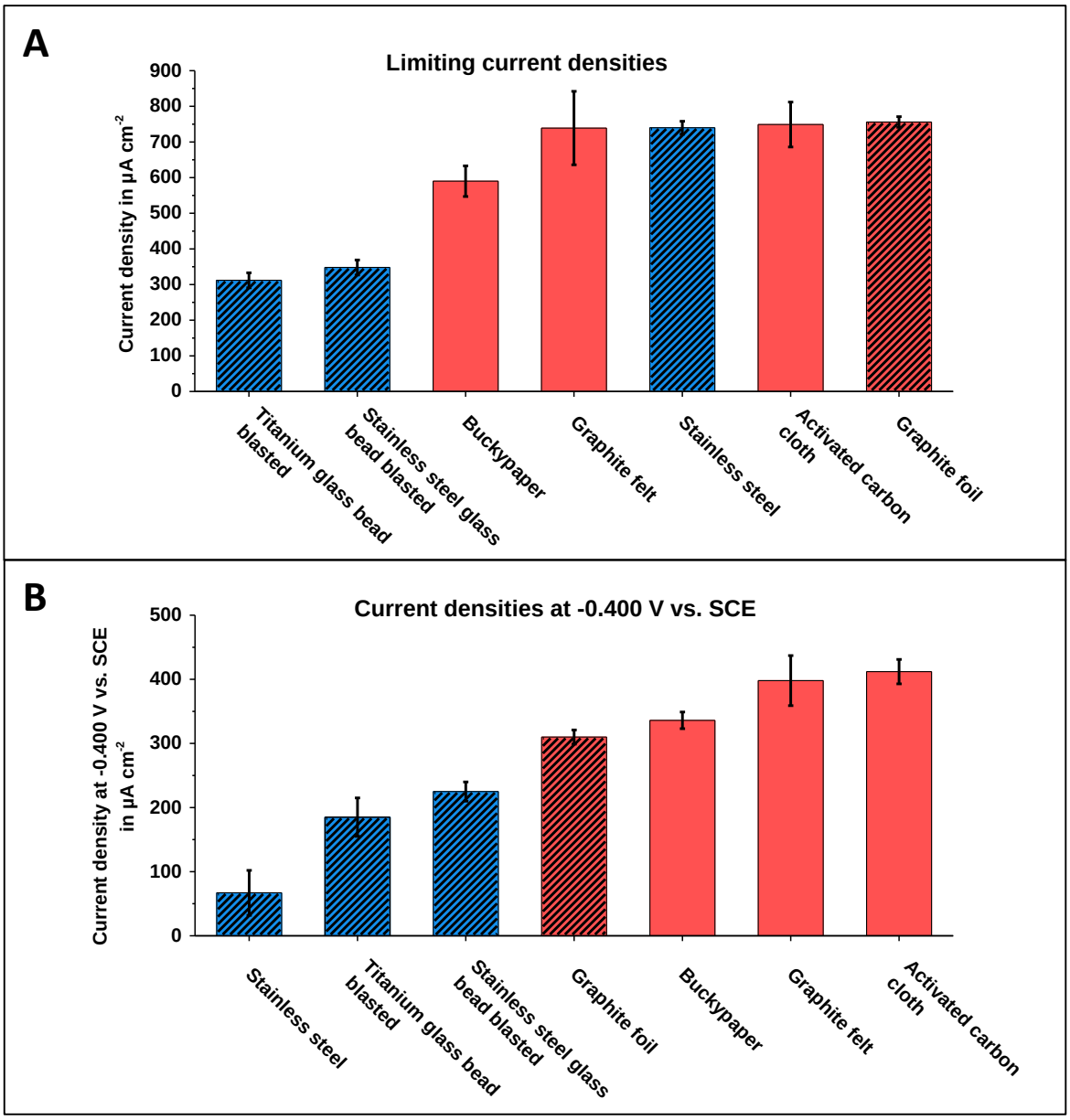

Figure 4.2: A) Limiting current densities and B) area-based current densities at −0.400 V vs. SCE extracted from polarization curves recorded using step-wise galvanostatic technique with *G. sulfurreducens*. The red bars depict the carbon-based and the blue bars the metal-based anode materials with error bars showing the sample standard deviation. The hatched bars indicate the materials for which a polarization curve with small current density steps (4.4 µA cm^{-2} every 6 h) was applied, whereas not-hatched bars indicate recording of the polarization curve with current density steps of 22.2 µA cm^{-2} every 6 h.

No current at all could be achieved with the untreated titanium anode. This can be attributed to the oxide layer of the titanium anode that forms upon contact with air and decreases the electron transfer rate [78, 170]. However, after glass bead blasting titanium delivered a maximum limiting current density of 312 ± 21 µA cm^{-2}, presumably due to the removal of the oxide layer. This surface treatment had a long-term effect as the glass bead

blasted titanium anodes were running for about 580 h until the limiting current density was reached.

Remarkably, untreated stainless steel showed a very high limiting current density of 740 ± 18 µA cm^{-2} at −0.038 ± 0.026 V vs. SCE, whereas glass bead blasted stainless steel delivered only 348 ± 21 µA cm^{-2} at an anode potential of −0.241 ± 0.040 V vs. SCE. In this context, there are some studies in literature linking the current densities achieved with stainless steel electrodes to their surface roughness. For instance, Pons et al. (2011) [171] showed that for stainless steel cathodes with a pure culture of *G. sulfurreducens* an increased mean arithmetic surface roughness (R_a) from 2.0 to 4.0 µm led to an increased current. In contrast, Pocaznoi et al. (2012) [80] could not observe any effects of the surface roughness of stainless steel anodes with an acetate-fed mixed consortium. The arithmetic mean roughness values (R_a) of our tested metal anodes are listed in Table 4.2. In case of stainless steel electrodes, the mean roughness value decreased after glass bead blasting from ~2–3 µm to 1.55 µm, and at the same time the limiting current density decreased by half. Interestingly, after glass bead blasting, titanium and stainless steel delivered similar limiting current densities (312 ± 21 µA cm^{-2} and 348 ± 21 µA cm^{-2}) although the materials differ in their surface roughness (0.53 µm vs. 1.55 µm). This clearly indicates that other factors such as the metal oxide layer play a larger role in current generation than the surface roughness – a topic that warrants further investigation beyond this work.

Table 4.2: Arithmetic mean roughness values R_a of selected non-porous anode materials in increasing order.

Material	Arithmetic mean roughness value R_a
Titanium glass bead blasted	0.53 µm
Titanium	0.77 µm
Stainless steel glass bead blasted	1.55 µm
Untreated stainless steel lengthwise	1.17 µm
Untreated stainless steel crosswise	2.73 µm
Graphite foil	5.03 µm

Compared to the carbon-based tested anode materials, the investigated steel and titanium electrodes show a significantly increased linear slope of the polarization curve which in general is related to higher ohmic losses of the half-cell, including among others the resistance of the flux of the electrons through the electrode material [172]. This effect may be explained by the presence of oxide layers with elevated resistance on the metal surface [82].

In summary, these results show that *G*. *sulfurreducens* can achieve similar high limiting current densities with graphite foil, activated carbon cloth, untreated stainless steel and graphite felt. That confirms our initial hypothesis that *G*. *sulfurreducens* is able to achieve current densities in a similar range with substantially different type of anode materials. This may be related to the fact that *G*. *sulfurreducens* is known to build up thick biofilms and to transfer its electrons via pili and loosely bound cytochromes through the biofilm network [31, 173]. Presumably, the microorganisms only need a surface to attach for starting biofilm formation in several layers. However, this observation is not true for all tested anode materials, as for buckypaper and the glass-bead blasted stainless steel and titanium anodes substantially lower limiting current densities were achieved. This clearly indicates that beside the available surface area for biofilm formation, also other factors such as biocompatibility and surface chemistry of the materials may play a significant role which requires further investigation.

4.4.1.2 Electrode behavior upon reaching the limiting current density

As can be seen from Figure 4.1 the polarization curves recorded using the step-wise galvanostatic technique show a rapid rise of the anode potential when the limiting current density is reached. Looking closer at the time point when the anode potential rises steeply to a potential where water electrolysis occurs (Figure 4.3), one can see that the potential rise does not occur directly after the increase of the current density step (which is 6 h long), but after some time later, typically after a couple of hours (Table 4.3). However, the time until the potential rises differs significantly also within identical triplicates, and thus no significant difference between the various materials can be observed. Our results show that initially the *G*. *sulfurreducens* biofilm is able to deliver the imposed current, but after a certain time (from minutes to hours) the microorganisms are no longer able to sustain the electron transfer rate at this level and the anode potential rises to a potential where water electrolysis occurs.

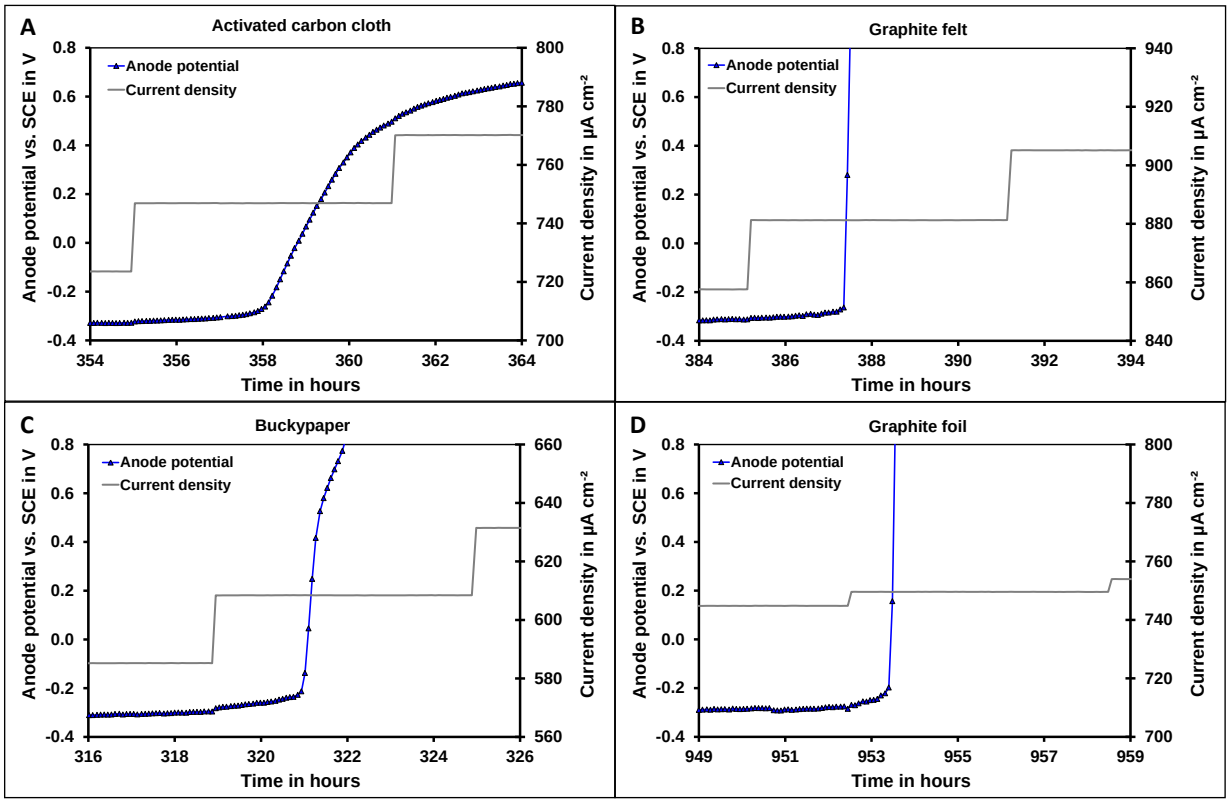

Figure 4.3: Anode potential–time curves shown for the time point when the anode potential rises steeply at a given current density step. Exemplarily shown for each carbon-based anode material: A Activated carbon cloth, B Graphite felt, C Buckypaper, and D Graphite foil. A-C were recorded with current density steps of 22.2 µA cm^{-2} every 6 h, D was recorded with current density steps of 4.4 µA cm^{-2} every 6 h.

Table 4.3: Time until the anode potential rises to a potential of water electrolysis in the current density step, and the corresponding current densities and anode potentials for the tested carbon- and metal-based materials.

Anode material	Time in current step till anode potential rises	Corresponding current density	Corresponding anode potential vs. SCE
Activated carbon cloth[a]	3.5 ± 1.5 h	772 ± 63 µA cm^{-2}	-0.275 ± 0.012 V
Graphite felt[a]	1.5 ± 1.0 h	762 ± 103 µA cm^{-2}	-0.299 ± 0.019 V
Buckypaper[a]	1.3 ± 1.1 h	613 ± 42 µA cm^{-2}	-0.209 ± 0.018 V
Graphite foil[b]	1.8 ± 2.1 h	761 ± 15 µA cm^{-2}	-0.220 ± 0.041 V
Untreated stainless steel[b]	3.6 ± 2.8 h	746 ± 16 µA cm^{-2}	+0.057 ± 0.034 V
Stainless steel glass bead blasted[b]	3.3 ± 2.8 h	351 ± 23 µA cm^{-2}	-0.175 ± 0.037 V
Titanium glass bead blasted[b]	2.6 ± 2.4 h	315 ± 19 µA cm^{-2}	-0.203 ± 0.032 V

[a] Standard polarization curve with 22.2 µA cm^{-2} every 6 h.

[b] Slow polarization curve with 4.4 µA cm^{-2} every 6 h.

In this context, Esteve-Núñez et al. (2008) [174], Malvankar et al. (2012) [175] and Fernandes et al. (2017) [176] proposed that *G. sulfurreducens* stores electrons in its periplasmic cytochromes to maintain its energy metabolism also during time periods when no external electron acceptor is available. The total charge accumulated in the cell internal cytochromes of a similar performing *G. sulfurreducens* biofilm amounts to approximately 0.06 C cm^{-2} [177].

If we consider the last current density step before the sudden rise in electrode potential and assume that the microorganisms still deliver the electrons of the previously imposed current density step, this cytochrome charge capacity would be depleted after 45 min and 3.8 h for the current density steps of 22.2 µA cm^{-2} and 4.4 µA cm^{-2}, respectively. This time span is clearly in the range of the experimentally observed time until the sudden potential rise occurs, as shown in Table 4.3. This indicates that *G. sulfurreducens* can sustain the electrons up to a certain limiting current density. The additionally imposed current density step can only be sustained until the stored electrons in the biofilm cytochromes are depleted which then results in the abrupt potential rise.

Here, our experimental results indicate that the *G. sulfurreducens* biofilm is still intact and delivering electrons up to a certain limiting current density. In general, the slope of potential rise corresponds to the discharge of the electrode material's double layer capacitance according to

$$\frac{dU}{dt} = \frac{I}{C} \tag{4.1}$$

with I being the current and C the anode material's double layer capacitance.

For instance, in case of activated carbon cloth with its double layer capacitance of 1.2 F cm^{-2} [178] this would result in a steady potential increase of 2.25 V h^{-1} when discharged at a constant current density of 750 µA cm^{-2} (when regarding only the material's double layer capacitance without biofilm). In contrast, the observed slope (Figure 4.3A) amounts to an approximately 10 times lower value of 0.28 V h^{-1}. This value would correspond to a capacitor discharge current of around 93 µA cm^{-2}. Considering the total current density of 750 µA cm^{-2}, this means that the biofilm still delivers approximately 657 µA cm^{-2}. In other words, the experimentally observed sudden rise in electrode potential is in agreement with the *G. sulfurreducens* biofilm still delivering electrons at a value in the range of the limiting current density.

Another reason for the sudden potential rise might be a potential-dependent shift in the electron transport pathway and an associated decrease in current generation during the

transition period. In this context, Yoho et al. (2014) [179] reported that in *G*. *sulfurreducens* at least two electron transport pathways exist which are expressed selectively dependent on the applied anode potential. When the anode potential changes *G*. *sulfurreducens* has to adapt its electron transfer pathways probably due to energy optimization in its respiration. However, they determined lower midpoint point potentials for the two electron transfer pathways (−0.399 V and −0.339 V vs. SCE) than the anode potentials in our work when the anode potential rises rapidly (Table 4.3). Still, this difference between the reported and measured potentials in our study might to a certain extent be explained with the potential drop across the electrolyte between the working electrode und the reference electrode. This potential drop, also called iR_u-drop, can be attributed to the uncompensated resistance R_U of the electrolyte which leads to a deviation of the measured anode potential to the actual potential [178].

However, according to the study of Yoho et al. (2014) [179] the shift in metabolic electron transfer pathways occurs on a time scale of minutes, whereas the abrupt potential rise in our study takes place in the range of hours. It is thus unlikely that the abrupt potential rise observed in our experiments is related to a metabolic pathway shift. Nevertheless, it is evident that the electron transfer of *G*. *sulfurreducens* is not yet completely understood and it requires further research in that field to completely elucidate the processes during electron transfer.

4.4.1.3 Comparison between step-wise galvanostatic and potentiostatic polarization

In the literature, potentiostatic control is commonly used for the evaluation of anode materials, but often tested at an anode potential which is too close to the oxygen reduction potential of the cathode and thus too high for practical fuel cell application. Theoretically, electroactive microorganisms could obtain more energy by transferring the electrons to an electron acceptor with a high potential, but only if the microbe has the ability to adapt its metabolic pathway to gain the available energy [180]. Studies have shown that in mixed communities the microbial community at the anode and therewith the current density is significantly influenced by the anode potential [40, 181]. Moreover, Torres et al. (2009) showed that at the higher anode potential of +0.37 V vs. SHE the current density was even decreased due to the fact that not the organisms which produce the highest current density but a mixed consortium dominated the electrode [40].

In general, comparison of current densities in literature is difficult, on the one hand because research groups use different anode potentials leading to different current densities for the investigated anode materials. On the other hand, different measurement techniques,

such as potentiostatic or a step-wise galvanostatic technique, are used. Potentiostatic control of the electrodes is often the preferred measurement technique, but not accessible in a high parallel fashion and only available at comparably high costs. On the other hand, the step-wise galvanostatic recording of polarization curves can be realized in a highly parallel fashion using an inexpensive testing equipment [55].

To demonstrate the comparability between polarization curves recorded under potentiostatic control or with the step-wise galvanostatic technique the four best performing anode materials graphite foil, activated carbon cloth, graphite felt, and untreated stainless steel identified in our study were additionally tested under potentiostatic control at the potentials of −0.400 V and +0.151 V vs. SCE (Figure 4.5, Figure 4.6).

At the applied high anode potential of +0.151 V vs. SCE higher current densities than the current densities at −0.400 V vs. SCE are delivered. However, this observation is not true for the stainless steel electrode. This may be related to the formation of an oxide layer with elevated resistance (see also section 4.4.1.1) on the metal surface [82] at the more oxidizing potential of 0.151 V vs. SCE.

At the high potential control of +0.151 V vs. SCE *G*. *sulfurreducens* delivers the highest current densities of 1022 ± 66 µA cm^{-2} and 926 ± 21 µA cm^{-2} with the materials graphite felt and activated carbon cloth, respectively. With graphite foil a lower current density of 653 ± 82 µA cm^{-2} at +0.151 V vs. SCE is achieved (duplicate measurement; with the third investigated electrode a lower current was observed: presumably *G*. *sulfurreducens* was not able to form a robust biofilm on one of the three graphite foil electrodes (Figure 4.6).

Remarkably, the current densities under potentiostatic control at +0.151 V vs. SCE of activated carbon cloth and graphite felt (926 ± 21 µA cm^{-2} and 1022 ± 66 µA cm^{-2}, respectively) are noticeably higher than the limiting current densities achieved using step-wise galvanostatic polarization (749 ± 63 µA cm^{-2} and 739 ± 103 µA cm^{-2}). Our results do not suggest that this higher current density is related to an increased amount of *Geobacter* cells on the electrode (e.g. thicker biofilm), since at the lower potential of −400 mV vs. SCE (experiment performed right after polarization at +0.151 V vs. SCE, see Figure 4.5) similar current densities are observed with both techniques (see Figure 4.4). If there were more bacterial cells attached, also at the lower potential a higher current density would be expected. In addition, this difference in limiting current density can also not be explained by the formation of a less dense biofilm at the higher potential, which would not as quickly be limited by a pH gradient. If this was the case, then this difference should also be observed

with the graphite foil, which is not the case. Further systematic research is required to investigate the significance of this effect and to elucidate the underlying phenomenon.

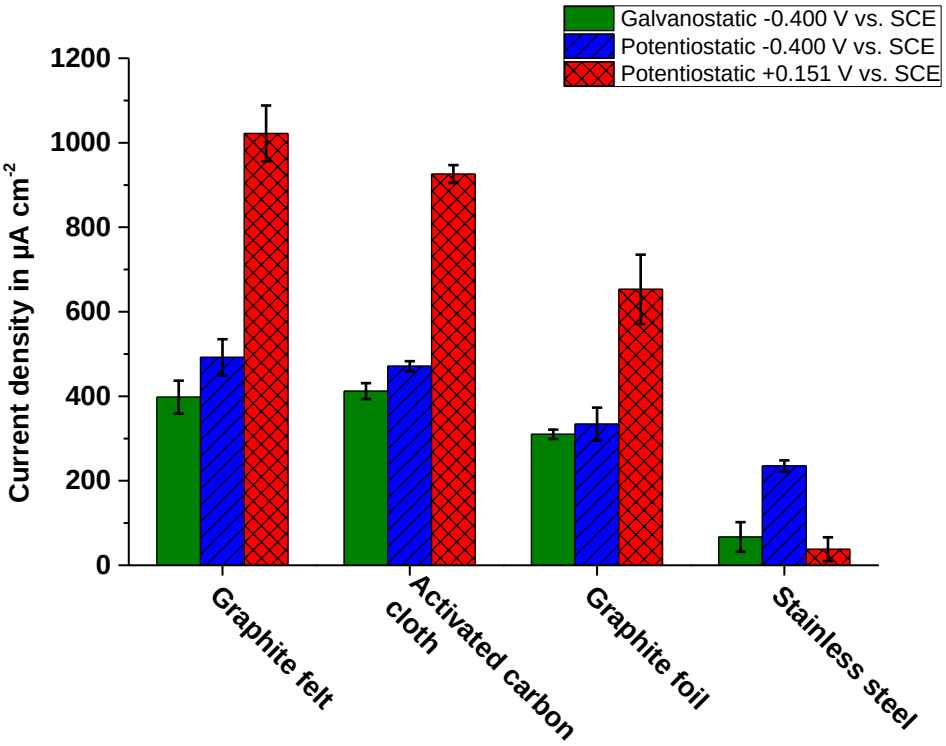

Figure 4.4: Comparison of the area-based current densities recorded at −0.400 V vs. SCE with the step-wise galvanostatic technique, and potentiostatic control at −0.400 V and + 0.151 V vs. SCE using *G. sulfurreducens* and the anode materials graphite felt, activated carbon cloth, graphite foil and untreated stainless steel. Each material is tested in triplicate, only for graphite foil at +0.151 V vs. SCE a duplicate measurement was used. Data for activated carbon cloth and graphite felt (step-wise galvanostatic technique) are cited from [167]. Bars correspond to the sample standard deviation.

At the more application-relevant anode potential of −0.400 V vs. SCE hardly any differences can be observed between the step-wise galvanostatic technique and potentiostatic control for the three materials activated carbon cloth, graphite felt and graphite foil (Figure 4.4). This implicates that from an applicational point-of-view both, galvanostatic or potentiostatic control are suitable methods. However, special attention has to be paid to choose sufficiently small current density steps (depending on the anode material) when using the step-wise galvanostatic technique. If the applied current is too high to be sustained by the growing culture of *G. sulfurreducens*, the anode potential rises rapidly to the potential range in which water electrolysis occurs. This cannot happen when polarization data is recorded under potentiostatic control, which is a clear advantage of this more expensive technique. Nevertheless, also with the step-wise galvanostatic technique

similar high limiting current densities can be achieved if sufficiently small current density steps are chosen.

Remarkably, in case of the stainless steel electrode a significant difference between the step-wise galvanostatic technique and potentiostatic control can be observed.

As can be seen from Figure 4.1, this difference stems from a pronounced polarization of the stainless steel electrode in the low current density regime (<100 µA cm^{-2}) with the step-wise galvanostatic technique. Commonly, polarization in this current density range is attributed to electrocatalytic activity of the electrode and the associated activation losses. However, since in our case all electrodes share the same microbial catalyst (*G. sulfurreducens*) it is more plausible that this observation is related to a change in stainless steel surface properties (e.g. formation of oxide layers, microstructure) and an associated effect on electron transfer and transport. This hypothesis is also supported by the fact that the glass bead blasted stainless steel electrodes do not show such a pronounced polarization in the low current density regime. To clarify this effect further investigation on a fundamental level is required.

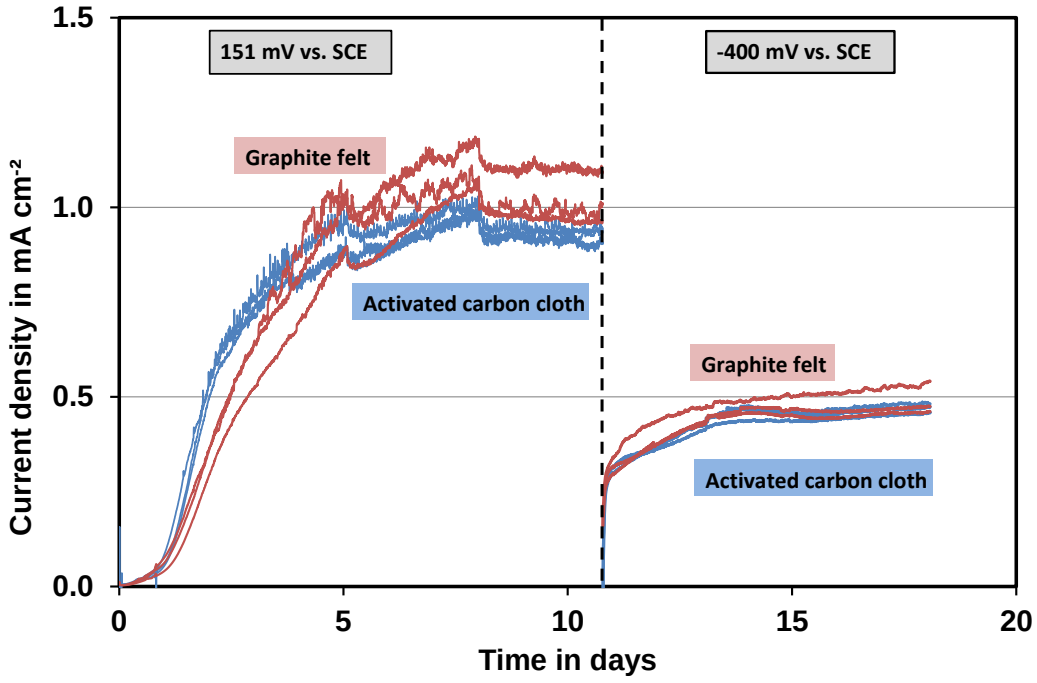

Figure 4.5: Current densities recorded under potentiostatic control with *G. sulfurreducens* at +0.151 V and −0.400 V vs. SCE, with the anode materials graphite felt and activated carbon cloth.

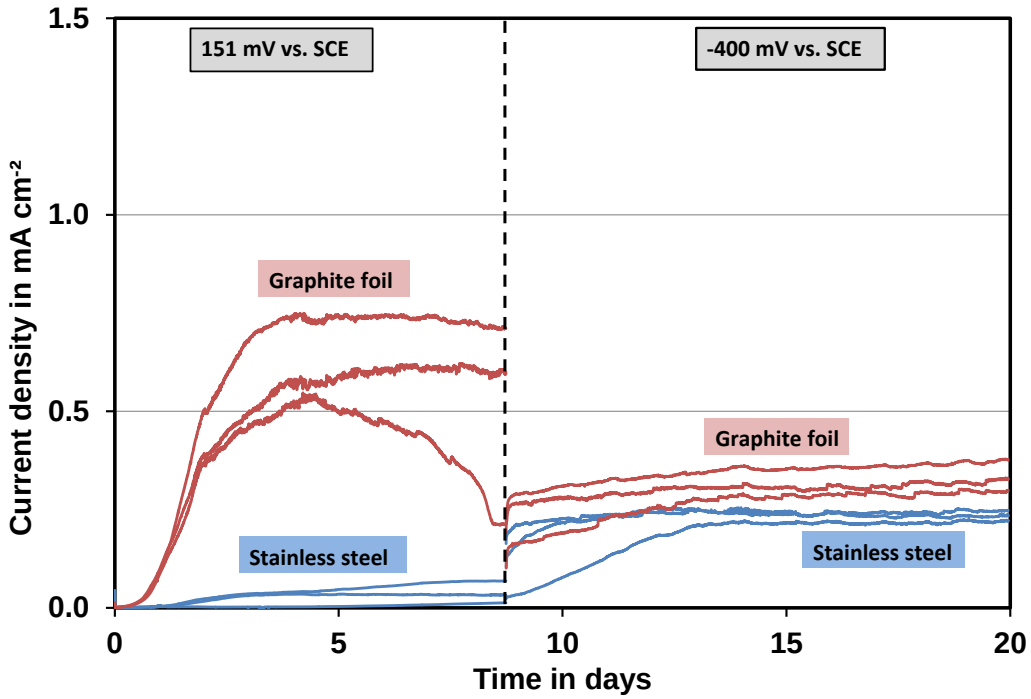

Figure 4.6: Current densities recorded under potentiostatic control with *G. sulfurreducens* at +0.151 V and −0.400 V vs. SCE, with the anode materials untreated stainless steel and graphite foil.

4.4.2 Comparison of the achieved current densities with literature values

In a recent study, Baudler et al. (2015) [78] achieved with a secondary biofilm fed with acetate and containing a high amount of *G. sulfurreducens* a current density of 984 µA cm^{-2} using a graphite electrode, but at a potential of +0.2 V vs. Ag/AgCl which is higher than the potential used in our study and not relevant for practical application. Using a copper electrode at the more negative potential of −0.2 V vs. Ag/AgCl, they achieved even 1515 µA cm^{-2} [78]. This is higher than the values achieved with a pure culture of *G. sulfurreducens* achieved in our study. However, they obtained this high current density with a mixed community and at an elevated temperature of 35 °C which might enhance the metabolic rate compared to the 30 °C we used (Arrhenius behavior). Such a behavior was also reported by Patil et al. (2010) who investigated the temperature dependence of wastewater derived biofilms. They could show that the biofilm formation time decreases at elevated temperatures and in addition, that biofilms grown at higher temperatures are electrochemically more active and lead to higher current densities [182].

When using porous materials not only the surface but also the inside of the material is available for *G. sulfurreducens* as long as sufficient nutrient supply, electron and proton

transport is ensured through the pores. On this account, for the porous materials graphite felt and activated carbon cloth the current densities were not only calculated based on the surface area but also on the volume of the material (for details the reader is referred to Appendix A4). Relating to the volume-based current densities activated carbon cloth is clearly superior to graphite felt, as activated carbon cloth shows similar current densities at a lower thickness which allows the construction of a microbial fuel cell with an optimized current-density-to-volume ratio. With respect to volumetric current densities reported in literature, Baudler et al. (2017) achieved 15.5 ± 5.0 mA cm^{-3} at −0.2 V vs. Ag/AgCl in a similar setup using a 3-dimensional copper-melamine-foam based anode [83]. This is comparable to the volumetric limiting current density of 14.98 ± 1.26 mA cm^{-3} achieved with activated carbon cloth at a more negative potential of −0.322 ± 0.007 V vs. SCE in our study.

4.4.3 Overview of the achieved results and discussion

In this comprehensive anode material study, we could show that *G. sulfurreducens* achieves the highest limiting current density of 756 ± 15 µA cm^{-2} at −0.253 ± 0.037 V vs. SCE with the anode material graphite foil. But similar high current densities were achieved with completely different anode materials, such as activated carbon cloth, untreated stainless steel and graphite felt. We could not observe an influence of the surface roughness of the used materials on the resulting current densities. This supports the hypothesis that *G. sulfurreducens* is able to achieve similar current densities with various substantially different types of anode materials.

However, in case of metal-based electrodes made from stainless steel or titanium the existence of a metal oxide layer can inhibit effective electron transfer to the electrode. Clearly, further research is needed to elucidate the surface effects and to identify the relevant material properties which promote or prevent current generation.

Nevertheless, the possibility to use a wide range of anode materials opens the possibility to focus on material properties such as conductivity, long-term stability, availability in large quantities and low production costs which are important factors regarding fuel cell application.

Besides, a second aspect needs to be taken into account: the polarization behavior and the appropriate recording using the step-wise galvanostatic technique. We showed in this study that some materials, for example graphite foil, require smaller current density steps for a material-dependent step-wise galvanostatic polarization curve to achieve steady-state conditions. Nevertheless, with this recording technique as high limiting current densities as

for the porous materials such as activated carbon cloth or graphite felt could be achieved (Figure 4.2A).

In any case, the comparison of the step-wise galvanostatic technique and potentiostatic control at the application relevant potential of −0.400 V vs. SCE showed that similar current densities for the investigated carbon-based anode materials were achieved (Figure 4.4). This underlines that, as long as there is enough process time for *G*. *sulfurreducens* to achieve steady-state conditions, the technique to record polarization is only of minor importance. From a practical point of view the step-wise galvanostatic technique is thus well suitable to record polarization curves in a highly parallel fashion, and may be an alternative to the use of the expensive potentiostatic setup. However, for the step-wise galvanostatic technique a longer process time needs to be taken into account, since first a one-week initial growth phase is applied and the step-wise polarization took about 40 days for example for graphite foil to achieve the limiting current density. The time until the limiting current density is reached fluctuates between 319 ± 12 h for buckypaper and 1134 ± 19 h for graphite foil (including the one week initial growth phase) depending on the material and the applied current-density steps. For the operation time of the other anode materials until the limiting current density is reached, the reader is referred to Appendix A4.

On the contrary, potentiostatic control only needed about 9 days to achieve steady-state conditions.

4.5 Conclusions

In this systematic and extensive anode material study with a pure culture of *G*. *sulfurreducens*, we showed that substantially different anode materials yield similar current densities under application-relevant conditions. The highest limiting current densities of up to 756 ± 15 µA cm^{-2} were achieved with graphite foil, but also with activated carbon cloth, stainless steel and graphite felt similar values were obtained. Further research is still needed to identify the influence of surface properties such as the metal oxide layer on the electron transfer mechanisms of *G*. *sulfurreducens*.

5 An air-breathing enzymatic cathode with extended lifetime by continuous laccase supply

This chapter has been published as original research article as follows (reprinted with permission from Elsevier):

E. Kipf, S. Sané, D. Morse, T. Messinger, R. Zengerle, S. Kerzenmacher: *An air-breathing enzymatic cathode with extended lifetime by continuous laccase supply*. Bioresource Technology 264 (2018) 306–310.

DOI: https://doi.org/10.1016/j.biortech.2018.04.086

Compared to the manuscript, the numbering of sections, figures, tables and references was adapted to the overall numbering of this dissertation. Minor improvements due to additional proof reading were implemented.

Contributions to this publication:

- Elena Kipf: Idea, Literature search and analysis, concept of the set-up, electrochemical experiments except the long-term experiment, planning and analysis of the experiments, and manuscript preparation.
- Sabine Sané: Scientific advice during experiments and manuscript preparation.
- Daniel Morse: Assistance during electrochemical experiments, experimental work during the long-term experiment.
- Thorsten Messinger: Assistance during electrochemical experiments.

- Roland Zengerle, Sven Kerzenmacher: Scientific advice during experiments and manuscript preparation.

Preface to chapter 5

As described in chapter 1, enzymes as biocatalysts are an inexpensive alternative to expensive noble-metal catalysts for the oxygen reduction cathode in a biofuel cell. Enzymes such as fungal laccase from *Trametes versicolor* exhibit a high electrocatalytic activity and selectivity for the oxygen reduction reaction. However, a major drawback of enzymatic cathodes is the limited enzyme lifetime due to enzyme denaturation leading to cathode lifetimes of only days and weeks. This restricts the application of enzymatic cathodes in hybrid microbial-enzymatic fuel cells with microbial anodes that show operation times of up to several years.

To overcome this problem, a novel concept towards a self-regenerating cathode was introduced by Rubenwolf et al. [114] and Sané et al. [115], who demonstrated that periodic re-supply of laccase to the electrode leads to an extended cathode lifetime. However, in their approach an immersed cathode was used which requires additional energy input for the active aeration of the catholyte. Moreover, the enzyme-containing solution was periodically and manually supplied which is not feasible for practical long-term applications.

These limitations are addressed in chapter 5, in which a novel concept is developed, which combines the advantages of a continuous enzyme supply for an extended cathode lifetime with the benefits of an air-breathing cathode design that makes energy-intensive aeration redundant and enables higher oxygen concentrations at the catalysts.

5.1 Abstract

We present a novel concept of an air-breathing enzymatic biofuel cell cathode combined with continuous supply of unpurified laccase-containing supernatant of the white-rot fungus *Trametes versicolor* for extended lifetime. The air-breathing cathode design obviates the need for energy-intensive active aeration. In a corresponding long-term experiment at a constant current density of 50 µA cm^{-2}, we demonstrated an increased lifetime of 33 days (cathode potential above 0.430 V vs. SCE), independent of enzyme degradation. The obtained data suggest that theoretically a longer lifetime is feasible. However, further engineering efforts are required to prevent clogging and fouling of the supply tubes. These results represent an important step towards the realization of enzymatic biofuel cell cathodes with extended lifetime and enhanced performance.

5.2 Introduction

Microbial fuel cells bear great potential for the generation of electricity from renewable resources such as wastewater or other organic residues [183]. However, the overall fuel cell performance is often limited by the sluggish kinetics of the oxygen reduction reaction at the cathode [94]. On this account, enzymatic biocatalysts such as laccase are an inexpensive alternative to expensive and rare noble metal catalysts such as platinum. The multicopper oxidase laccase exhibits high electrocatalytic activity for oxygen reduction, that compares favorably to platinum [184]. In nature, laccase is for instance secreted by the white rot fungus *Trametes versicolor*. It catalyzes the oxidation of phenolic compounds in timber with the simultaneous four electron reduction of dioxygen to water [185, 186]. In addition, it is capable of direct electron transfer for instance to carbon-based electrodes, which obviates the need for artificial electron mediators [187]. However, the long-term application of enzymes is significantly impaired by the intrinsic protein instability and the associated loss of biocatalytic activity. The lifetime of enzymes is typically in the range of days. For instance, in case of laccase dissolved in citrate buffer (pH 5), a half-life time in the range of only 9 days has been reported [114]. In contrast, microbial fuel cells can typically be operated over periods of several years [123], and probably beyond. Therefore, to be combined with microbial anodes (hybrid microbial-enzymatic fuel cell) the lifetime of enzymatic cathodes has to be significantly increased.

In literature, different approaches to extend the enzyme lifetime are reported, which include stabilization by genetic engineering of the enzyme's amino acid sequence, by immobilization of the enzymes by binding to an external matrix, or by reduced interactions with the solvent [118, 188, 189]. Although considerable improvements have been achieved, these methods typically only decrease the enzyme's denaturation rate but do not fully prevent degradation and the associated loss of bioelectrocatalytic activity over extended periods of time. To decouple enzyme lifetime from the lifetime of the electrode, Rubenwolf et al. (2012) [114] previously introduced the periodic renewal of purified laccase enzyme reversibly adsorbed to a carbon-based cathode. This approach was further developed by Sané et al. (2013) [115] who showed that the periodic re-supply of crude laccase-containing supernatant of *T. versicolor* (without purification) to a cathode leads to a more than 5 times extended electrode lifetime of at least 120 days. Furthermore, they demonstrated that it is not necessary to perform time-consuming and expensive enzyme purification processes to apply laccase as oxygen-reduction catalyst in biofuel cells. However, a limitation of these previous studies is the use of cathodes submerged in the enzyme containing catholyte, which has to be actively aerated to supply oxygen [115]. A further drawback of immersed cathodes is the low oxygen solubility in aqueous electrolytes. Thus, the focus of recent research lies on air-breathing cathodes to maximize the oxygen concentration at enzymatic cathodes, however only few studies on this topic have been published so far [188, 190, 191].

In the present work, we demonstrate that the promising concept of enzyme renewal can also be applied in an air-breathing gas-diffusion cathode design. This work significantly exceeds the partial results already communicated in earlier conference proceedings [192, 193], and to the best of our knowledge, this combination has never been shown before. Relying purely on diffusive O_2 supply, this concept enables passive operation of the cathode without the need for energy-intensive aeration – which is of high relevance for practical application in a biofuel cell. The novel cathode design features an integrated flow-through system to continuously supply laccase-containing supernatant of a *T. versicolor* culture, and a silicone rubber membrane as diffusion layer, which enables passive oxygen diffusion. Silicone rubber is an alternative to PTFE which is used in conventional air-breathing cathodes, since it has a higher permeability for oxygen compared to PTFE [194]. Furthermore, applied as a dense layer it overcomes the typical problems of conventional microporous gas diffusion layers such as electrolyte leakage and salt precipitation [53, 195] which often lead to a performance loss due to clogged micropores in the catalyst layer [196].

5.3 Materials and methods

5.3.1 Culture conditions

To supply laccase the strain of the white rot fungus *T. versicolor* ATCC 32745 was used in this study. It was cultivated according to the procedure described elsewhere [115]. In short, every week a new liquid culture of *T. versicolor* was prepared by transferring three pieces (0.5×0.5 cm^2 each) of mycelium grown on a YDP agar plate, onto the surface of 150 mL sterile synthetic complete laccase medium (SCL, pH 5) in a 250 mL Erlenmeyer flask. This culture was cultivated for two weeks in the dark under non-shaking conditions at 30 °C. In the next step, after this cultivation time the supernatant was harvested, centrifuged for 10 min at 9511*g*, and then sterile filtered using a PES filter with 0.2 µm pore size (514–0030, VWR, Bruchsal, Germany). Afterwards the pH value and the enzyme activity were analyzed as described elsewhere [115]. One unit of enzyme activity (1 U) is defined as the amount of enzyme required to oxidize 1 µmol of ABTS per minute at pH 5 and a temperature of 30 °C.

In the long-term experiment, different supernatant batches with differing enzyme activities were used to supply the cathode throughout the experiment, as indicated in Figure 5.3. To this end, every week a new flask with SCL medium was inoculated with *T. versicolor* as described above (described as batches A-G). The cultivation time until supernatant was harvested is listed in Table 5.1. After harvesting approx. 30 mL of supernatant from a flask, this flask was further cultivated until the next time point when supernatant was harvested (batches 1, 2, …).

As comparison to the culture supernatant of *T. versicolor*, commercial laccase from *T. versicolor* (Sigma-Aldrich, Germany) dissolved in 0.1 M sodium acetate buffer (pH 5) (approx. 3.6 U mL^{-1} towards ABTS) was used as catholyte.

Table 5.1: Batches of the flasks cultivating *T. versicolor* (A-G), the corresponding enzyme activity and culturing time. Numbers indicate the different harvesting time points of one batch. In addition, the pH values of the respective batches at the inlet and outlet of the flow-through cathode and the corresponding HRTs are listed.

Culture flask	Enzyme activity [U mL^{-1}]	Culturing time [days]	pH at cathode inlet	pH at cathode outlet	HRT
A.1	2.5	16	3.9	4.6	2.4 h
A.2	3.5	18	4.1	4.8	
B.1	3.1	14	4.1	4.8	
B.2	2.7	16	4.1	5.1	
C.1	2.7	11	4.5	5.1	
C.2	3.9	14	4.3	5.0	
C.3	4.1	16	4.1	4.9	
C.4	3.7	18	4.2	4.9	
D.1	3.8	14	4.2	4.9	
D.2	3.8	16	4.2	4.7	1.2 h
D.3	4.0	18	4.2	4.6	
E.1	2.0	16	4.5	4.7	
E.2	2.5	18	4.5	4.8	
F.1	1.8	16	4.4	-	
G.1	0.9	15	-	-	

5.3.2 Electrode and reactor set-up

To construct the air-breathing cathode, at first a buckypaper electrode was prepared from dispersed carbon nanotubes (Baytubes C150 HP, Bayer Material Science AG, Germany) as described elsewhere [136, 197]. For the detailed procedure of the buckypaper preparation the reader is referred to the supplementary data of our previous report [152]. The buckypaper electrode was then equipped with a 0.5 mm thin silicone rubber membrane (Ketterer + Liebherr, Freiburg, Germany) as gas diffusion layer, which enables sufficient passive oxygen supply and prevents electrolyte leakage and salt precipitation. A schematic of the flat-plate construction of the air-breathing cathode is shown in Figure 5.1. The buckypaper side with the carbon nanotubes faced towards the silicone rubber membrane and the nylon filter support faced the catholyte chamber. The overall exposed area of the air-breathing cathode was 1 cm^2.

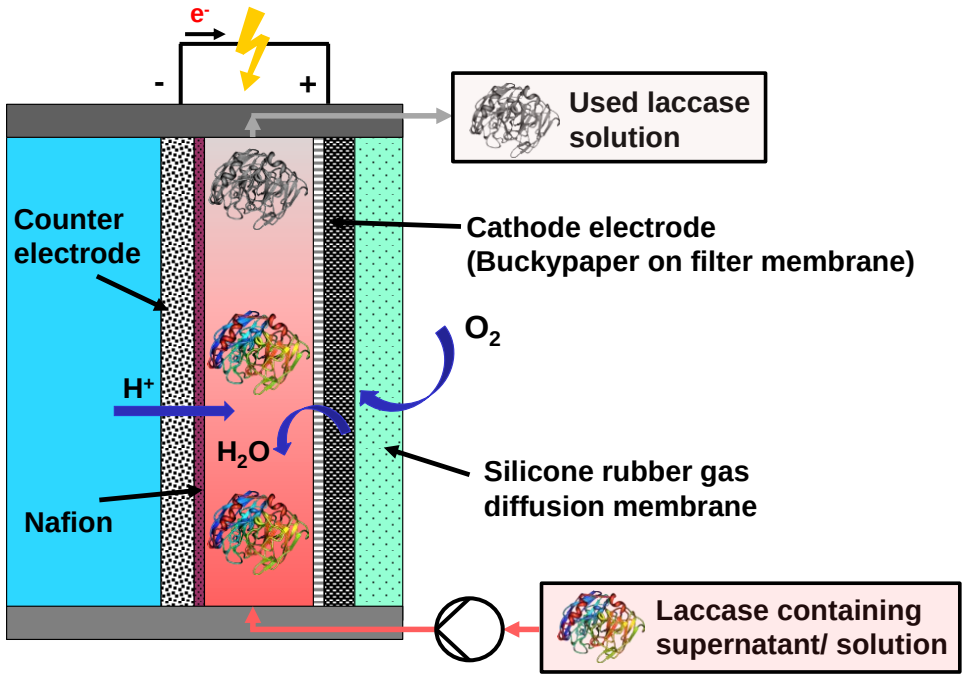

Figure 5.1: Schematic of the flat-plate construction of the air-breathing laccase cathode with continuous flow-through. The image of the laccase enzyme was created using the protein data bank (PDB) and the software Protein Workshop.

The cathode was operated in a half-cell setup against a platinum mesh counter electrode (Goodfellow, Bad Nauheim, Germany), separated by a Nafion membrane (Nafion 115, Quintech, Göppingen, Germany). As reactor an octagonal polycarbonate vessel with a liquid volume of 300 mL was used. To its outside eight air-breathing cathodes were attached using different polycarbonate frames and silicone gaskets. The cavity between the porous filter backside of the buckypaper cathode and the Nafion membrane (see Figure 5.1) amounted to only 0.2 mL volume. The reactor was filled with 300 mL of 0.1 M sodium acetate buffer (pH 5), and its interior volume was continuously purged with nitrogen. This thin flat-plate configuration was investigated in both, batch mode and continuous mode. In continuous mode, laccase solution or laccase-containing supernatant was continuously supplied through this cavity at different hydraulic retention times (HRTs) of 0.8 h, 1.2 h and 2.4 h using a peristaltic pump (Reglo Digital, Ismatec, Wertheim, Germany). Before filling the cavity of the air-breathing cathodes with sterile-filtered laccase solution, the test reactor was autoclaved at 121 °C for 20 min to provide sterile conditions.

5.3.3 Electrochemical characterization

For electrochemical characterization the electrical testing environment described elsewhere was used [55]. The test setup consists of an electronic load (STG 2008 stimulus

generator, Multichannel Systems, Reutlingen, Germany) to apply load current to the cathode half-cell, and a data acquisition unit (Keithley 2700, Germering, Germany) to simultaneously record the cathode potentials against a reference electrode every 5 min. As reference electrode a saturated calomel electrode (SCE, +0.244 V vs. SHE, KE 11, Sensortechnik Meinsberg, Ziegra-Knobelsdorf, Germany) was used. The electrochemical experiments were conducted as described elsewhere [115]: Prior to all electrochemical experiments, the enzyme was allowed to adsorb to the electrode for 12 h under open circuit conditions. For the step-wise galvanostatic polarization the current density was increased in steps of 5 µA cm^{-2} every hour. For the long-term experiment, a constant current density of 50 µA cm^{-2} was applied. All measurements were conducted at a constant temperature of 30 °C. The measurements for the long-term experiment and the galvanostatic polarization were conducted in triplicates, except for the experiments with commercial laccase solution at a HRT of 2.4 h, which were performed as quadruplicate.

5.4 Results and discussion

5.4.1 Effect of hydraulic retention time on the cathode polarization curve

Figure 5.2 shows cathode polarization curves of the air-breathing cathodes supplied with either commercial laccase in sodium acetate buffer or with cultivated supernatant of *T. versicolor* at different hydraulic retention times. Similar enzyme activities of approx. 3.6 U mL^{-1} were used in all fuel cells. Significantly higher current densities (53 ± 4 µA cm^{-2} at 0.4 V vs. SCE) were achieved with commercial laccase in sodium acetate buffer at a hydraulic retention time (HRT) of 2.4 h, as compared to batch mode (12 ± 3 µA cm^{-2} at 0.4 V vs. SCE). The lower current density in case of batch operation can be explained by the relatively little amount of laccase that can be supplied to the electrode from the total cavity volume of only 0.2 mL. In contrast, with continuous flow-through more laccase molecules can be supplied and adsorb to the electrode.

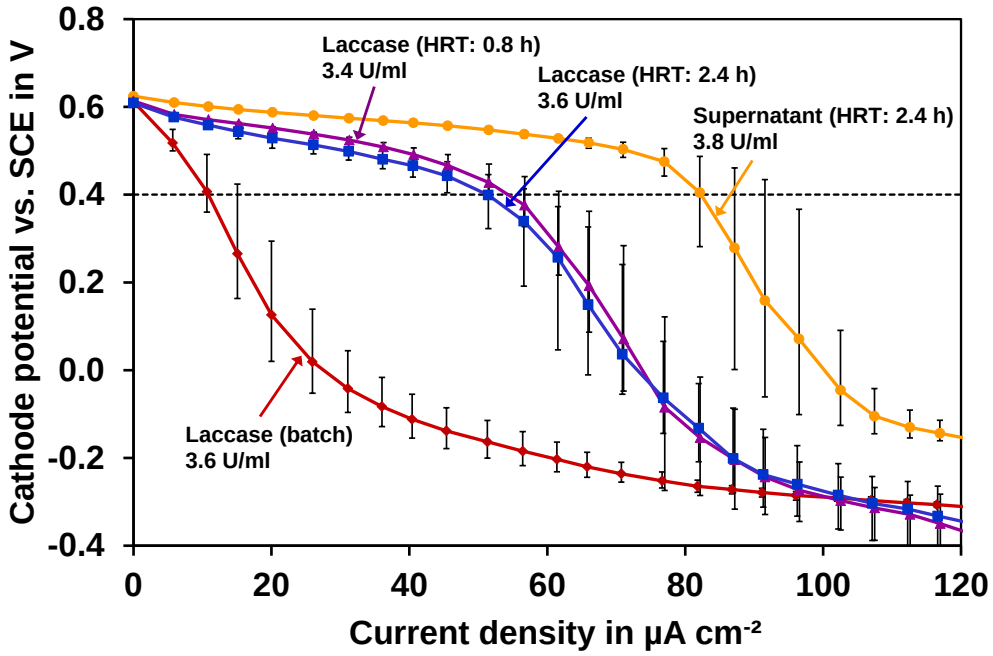

Figure 5.2: Cathode polarization curves of air-breathing cathodes, recorded either in batch-mode, or with continuous supply of commercial laccase solution in sodium acetate buffer or cultivated supernatant of *T. versicolor*. Different hydraulic retention times (HRTs) were tested, as indicated. In all cases similar enzyme activities were used (approx. 3.6 U mL^{-1} towards ABTS). Data points depict the mean values and bars correspond to the maximum and minimum values of at least triplicate experiments.

The increase of the flow rate by a factor of three (decrease of the HRT from 2.4 h to 0.8 h) did not lead to a change of the cathode performance (with HRT of 0.8 h: 56 ± 6 µA cm^{-2} at 0.4 V vs. SCE). This indicates that the electrode is already saturated with adsorbed laccase at the higher HRT of 2.4 h. Even under these conditions (HRT of 2.4 h), an abrupt potential drop occurs at higher current densities, which can be related to mass-transfer limitations. This rapid potential drop stabilizes at around −0.444 V vs. SCE (−0.200 V vs. NHE), which corresponds to a potential range at which the oxygen reduction reaction occurs on the buckypaper electrode without enzymes [197]. This indicates that the potential drop is caused by a limited amount of laccase enzymes attached to the electrode instead of an oxygen limitation. Remarkably, an increased current density of 86 ± 8 µA cm^{-2} at 0.4 V vs. SCE could be achieved when using the cultivated laccase-containing supernatant of *T. versicolor* with a HRT of 2.4 h. This result clearly underlines the practical applicability of crude supernatant of *T. versicolor* to supply laccase obviating the need for time-consuming and expensive purification as previously shown [115]. A control polarization curve using only SCL medium without enzyme was conducted by Sané et al. (2013) [115]. The observed open circuit potential (OCP) was significantly lower (0.168 V vs. SCE), corresponding to the limited catalytic activity for oxygen reduction of the buckypaper electrode.

Comparing our results with air-breathing enzymatic cathodes in literature is rather difficult, due to the differences in enzymes, construction principles, experimental methods, and operation conditions. In addition, hardly any data on long-term operation is available. For instance, Kontani et al. (2009) achieved current densities of up to 20 mA cm^{-2} using cyclic voltammetry with a copper efflux oxidase (CueO) adsorbed onto hydrophobic Ketjen black modified carbon paper [198]. However, these current densities were achieved at a cathode potential of −0.2 V vs. Ag/AgCl, which is by approx. 600 mV more negative compared to the values in our work. Furthermore, Ciniciato et al. (2012) presented an air-breathing paper-based bilirubin oxidase cathode yielding about 300 µA cm^{-2} at a cathode potential of 300 mV vs. Ag/AgCl [199]. Santoro et al. (2016) even investigated the long-term performance of a bilirubin oxidase air-breathing cathode at a constant potential of 300 mV vs. Ag/AgCl, but they observed a strong continuous decrease of the current density: an initial current density of 350 µA cm^{-2} was shown, followed by a rapid decrease of ∼60 µA cm^{-2} day^{-1} in the first three days which slowed down to a rate of 1.5 µA cm^{-2} day^{-1} after 9 days and resulted in a final current density of ∼48 µA cm^{-2} after 45 days [191]. In the study of Gupta et al. (2011) [200] gas-diffusion cathodes using immobilized laccase from *Trametes hirsuta* yielded current densities of up to 1 mA cm^{-2}, however in this case the cathode was operated with pure oxygen instead of air. Though our air-breathing laccase cathode exhibits extended lifetime (see Section 5.4.2), its limiting current density of up to 100 µA cm^{-2} is still lower compared to literature values. A possibility to further improve its limiting current density is the optimization of the electrode thickness. However, this has not been the focus of the present work.

5.4.2 Long-term stability of the air-breathing cathode with continuous laccase supply

The integrated flow-through system offers the opportunity to sustain the electrocatalytic activity of the air-breathing cathode over time by a continuous supply of fresh laccase. This was tested with cultivated supernatant of *T. versicolor* of different batches with differing enzyme activities (Table 5.1). The evolution of the cathode potential over time at a constant current density of 50 µA cm^{-2} is shown exemplarily for the curve with the longest lifetime in Figure 5.3. Starting from an initial cathode potential of 0.557 V vs. SCE, the electrode potential could be kept at values above 0.430 V vs. SCE for up to 33 days. Then, irreversible clogging of the supernatant supply tubes occurred and the experiment had eventually to be stopped. In a similar experiment (submerged cathode) without the continuous re-supply of laccase-containing supernatant, the cathode potential

dropped already after 23 days to a significantly lower potential of less than -0.050 V vs. SCE [115]. In a control long-term experiment without flow-through using our novel setup, only the cavity was filled with *T. versicolor* supernatant (data not shown). Here, the potential of the air-breathing cathode dropped immediately upon applying the current density of 50 µA cm^{-2}. This indicates that the number of enzymes that can be provided by the small cavity volume of 0.2 mL is too small to sustain this current density.

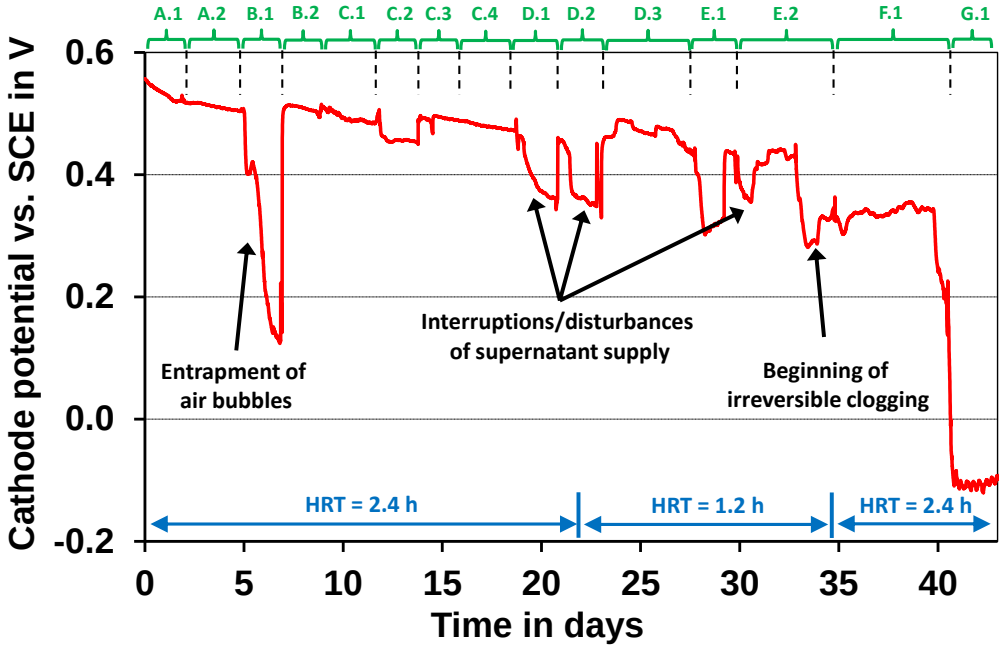

Figure 5.3: Evolution of the cathode potential over time with continuous supply of laccase-containing supernatant of *T. versicolor* at a constant current density of 50 µA cm^{-2}. A representative curve is shown. At indicated time points different supernatant batches with varying laccase activities were used. HRTs were adjusted as indicated. Shown is the curve with the longest lifetime. Replicate experiments showed only lifetimes of 17 days and 9 days, respectively, due to the excessive clogging of the supply tubes and additional issues with the electrical connections. Data cited from [193].

Several times throughout the long-term experiment a disturbance or an interruption of the supernatant occurred, as indicated by arrows in Figure 5.3. These were mainly caused due to entrapped air bubbles in the supply tubes, by leakage, and by biofouling of the tubes. Especially the exit of the supply tubes, which were closed with sterile filters to maintain a sterile environment in the reactor, were prone to fouling which frequently led to a complete blockage and interruption of the laccase supply. Interestingly, the enzyme activity of the cultivated supernatant (Table 5.1) had no noticeable effect on the cathode potential under load in the investigated setup. This can be explained by operation of the electrode at a value below the limiting current density.

In summary, we successfully demonstrated an air-breathing laccase cathode which is continuously supplied with enzyme-containing supernatant of *T. versicolor* to achieve an

extended lifetime, which is decoupled from enzyme degradation. Our results indicate that theoretically a longer lifetime is feasible if the observed issues of blocking and biofouling can be alleviated. Nevertheless, as can be seen from Figure 5.3, there is a small but noticeable decrease of the cathode potential over time, which points towards a gradual loss of electrocatalytic activity. Remarkably, such a behavior has not been observed in previous experiments with submerged cathodes [115]. Future research is necessary to investigate the magnitude of this effect and to clarify whether it is related to the secretion of inhibitory by-products by the *T. versicolor* culture. For instance, in separate experiments with shaken cultures of *T. versicolor* (data not shown) we observed a rapid decrease of the cathode potential – presumably caused by by-products secreted under these culture conditions.

With respect to practical application of our concept to microbial fuel cells, the pH gradient between the anode and cathode compartment due to limited proton transport through the membrane and the associated performance loss, is of particular concern [60]. Here our cathode design featuring the continuous flow-through may provide an engineering solution to maintain a stable pH value at the cathode by adjusting a suitable flow-rate. For instance, in the long-term experiments with a HRT of 2.4 h the pH at the exit of the flow-through cathode chamber increased by only about 0.6–1.0 units (the inlet pH of *T. versicolor* supernatant was at pH 3.9–4.5). The pH difference between inlet and outlet could even be decreased to 0.2–0.5 pH units at the lower HRT of 1.2 h (see Table 5.1).

Important points are the economics and the sustainability of a system that continuously requires fresh enzyme solution. These aspects need further detailed investigations and optimizations of the system, e.g. of enzyme supply rates and hydraulic retention times. In this context, the possibility of *T. versicolor* to produce laccase from growing on abundant organic residues such as by-products of the pulp and paper industry [201] or agricultural waste containing lignocellulosic material [202] may be of advantage with respect to economic feasibility and ecological sustainability.

5.5 Conclusions

We successfully demonstrated an air-breathing laccase cathode based on the continuous supply of enzyme-containing supernatant of *T. versicolor*. In contrast to previous works, the new concept obviates the need for energy-intensive aeration. It is a significant step towards the realization of hybrid microbial-enzymatic biofuel cells with enhanced performance and increased lifetime. Future engineering work will have to focus on an

optimized construction to prevent leakage, biofouling, and clogging of the supply tubes and filters to further increase the operation time of the cathode.

6 Overall conclusions and outlook

6.1 Overall summary and conclusions

Overall, this thesis has several major outcomes which were derived in each chapter. Therefore, a short summary of the individual chapters and the respective conclusions are listed. Subsequently, a general conclusion of this doctoral thesis is given.

In chapter 2 of this thesis a systematic screening of different carbon-based anode materials was conducted with the microbial fuel cell model organism *Shewanella oneidensis* MR-1. Under the tested anoxic conditions the anode material activated carbon cloth C-Tex 13 showed the highest current density of 0.24 A m^{-2} at -0.2 V vs. SCE. Compared to the state of the art of anode materials operated with *S. oneidensis*, as listed in Table 1.1, this current density is in a similar range as values reported in literature, but at a significantly lower and thus more favorable anode potential of -0.2 V vs. SCE. In order to reduce the overall size of the fuel cell and thus the costs of the overall system also the volumetric current density needs to be considered. In that respect, the only 500 µm thick activated carbon cloth C-Tex 13 delivers ~0.5 mA cm^{-3} at -0.2 V vs. SCE based on the anode electrode volume. This is only surpassed by the tested buckypaper electrode (thin film of multi-walled carbon nanotubes) which exhibits a volumetric current density of 1 mA cm^{-3} at the slightly higher anode potential of -0.164 V vs. SCE. Compared to literature, only Sanchez et al. [90] reported a higher volumetric current density of 2.4 mA cm^{-3} with *S. oneidensis* and a carbon nanofiber mat anode, however this value was recorded at a 200 mV more positive anode potential compared to the results presented in chapter 2.

The superior performance of the activated carbon cloth anode material is attributed to the high specific surface area of this nanoporous material which is presumably available for mediated electron transfer via self-secreted flavins of *S. oneidensis.* Nevertheless, since the detailed electron transfer mechanisms are not yet completely understood, different hypotheses for the role of flavins in the extracellular electron transfer exist. For example, Okamoto et al. [52] proposes that flavins do not act as redox mediators in the form of free electron shuttles for mediated electron transfer, but form instead a flavin/outer membrane

cytochrome complex in which flavins function as bound co-factors for the direct electron transfer. This hypotheses is supported by recent research of Xu et al. [203] who also concluded that during electron transfer of *S. oneidensis* to high surface carbon cloth electrodes, flavins primarily act as bound co-factors accelerating the direct electron transfer, rather than as free electron shuttles. This new model for the extracellular electron transfer mechanism of *S. oneidensis* emphasizes that research on the detailed processes and the involved compounds is not yet completed and requires further investigation and validation.

As reported in chapter 2 when normalizing the current density to the anode area, activated carbon cloth delivers the highest current density, but when normalized to the BET-surface it is significantly outranged by porous materials with larger pores (graphite felt, carbon paper, buckypaper). This fact clearly indicates that the large specific surface area of activated carbon cloth seems to be unused to a great extent by mediators and microorganisms. That is presumably due to diffusion limitations occurring on the nanoporous and macroporous level. With this information, the anode electrode structure can be further optimized for its application with *S. oneidensis*. For instance, the pore size needs to be increased in the nanoporous as well as in the macroporous structure to prevent limitations of the mediator diffusion and of the bacteria migration. From a practical point of view, this could be realized for example by electrospinning of loosely connected polymer fibers leading to larger pores in the macroporous structure, which are then carbonized and treated with an activation step to increase the specific surface area on a nanoporous level.

In chapter 2 also the influence of aeration on the achieved current density with the aero-tolerant strain *S. oneidensis* was investigated. Under aerated conditions the current density could be increased about three times, however at the expense of the coulombic efficiency. The increased current density was attributed to the formation of thicker biofilms under aerobic conditions, as described by Rosenbaum et al. [28]. However, in regard of the novel electron transfer model for *S. oneidensis* which proposes that flavins act as co-factors in the form of flavin-bound cytochromes enhancing the direct electron transfer rate [52, 203], the increased current density could also be a result of the increased flavin production under aerated conditions, as it was reported by TerAvest et al. [91]. Interestingly, in chapter 2 no influence of the specific surface area could be observed under aerated conditions, which was related to a shift from mediated to direct electron transfer.

In contrast to the above observed increased current density with *S. oneidensis* under aerated conditions, Rosenbaum et al. [204] reported in their transcriptional analysis that the proteins necessary for electrode reduction (c-type cytochromes) are down-regulated under aerobic conditions. That contradiction can be explained with the fact that although in the

bulk liquid aerobic conditions maintain, inside the biofilm mostly micro-aerobic or anoxic conditions are prevailing due to limited oxygen diffusion into the biofilm. That means that bacteria in close proximity to the anode surface still need to perform external electron transfer to the electrode for anaerobic respiration. With oxygen the biomass growth can be enhanced and thus the number of the electrochemically active cells on the electrode can be increased, which is presumably responsible for the increased current density under aerobic conditions. Nevertheless, regarding the coulombic efficiency oxygen is considered detrimental as it competes with the anode electrode for the electrons. Thus, in chapter 2 first an aerobic growth phase to increase the number of electroactive cells on the electrode followed by anaerobic operation is proposed.

With this study in chapter 2, it could be demonstrated that the electrode material has a significant influence on the anode performance of *S. oneidensis*. It was concluded that the high surface area is presumably available for mediated electron transfer via flavins which leads to an enhanced current density with *S. oneidensis*. This is a particularly important result for applications using pure cultures of *S. oneidensis.* This includes for example bioproduction of precursor chemicals by using unbalanced fermentation of genetically modified *S. oneidensis* [205]. In conventional fermentation the oxidation state of the substrate and the fermentation end products has to be intrinsically identical, which typically leads to the formation of mixed end products by the microorganisms. Unbalanced fermentation overcomes this limitation by introducing an external electron acceptor that cannot be depleted, which is an electrode. Proof of principle of unbalanced fermentation was shown by Flynn et al. [206] who developed an *S. oneidensis* strain that catalyzed the formation of ethanol from glycerol, a waste product of the biodiesel production. Due to the more reduced state of glycerol compared to ethanol, this conversion without interfering by-products would not be possible in conventional fermentation. A recent example for unbalanced fermentation is the bioproduction of acetoin, an important platform chemical, in genetically modified *S. oneidensis* by using lactate as substrate [205].

Another application, in which *S. oneidensis* is used as a pure culture which can benefit from an improved anode material as presented in chapter 2, is the application of *S. oneidensis* as a biosensor. Proof of principle was demonstrated by Golitsch et al. [16] with a pure culture of genetically modified *S. oneidensis* which produces electrical current in response to the analyte of interest – in this case the model compound arabinose. Webster et al. [207] went beyond this proof of principle by developing a biosensor with genetically engineered *S. oneidensis* for the environmentally relevant analyte arsenic. In the absence of the analyte of interest, the genetically modified *S. oneidensis* cannot use the anode as

electron acceptor, since the genes for the expression for the outer membrane complex are only induced in the presence of the analyte of interest. In order to survive under these conditions, *S. oneidensis* as a facultative anaerobic microorganism uses oxygen as electron acceptor. Thus, the coulombic efficiency plays only a minor role in that type of application.

Maintaining anoxic conditions can mean too much effort, especially in practical applications such as scaled-up microbial fuel cell operation. In that context, the application of an aero-tolerant exoelectrogenic strain such as *S. oneidensis* may be of advantage. Moreover, oxygen intrusion which might occur by e.g. cross-over from an air-breathing cathode to the anode compartment can promote the *S. oneidensis* biofilm growth on the anode electrode. In addition, in applications in which the substrate is derived from abundant organic residues or waste, the reduced coulombic efficiency under aerated conditions is of only minor importance. Furthermore, when degradation of organic residues is the primary focus besides current generation as it is the case in wastewater treatment, the additional substrate degradation by bacteria that use oxygen instead of the electrode as electron acceptor can be desired.

In chapter 3 a comparison of the two microbial fuel cell model organisms *Geobacter sulfurreducens* and *Shewanella oneidensis* is accomplished, each relying on completely different electron transfer mechanisms, which are direct and mediated electron transfer, respectively. In addition, in this study two different anode materials that vary significantly in their specific surface area, high-surface area activated carbon cloth and low-surface area graphite felt, are investigated. Remarkably, *G. sulfurreducens* achieves with both anode materials up to 700 µA cm^{-2}, independent of the specific surface area. The insignificant influence of the surface area on the current density is attributed to the fact that *G. sulfurreducens* forms thick conductive biofilms on the anode material and performs only direct electron transfer. This finding could open the possibility of using a broad spectrum of anode materials largely independent of the material's specific surface area. *S. oneidensis* in contrast, achieves significantly higher current densities with the high-surface area activated carbon cloth compared to the low-surface area graphite felt, but at a substantially lower level than *G. sulfurreducens*. Nevertheless, the fact that *S. oneidensis* can apparently make use of the high surface area of activated carbon cloth is associated with its availability for the self-secreted electron shuttles in the mediated electron transfer of *S. oneidensis.*

The results of chapter 3 affirm the in the beginning of this thesis raised research question whether the two model organisms which rely on significantly different electron transfer mechanisms interact differently with the investigated anode materials. Moreover,

the obtained results suggest that the prevailing electron transfer mechanism of the microorganisms plays a role for the choice of the anode material.

However, as discussed above the underlying mechanisms of the electron transfer are still under investigation and need further research. Especially, the role of flavins in the mediated electron transfer, either as free electron shuttles or as bound co-factors at the cytochromes is still under discussion. In this regard, Okamoto et al. [208] suggested that flavins play not only a decisive role in the electron transfer mechanism of *S. oneidensis*, but also in *G. sulfurreducens.* They proposed a similar electron transfer mechanism for both microorganisms involving flavins which are bound to cytochromes and act as co-factors for an enhanced electron transfer rate. In addition, they reported that *G. sulfurreducens* is also able to self-secrete these flavins [164], which is a novel finding compared to previous literature. Besides that, it is worth noting that also some medium components may be redox active and act as electron mediators. For example, sulfate can act as electron shuttle by being reduced by sulfate-reducing bacteria to sulfide, which is then re-oxidized at the anode [145]. This must also be taken into account when further research on electron transfer mechanisms is conducted.

The tendency that *G. sulfurreducens* is able to achieve substantially higher current densities compared to *S. oneidensis* is confirmed in the literature data overview of Table 1.1, which shows that the obtained current density depends not only on the electrode material, but also on the fed substrate and the applied microorganisms. As can be seen in this table, in acetate-fed biofilms in which the microorganism *G. sulfurreducens* is dominating, the current density is significantly higher than in pure cultures of *S. oneidensis* fed with lactate. Consequently, *G. sulfurreducens* is the preferred electroactive microorganism for applications demanding high current densities. Nevertheless, since *G. sulfurreducens* is sensitive to the presence of oxygen [151], *S. oneidensis* as aero-tolerant strain may have its advantage in environments where oxygen intrusion cannot be prevented, or in applications requiring pure cultures of genetically modified *S. oneidensis* such as in a biosensor [16, 207] or in unbalanced fermentation [205, 206], as described above.

Chapter 4 describes an extensive and systematic anode material screening with the model organism *G. sulfurreducens.* In this study, a large range of substantially different carbon- and metal-based anode materials were investigated under application-relevant conditions. *G. sulfurreducens* achieves the highest limiting current density of 756 ± 15 µA cm^{-2} (~7.6 A m^{-2}) at -0.253 ± 0.037 V vs. SCE with graphite foil, but also with the completely different anode materials activated carbon cloth, graphite felt and untreated

stainless steel similar high current densities were reached. The electrochemical stability of stainless steel is not a problem in microbial anodes, since stainless steel is a passivating material whose oxide layer protects itself from being oxidized at higher potentials [78]. Comparing these current densities with state of the art of acetate-fed biofilms in literature (see Table 1.1), the achieved current densities are mainly in the same order of magnitude. For example, Baudler et al. [78] achieved current densities of up to 10 - 15 A m^{-2} with the anode materials graphite, silver, gold and copper using an acetate-fed secondary biofilm derived from wastewater. The slightly higher current densities compared to the results from chapter 4, could be explained by the fact that they used a mixed consortium instead of a pure culture of *G. sulfurreducens*, by the elevated temperature they used (35 °C vs. 30 °C) which might enhance the bacterial metabolism and thus the electron transfer rate, and by the higher (and less favorable) anode potential which was applied (+0.2 V vs. Ag/AgCl, only for copper -0.2 V vs. Ag/AgCl).

The results obtained in chapter 4 indicate that *G. sulfurreducens* is able to achieve high current densities with a wide range of substantially different anode materials, largely independent of the specific surface area of the electrode. In that context, it was shown that *G. sulfurreducens* was able to achieve one of the highest current densities with both, high surface area activated carbon cloth and low surface area graphite felt as anode material. This result is presumably attributed to the formation of thick conductive biofilms on the anode surface, together with the direct electron transfer mechanism of *G. sulfurreducens*. The possibility to use a great variety of anode materials allows to focus on availability, manufacturing costs, long-term stability and robustness, electrical conductivity, and scaling-up of the electrode material.

New developments in literature are composite materials which combine the advantages of several materials, such as electrical conductivity and improved microbe-electrode interaction and thus represent a promising concept. For example, composite materials made of carbon black coated stainless steel or copper coated polymer foams were demonstrated to be promising anode materials using acetate-fed secondary biofilms derived from wastewater [83, 87]. However, a disadvantage is the complex fabrication process which is expensive and laborious, and may complicate the scale-up process required for practical application. In addition, long-term stability and functionality of the composite structures under application-relevant conditions still need to be demonstrated.

Depending on the type of application, not always the best performing electrode but an inexpensive electrode material may be advantageous from an economic point of view. Thus, often a compromise between low cost and good performance of the electrode material

needs to be found [63]. In that context, Blanchet et al. [93] proposed that under industrially-scalable conditions, 2-dimensional electrodes should be considered as a worthwhile alternative to more complex and expensive 3-dimensional porous anodes, as they showed a similar performance during long-term operation for both types of anodes, due to biofilm growth and pore clogging. This result is supported by Baudler et al. [83] who described a decline of the current density of a 3-dimensional anode to values even below that of a solid planar 2-dimensional anode, which was related to clogging of the porous structure and the resulting mass transfer limitations. Moreover, the transfer of inexpensive, 2-dimensional anodes to more complex 3-dimensional electrodes does not necessarily lead to remarkably higher volumetric current densities due to the increasing mass transfer limitations inside the pores [63]. These findings underline the importance regarding practical application of the in chapter 4 obtained high current densities using planar, 2-dimensional anodes with *G. sulfurreducens*.

Moreover, in chapter 4 highly parallelized and inexpensive step-wise galvanostatic polarization was compared to state-of-the-art and cost-intensive potentiostatic control. At the application-relevant potential of -0.4 V vs. SCE, similar current densities were obtained for the investigated carbon-based materials with both measurement techniques. Only in case of stainless steel the two measurement techniques resulted in considerably different current densities. In detail, the use of potentiostatic control led to significantly higher current densities at -0.4 V vs. SCE compared to galvanostatic control due to the pronounced polarization of stainless steel in the low current density regime with the step-wise galvanostatic technique. This can presumably be related to the surface properties of the stainless steel material, e.g. the presence of a metal oxide layer that impedes the electron transfer. In addition, the step-wise galvanostatic technique required a longer start-up time for achieving the limiting current density compared to potentiostatic control. However, from an applicational point of view, this longer start-up time in the range of days or a few weeks is negligible compared to the operation time of a microbial fuel cell of up to several years. Moreover, when using step-wise galvanostatic polarization special attention needs to be paid to choose sufficiently small steps for the individual anode materials, otherwise the growing culture of *G. sulfurreducens* is not able to sustain the high current and the anode potential rises abruptly to a potential where water electrolysis occurs. This does not happen when using potentiostatic control, which is a clear advantage of this more expensive technique that is commonly used in literature for the evaluation of anode electrodes. Nevertheless, in contrast to potentiostatic control, the step-wise galvanostatic technique can be applied in a highly parallel fashion by using inexpensive equipment [55], which is a great advantage of this measurement technique.

In chapter 5 a novel concept for an air-breathing enzymatic laccase cathode with extended lifetime by continuous supply of the supernatant of the fungus *T. versicolor* is demonstrated. This novel concept is based on the approach of Sané et al. [115] who showed that manual, periodic re-supply of enzyme-containing, unpurified supernatant of *T. versicolor* extends the cathode lifetime. Nevertheless, in their work an immersed cathode was used, which on the one hand requires energy-intensive active aeration, and on the other hand can limit the oxygen supply due to mass transfer limitations as a result of the limited oxygen solubility in aqueous solutions. Moreover, for an immersed cathode a separate cathode chamber is needed.

These limitations are overcome by the novel air-breathing cathode concept that is demonstrated in chapter 5. The air-breathing laccase cathode obviates the need for additional energy-input for aeration and at the same time, it allows for higher oxygen concentrations at the cathode catalyst due to the direct oxygen diffusion to the catalyst particles. In addition, it enables the construction of a favorable 1-compartment fuel cell with decreased internal resistance. Furthermore, in the work of Sané et al. [115] a periodic and manual enzyme re-supply was conducted, which is however not suitable for practical long-term application. Thus, additionally a continuous supply system for the enzyme-containing supernatant was developed in chapter 5.

With the novel air-breathing cathode design and the continuous enzyme supply of the supernatant of *T. versicolor,* a cathode lifetime of 33 days at a constant current density of 50 µA cm^{-2} could be demonstrated, independent of the enzyme lifetime. In a control experiment without flow-through, when only the cavity of the air-breathing cathode was filled with *T. versicolor* supernatant, the potential dropped immediately upon applying the current density of 50 µA cm^{-2}. That points out that the small cavity volume of only 0.2 mL provides a too small number of enzymes to sustain this current density. Thus, the continuous re-supply of the enzymes is required to connect enough enzymes to the electrode.

In literature, state of the art to extend the enzyme lifetime involves typically enzyme immobilization which in general means inclusion of the enzymes into several matrices or binding of the enzymes to a surface, which leads to an increased enzyme stability [209]. In that respect, Santoro et al. [191] investigated the performance of an immobilized bilirubin oxidase air-breathing cathode at a constant potential of 300 mV vs. Ag/AgCl over a time period of 45 days. Despite the enzyme immobilization, they observed a severe and rapid decrease of the current density. In detail, the current density dropped from initial 350 µA cm^{-2} to only 175 µA cm^{-2} after already 3 days, to 100 µA cm^{-2} after 9 days. After 45 days a final current density of only 48 µA cm^{-2} was obtained.

Rubenwolf et al. [114] presented for the first time the novel concept that the cathode lifetime can be decoupled from the enzyme lifetime by regular re-supply of fresh enzymes. In detail, they demonstrated a cathode lifetime of 19 days at a constant current density of 110 µA cm^{-2} by periodic re-supply of fresh laccase to the electrode. This approach was further developed by Sané et al. [115] who supplied crude supernatant of *T. versicolor* without purification to an immersed cathode and obtained a remarkable cathode lifetime of 120 days, operated at a constant current density of 50 µA cm^{-2}. This result definitely exceeds the lifetime of 33 days obtained in chapter 5 with the novel concept of the air-breathing laccase cathode and the continuous supply system for the laccase-containing supernatant. Nevertheless, technical problems such as irreversible clogging and fouling of the supply tubes were the reasons to the stop this long-term experiment. Thus, theoretically a longer lifetime of this novel air-breathing laccase cathode is feasible if the observed technical issues can be solved, which is clearly a topic that needs to be addressed in future research.

In the long-term experiment a small but progressing decrease of the cathode potential over time was visible which points towards a gradual loss of the electrocatalytic enzyme activity. This can be due to the accumulation of inhibitory by-products secreted during the cultivation of *T. versicolor,* which might lead to poisoning of the electrode. Interestingly, this behavior was also observed in the work of Rubenwolf et al. [114] who used purified laccase in citrate buffer, but not in the study of Sané et al. [115] who also applied crude supernatant of *T. versicolor*. Thus, further research is necessary to investigate the impact of this effect and to identify whether it is caused by the secretion of inhibitory by-products by *T. versicolor.* The latter could be addressed by optimization of the culture conditions (e.g. temperature, shaking speed, etc.) or by changing the media composition.

In chapter 5 also the electrochemical characterization of the air-breathing laccase cathode by galvanostatic polarization was shown. Therein, a maximum limiting current density of 86 ± 8 µA cm^{-2} at 0.4 V vs. SCE could be achieved with continuous supply of the laccase-containing supernatant of *T. versicolor* at a HRT of 2.4 h. The comparison with literature data showed that Gupta et al. [210] even reached up to 350 µA cm^{-2} at 0.5 V vs. Ag/AgCl using an immobilized bilirubin oxidase in a gas-diffusion cathode. Also Ciniciato et al. [199] obtained a high limiting current density in the same range of ~300 µA cm^{-2} at 0.25 V vs. Ag/AgCl with an air-breathing paper based bilirubin oxidase cathode. Thus, evidently the in chapter 5 achieved limiting current density of 86 µA cm^{-2} at 0.4 V vs. SCE with the novel concept of an air-breathing laccase cathode is still lower than literature values. Remarkably, also Sané et al. [115] obtained higher limiting current densities (129 µA cm^{-2} at 0.4 V vs. SCE) with laccase-containing crude supernatant of *T. versicolor*, although in their work an

immersed cathode was used, which theoretically leads to lower current densities than an air-breathing cathode due to the limited oxygen solubility in aqueous solutions and the related mass transfer limitations [190, 199]. Consequently, there is still plenty of room for further improvements, including the optimization of the electrode thickness and the size of the cavity, and associated the internal resistance of the cathode, as well as the oxygen transfer rate through the gas diffusion membrane and the enzyme supply rates.

This novel concept presented in chapter 5 combines the advantages of an air-breathing cathode design with the continuous supply of unpurified laccase-containing supernatant of *T. versicolor* for an extended cathode lifetime. Nevertheless, the ecological sustainability of a system which uses a continuous flow-through system and requires constant supply of fresh enzymes needs to be considered. But in this regard, the fungus *T. versicolor* offers the possibility to produce laccase by growing on abundant resources such as by-products from the pulp and paper industry [201], which makes this approach economical and sustainable.

Overall of this PhD thesis regarding the anode of a microbial fuel cell, systematic anode material screenings were presented in chapter 2-4 with the fuel cell model organisms *S. oneidensis* and *G. sulfurreducens.* These systematic investigations of different carbon- and metal-based anode materials suggest that the anode materials need to be chosen according to the employed electroactive microorganism. This result is particularly important for applications using pure cultures of *S. oneidensis* such as in unbalanced fermentation [205, 206], since it could be shown that a high surface area anode material significantly increases the current density obtained with *S. oneidensis.* This was related to the high surface area of the anode material which is presumably available for the self-secreted flavins that act as electron shuttles in the mediated electron transfer of *S. oneidensis*. From a scientific point of view, however, there is still a need for a better understanding of the detailed electron transfer mechanisms, especially with regard to the role of flavins, which according to recent literature mainly act as cytochrome-bound co-factors that enhance the direct electron transfer rate, and not as free electron shuttles [208]. Only when the complex electron transfer mechanisms of the electroactive microorganisms are completely elucidated, a reliable conclusion regarding the microbe-electrode interaction is possible.

In contrast to *S. oneidensis*, it was demonstrated that *G. sulfurreducens* can achieve high current densities with completely different anode materials without any recognizable influence of the specific surface area. This result allows concentrating on material properties that are important for scale-up in practical fuel cell applications, e.g. electrical conductivity, durability, material costs, long-term stability, etc. In that regard, studies have demonstrated

that the influence of additional surface modifications of anode materials diminishes over time due to biofilm formation on the electrode surface [71, 211]. Moreover, it was shown that advantageous 3-dimensional porous anode structures are prone to biofilm clogging during long-term operation, which leads to mass transfer limitations, and eventually to anode performances comparable to flat, 2-dimensional anodes [83, 93]. This result favors the use of cost-efficient 2-dimensional anode materials, especially with respect to practical long-term applications in scaled-up microbial fuel cells. Furthermore, it underlines the importance of the high current densities achieved with *G. sulfurreducens* in chapter 4 using the planar anode materials graphite foil, graphite felt, activated carbon cloth, and untreated stainless steel.

In this thesis only pure cultures of the anode model organisms *S. oneidensis* and *G. sulfurreducens* were used in order to investigate the individual microbe-electrode interactions of the respective microorganisms. However, the next step towards practical application, e.g. treatment of wastewater which is typically comprised of many types of bacteria, is the application of a mixed microbial consortium at the anode. Interestingly, in that context a previous study has shown that the anodic bacterial communities fed with winery or domestic wastewater are dominated by *Geobacter* species [38]. The question therefore arises whether the results obtained in this thesis with *G. sulfurreducens* may be transferable to a mixed microbial community in which *Geobacter* is the dominating species. To answer this question, a fundamental study which investigates the interaction of a biofilm derived from a mixed microbial consortium and the electrode is required.

With respect to the application of mixed microbial communities at the anode, a promising approach may be the co-cultivation of *S. oneidensis* and *G. sulfurreducens.* In this case, the usually unwanted oxygen intrusion into the anode compartment, e.g. by an air-breathing cathode or by excluding a separator membrane, can be of advantage by using the facultative anaerobic microorganism *S. oneidensis*. As shown in this thesis, oxygen can promote the current generation of *S. oneidensis* presumably due to the formation of thicker biofilms and associated a higher number of electroactive cells. By using *S. oneidensis* in a co-cultivation with the oxygen-sensitive, high-performance strain *G. sulfurreducens*, *S. oneidensis* could metabolize the intruding oxygen and thereby shielding the anaerobic biofilm of *G. sulfurreducens*. In addition, at the anode surface inside the biofilm where anoxic conditions prevail, *S. oneidensis* metabolizes lactate only to acetate, which is in turn the preferred substrate of *G. sulfurreducens.* However, this synergistic effect still needs to be validated in practical applications. With this approach, the advantages of a co-cultivation of

these two electroactive microorganisms as well as the microbe-electrode interactions in the environment of a mixed consortium could be investigated.

Overall of this PhD thesis regarding the enzymatic cathode for microbial fuel cells, it can be concluded that the novel concept of an air-breathing cathode developed in this thesis could be successfully combined with the enzyme re-supply for an extended cathode lifetime. That approach of a self-regenerating cathode by periodic enzyme renewal to extend the electrode lifetime decoupled from the enzyme lifetime was previously demonstrated by Rubenwolf et al. [114] and Sané et al. [115]. In this thesis, a new and innovative concept of an air-breathing cathode design is demonstrated which on the one hand obviates the need for energy-intensive aeration, and on the other hand allows for higher current densities than in immersed cathodes, because the problem of limited oxygen solubility in aqueous solution can be overcome. Moreover, a continuous supply system for the enzyme-containing supernatant of *T. versicolor* was developed and integrated into the air-breathing cathode concept. This enables a constant supply rate of fresh enzymes and simultaneously a constant removal of desorbed enzymes, which leads to fewer fluctuations of the cathode potential compared to the periodic enzyme re-supply that was previously shown by [114, 115]. In addition, the continuous enzyme supply allows for a self-sufficient fuel cell operation, e.g. in remote areas, which is in contrast to the manual and labor-intensive periodic enzyme re-supply that is not suitable for practical application. Another positive aspect of a continuous enzyme supply system is related to the reported increase of the pH value at the cathode side leading to fuel cell performance loses [60]. By adjusting an appropriate flow-rate of the continuous supply system, it may be possible to maintain a stable pH value to prevent pH shifts which on the one hand can negatively affect the laccase activity [212], and on the other hand decrease the cathode potential. All in all, this novel application-oriented concept of an air-breathing laccase cathode combined with a continuous enzyme supply system for extended lifetime describes one more step towards practical application.

However, it is also evident that there is still a great need to further extend the lifetime of the enzymatic cathode. Only when the lifetime of the microbial anode and the enzymatic cathode are both in a comparable range, the construction of a hybrid microbial-enzymatic fuel cell becomes relevant for practical applications. For the microbial anode an operation time of up to several years has already been reported in literature [123], but the demonstration of this time span for an enzymatic cathode is still pending. Therefore, further research is needed to solve the technical issues observed in this thesis in order to realize an enzymatic cathode lifetime in the range of months or years.

6.2 Outlook

In order to carry out the next steps towards practical application of microbial fuel cells further research topics require in-depth investigation. These topics are listed below, divided into separate sections for the anode and the cathode electrode.

At the anode a detailed investigation of the underlying electron transfer mechanisms of the electroactive strains *S. oneidensis* and *G. sulfurreducens* is necessary in order to explain the different microbe-electrode interactions observed in this PhD thesis. Therein, a significant difference in the achieved current densities of the two model organisms with high and low specific surface area anode materials was visible, which was related to the different electron transfer mechanisms (mediated and direct electron transfer) which are associated with the two microorganisms. Recent literature results, however, suggest different and partly contradictory electron transfer mechanisms for *G. sulfurreducens* and *S. oneidensis,* especially with regard to the role of flavins in mediated and direct electron transfer [52, 208]. Hence it is of major importance for future research to clarify the underlying electron transfer mechanisms for both electroactive strains. In particular, the role of the self-secreted flavins, either as free electron shuttles in the mediated electron transfer or as cytochrome-bound co-factors, must be investigated in detail under both anoxic and aerated conditions. In that regard, also the effect of media components which might act as electron shuttles needs to be taken into account. Furthermore, the influence of the applied anode potential on the electron transfer mechanisms and the biofilm formation of the respective microorganisms should be examined. In addition, the influence of metal oxide layers of e.g. stainless steel on the electron transfer could not be conclusively clarified in this thesis and requires further fundamental research.

The next step towards practical application is the use of real wastewater comprising a large variety of electroactive and non-electroactive bacteria, and related the application of a mixed microbial consortium at the anode. In that regard, it is of high importance to figure out how the investigated anode materials will perform with a mixed consortium instead of pure cultures of microbial fuel cell model organisms as it was investigated in this thesis. Interestingly, Torres et al. [40] demonstrated that the composition of the anodic microbial community depends severely on the applied anode potential and can thus vary significantly in their content of *Geobacter* species. In this context, it is important to investigate which anode potential has to be applied to maximize the anodic current densities. However, it has to be considered that the anode potential must be within an application-relevant range which enables the operation of a complete fuel cell together with a cathode electrode.

Moreover, it is of great interest to find out whether an anodic bacterial community dominated by *Geobacter* species will deliver similar results to those obtained in this thesis with a pure culture of *G. sulfurreducens*. Therefore, a thorough investigation of the microbe-electrode interaction in the environment of a mixed consortium is required which is relevant for practical applications of e.g. wastewater treatment.

Further challenges will arise when transferring the results obtained in this thesis with pure cultures that were operated in synthetic medium with easily degradable carbon compounds to a real wastewater environment. These include, for example, the much lower solution conductivity and buffer capacity of wastewater which contribute significantly to the internal resistance und thus considerably reduce the power output of a microbial fuel cell [35]. This needs to be considered in future reactor designs, e.g. minimized electrode spacing in a 1-compartmet fuel cell flat-plate design, and in the reactor operation, which typically involves a continuous flow through the anode as it is usual in wastewater treatment. Moreover, it should be noted that wastewater is usually operated at significantly lower temperatures compared to laboratory conditions, and additionally contains complex long-chained organics substances which first need to be converted by the anodic bacteria into smaller organic compounds, which can further decrease the energy output in microbial fuel cells.

Another step towards practical application comprises not only the investigation of the anode electrodes in a half-cell configuration, but also in a complete microbial fuel cell together with a cathode electrode, e.g. an abiotic or enzymatic cathode, and if required, a separating membrane. This is needed in order to study maximum power densities, the influence of substrate and oxygen cross-over as well as the occurrence of pH shifts on the microbial fuel cell performance. In addition, research on the long-term stability of the promising 2-dimensional anode materials proposed in this thesis is necessary for future applications of microbial fuel cells that can be operated self-sufficiently over months and years.

With regard to the enzymatic cathode, further research is required to improve the long-term performance of the novel concept of an air-breathing laccase cathode with continuous enzyme supply presented in this thesis. The demonstrated lifetime of up to 33 days needs to be further extended for practical application, e.g. in a hybrid microbial-enzymatic fuel cell with possible operation times of up to several years. As biofouling and clogging of the supply tubes occurred regularly by using the unpurified supernatant of *T. versicolor*, a robust supply setting with appropriate peripherals needs to be set up in the future. In addition, the cultivation of *T. versicolor* has to be optimized to reduce the secretion of inhibitory and

clogging by-products and to maximize the laccase yield. This can involve changing the cultivation conditions such as the cultivation period and temperature, or the media composition. In order to increase the current density of the air-breathing laccase cathode, the optimization of the electrode thickness, the enzyme supply rates and thus the hydraulic retention times as well as the size of the enzyme cavity is crucial. Moreover, other aspects such as the influence of the enzyme supply rate on the cathodic pH value, and the maximum amount of oxygen that can intrude into the anode chamber without inhibiting the anodic microorganisms require further and fundamental research.

All in all, anode and cathode electrodes are still parts of a whole system and it is important to note that finally the electrochemical reactions at both electrodes need to occur at same rate. Therefore, the anode and cathode need eventually to be evaluated in a complete fuel cell to characterize the interactions of all components and to discover the remaining performance limitations.

Glossary

This glossary was not solely created by the author of this thesis. In fact, it builds on definitions given by previous PhD students of the bioelectrochemical systems group of Prof. Sven Kerzenmacher and by the glossary used within this research group, and as well on definitions commonly used in literature.

Activation loss	Refers to the polarization of an electrode that occurs at low current densities and is related to the kinetics of the redox reactions. It is due to an energy barrier that needs to be overcome to transfer electrons from the fuel to the electrode or from the electrode to the oxidant (see chapter 1.1.4 in this work).
Active site	The part of an enzyme that interacts with the substrate.
Adsorption	Adhesion of molecules such as gas, liquid, or dissolved solids (e.g. enzymes) to a surface (e.g. an electrode).
Aerobic bacteria	Bacteria which utilize oxygen for growth and oxygen-based metabolism.
Anaerobic bacteria	Bacteria that are capable of living in the absence of molecular oxygen.
Anode	The electrode in an electrochemical cell at which the oxidation of the fuel occurs. Its potential is more negative than that of the cathode in a fuel cell.
Anolyte	The electrolyte at the anode compartment of an electrochemical cell (see catholyte).
Anoxic	For example an environment or condition that lacks oxygen.
Batch process	A bioprocess in which the bioreactor is filled with medium and inoculum without the addition of medium and nutrients until the bacterial growth is finished.
(Bio)catalyst	A (biological) substance that increases the rate of a chemical reaction by providing an alternative reaction pathway of lower activation energy. Examples for catalysts are platinum and enzymes.
Biofilm	A group of microorganisms in which the cells aggregate and stick to each other and to a surface. The cells are typically embedded in an extracellular

	matrix that is composed of extracellular polymeric substances such as polysaccharides.
Biofouling	The accumulation of microorganisms, plants, algae, or animals on wetted surfaces.
Buckypaper electrodes	Porous, self-entangled mat of carbon nanotubes that is used as an electrode. It is fabricated by filtering a suspension of carbon nanotubes through a filter membrane that also acts as a mechanical support.
Catalytic activity	A measure for the ability of a catalyst to catalyze a chemical reaction, expressed in mol/s. In case of enzymes often measured using a redox indicator (see also U).
Cathode	The electrode in an electrochemical cell at which the reduction occurs. It is the positive electrode in a fuel cell (see also anode).
Catholyte	The electrolyte at the cathode compartment of fuel cell (see also anolyte).
Cell voltage	The electrical potential difference between the anode and cathode of an electrochemical cell.
Cellular respiration	A series of metabolic processes that take place within a cell in which biochemical energy is harvested from organic substance (e.g. glucose) and stored as energy carriers (ATP) for use in energy-requiring activities of the cell.
Cofactor	A non-protein chemical compound that is required for an enzyme's activity.
Concentration loss	Refers to the considerable polarization of an electrode usually observed at high current densities. It occurs mainly due to a concentration gradient of reagents and products in the proximity of the electrode, caused by mass transport limitations (e.g.limited diffusion within the porous electrode) (see chapter 1.1.4 in this work).
Consortium	A microbial consortium consists of two or more microorganisms that live symbiotically.
Coulombic efficiency	It describes the fraction of electrons recovered as current versus the electrons available in the organic substrate which is oxidized by the bacteria in a microbial fuel cell.
Counter electrode	The counter electrode is used to set a potential or maintain a current at the working electrode. Working electrode, counter electrode and electrolyte form a closed electrochemical circuit. In this work, the counter electrode consists of a platinum mesh.

Crude culture supernatant	Cell free filtrate of a liquid culture.
Cytochromes	Proteins that contain heme-groups. They work as electron donors as well as electron acceptors since the central Fe atom allows for a reversible change of Fe2+ to Fe3+.
Diffusion	The net movement of molecules from a region of high concentration to a region of low concentration as a result of random motion of the molecules.
Double layer capacitance	Storing of electric charge at the interface between a conductive electrode and an adjacent liquid electrolyte.
Electroactive bacteria	Bacteria that are able to perform extracellular electron transfer to an electrode.
Electro-catalyst	Catalyst that takes part in electrochemical reactions.
Electrochemical cell	Consists typically of an anode, a cathode, in contact with an electrolyte. Sometimes an ion-conductive separator is used between anode and cathode.
Electrode	The electrically conductive part of an electrochemical cell. The electrochemical reactions take place at the interface between the electrode and the electrolyte (see also anode and cathode).
Electrode potential	Electrical potential of a half-reaction (oxidation/reduction) with respect to a reference electrode.
Electrolyte	Typically a liquid that contains mobile ions (usually salts, acids or bases).
Enzymatic fuel cell	An electrochemical device that converts chemical energy into electrical energy with the use of enzymes as catalysts.
Enzyme	Biological catalyst, converts substrates into products, e.g. oxygen into water at the cathode.
Enzyme activity	Moles of substrate converted per unit time, generally expressed in enzyme units (U = µmol/min).
Enzyme activity	Moles of substrate converted per unit time, generally expressed in enzyme units (U = µmol/min).
Enzyme denaturation	Process of partial or total alteration of the native secondary, and/or tertiary, and/or quaternary structures of an enzyme resulting in a loss of the catalytic activity.
Enzyme purification	Isolation of a protein from a complex mixture, such as whole organisms or culture supernatants.

Flavin	A derivative of riboflavin (vitamin B2) which is able to undergo oxidation-reduction reactions. It is secreted as an electron shuttle by *S. oneidensis*.
Fuel cell	An electrochemical device that converts chemical energy directly into electricity and can theoretically operate as long as fuel and oxidant are supplied to its electrodes.
Galvanostatic control	The current flow between the electrodes is controlled, whereas the potential difference is monitored.
Gram-negative	Gram-negative bacteria do not retain a crystal violet stain used in the gram-staining method. They are characterized by a thin peptidoglycan cell wall sandwiched between an inner cell membrane and a bacterial outer membrane.
Half-cell set up	Electrochemical experiment where the potential or current of either anode or cathode is of interest. The potential of the electrode of interest is set in reference to or measured with the help of a reference electrode. A counter electrode is used to close the circuit.
Hungate tube	Culture tube for growing and maintaining anaerobic bacteria and culture conditions.
Hydraulic retention time (HRT)	A measure of the average time that a soluble compound remains in a bioreactor. It can be calculated by dividing the volume of the bioreactor by the flow rate.
Initial growth phase	First phase of bacterial growth in which the bacteria adapt themselves to the growth conditions. It is defined in this thesis as 1 week at 4.4 µA cm^{-2} using galvanostatic control for the two organisms *S. oneidensis* and *G. sulfurreducens.*
Inoculation	The introduction of a microorganism into a culture medium.
Inoculum	The microorganisms used in an inoculation to start a culture.
Laccase	An enzyme secreted by several plants and microorganisms, especially white-rot fungi, able to reduce oxygen at the cathode.
Limiting current density	Current d density at which the anode potential rises steeply to a potential where water electrolysis occurs [17].
Macroporous material	Material which contains pores in the size of 50 nm – 1 µm.
Mass transport	Transport (usually by diffusion and/or convection) of fuel and oxidant to the reaction sites in the electrode and transport of products away from the electrode.

Mediator	Redox active molecule that can be oxidized and reduced and thus is able to transfer electrons between bio-catalyst and electrode. Sometimes also called “electron shuttle” or “redox shuttle”.
Metabolism	All chemical reactions of living cells and that sustain life. The reactions are catalyzed by enzymes. Metabolism can be divided in catabolism, which is the breakdown of molecules to obtain energy, and anabolism, in which all compounds needed by cells are synthesized.
Microbial fuel cell	An electrochemical device that converts chemical energy into electrical energy with the use of microorganisms as catalysts.
Microorganism	A microscopic unicellular or multicellular organism.
Model organism	A non-human species that is extensively studied to understand biological phenomena with the expectation that this will provide insight into the workings of other organisms.
Nanoporous material	Material which consists of a regular, porous structure with pores of 100 nm or smaller.
Nanowires	Electrically conductive appendages found on the surface of many bacteria most notably from Geobacter and Shewanella species.
Ohmic loss	Refers to the polarization of an electrode affected by the rate of electron transfer through the electrodes and by the ion transfer through the electrolyte. It shows linear behavior and is determined by the resistivity of the different conductors (electrode, current collectors, electrolyte and eventually membranes) and by the configuration of the fuel cell (see chapter 1.1.4 in this work).
Optical density	Measure of the transmittance of an optical medium for a given wavelength. It is a common method for estimating the concentration of bacterial or other cells in a liquid.
Overpotential	Potential difference between a thermodynamically determined reduction potential and the potential at which the redox reaction is experimentally observed caused by activation, ohmic, and concentration losses.
Oxidant	A substance that accepts electrons from another substance and is being reduced during the reaction.
Oxidase	Enzymes able to oxidize substrates.
Oxidation	The loss of electron(s) by a chemical species such as a molecule, atom or ion.
Pilus	A hair-like appendage found on the surface of many bacteria (plural: pili).

Planktonic cells	Microorganisms in a solution that do not colonize a surface or form large aggregates.
Polarization	The change of potential of an electrode from its open circuit potential due to current flowing.
Polarization curve	A plot that shows the dependency of potential and current or current density of an electrochemical cell (also called load-curve).
Potentiostatic control	The potential difference between the electrodes is controlled, whereas the current flow is monitored.
Protein expression	Protein production by an organism by transcribing information of DNA genes to mRNA which is then translated into a protein.
Quasi-steady-state	A system or process that is changing slowly enough that it can be considered to be constant (steady-state).
Redox reaction	Chemical reaction involving electron transfer between chemical species.
Reduction	The gain of electron(s) by a chemical species such as a molecule, atom or ion.
Reference electrode	An electrode with a well-known and stable electrode potential that serves as a reference point.
Renewable resource	An organic natural resource that can replenish either through biological reproduction or other naturally reoccurring processes, in a sufficient time compared to its usage.
Secondary biofilm	The progeny of cells which initially colonize a surface and build the primary biofilm cells.
Sessile cells	Bacterial cells which colonize a surface, in contrast to planktonic cells.
Specific surface area	Total surface area of a material per unit of mass.
Steady-state	Describes a system or process in which the variables which define the behavior of the system or the process are unchanging over time.
Substrate	Organic compounds such as acetate or lactate, that are oxidized by bacteria for their metabolism.
Volumetric current density	Current density normalized to the volume of the electrode, e.g. the anode.
Water electrolysis	It describes the decomposition of water into oxygen and hydrogen due to an electric current which passes through the water.

Working electrode	The electrode in an electrochemical system at which the reaction of interest takes place.

Abbreviations

A	Ampere (unit of the electrical current)
ABTS	2,2'-azino-bis(3-ethylbenzothiazoline-6-sulphonic acid) (chemical compound used as redox indicator)
ACC	Activated carbon cloth
Ag/AgCl	Silver/ silver chloride electrode (reference electrode)
ATP	Adenosine tri-phosphate
BET	Brunauer-Emmett-Teller (theory explaining the adsorption of gas molecules on solid surfaces, can be applied for surface area determination of porous solids)
CNTs	Carbon nanotubes
CoTMPP	Cobalt tetramethylphenylporphyrin
CueO	Copper efflux oxidase (enzyme)
DET	Direct electron transfer
FePc	Iron(II) phthalocyanine
G. sulfurreducens	*Geobacter sulfurreducens* (bacterial strain)
GDL	Gas diffusion layer
HRT	Hydraulic retention time
LB medium	Lysogeny broth medium (nutritionally rich medium, primarily used for the growth of bacteria)
MFC	Microbial fuel cell
MnO_x	Manganese oxides
MPP	Maximum Power Point
MtrC	Metal reducing protein C
MWCNTs	Multi-walled carbon nanotubes
NADH	Nicotinamide adenine dinucleotide (reduced form)
NHE	Normal hydrogen electrode (reference electrode)

OCP	Open circuit potential
OD_{600}	Optical density measured at a wavelength of 600 nm
OmcA	Outer membrane cytochrome A
OmcZ	Outer membrane cytochrome Z
ORR	Oxygen reduction reaction
PBS	Phosphate buffered saline
PDMS	Polydimethylsiloxane
PEM	Proton exchange membrane
PTFE	Polytetrafluoroethylene
R_a	Arithmetic surface roughness (describes the arithmetic average of the absolute values of height deviations from the mean line)
R_U	Uncompensated resistance
RVC	Reticulated vitreous carbon
S. oneidensis	*Shewanella oneidensis* (bacterial strain)
SCE	Saturated calomel electrode (reference electrode, +244 mV vs. SHE)
SCL medium	Synthetic complete laccase medium
SEM	Scanning electron microscope
SHE	Standard hydrogen electrode (reference electrode)
T. versicolor	*Trametes versicolor* (white-rot fungus)
U	Unit (a measure for enzyme activity)
V	Volt (unit for the electrical potential and potential difference)
wt/vol	weight/volume
YPD medium	Yeast peptone dextrose medium

Physical measures

Latin letters

A	Geometric area in cm^2
C	Capacitance in F
c	Concentration in mol l^{-1} or g l^{-1}
D	Diffusion coefficient in m^2 s^{-1}
E^0	Electrode potential at standard conditions in V
I	Current in A
j	Current density in µA cm^{-2}
	or Diffusion flux in mol m^{-2} s^{-1}
m	Mass in g
p	Pressure in Pa
pH	Negative decadic logarithm of H^+ concentration in mol l^{-1}
R	Electrical resistance in Ω
T	Temperature in K or °C
t	Time in s
U	Voltage in V
V	Volume in l

Greek letters

η_{ohm}	Ohmic potential loss in V
σ	Electrical conductivity in S m^{-1}

Physical constants

F	Faraday constant: 96485 C mol^{-1}
g	Earth-surface gravitational acceleration: 9.807 m s^{-2}

mol	Amount of substance: $6.022 \cdot 10^{23}$ mol^{-1}
p_0	Sea level standard atmospheric pressure: 101325 Pa
R	Gas constant: 8.314 J mol^{-1} K^{-1}

Appendix

A2 Appendix to Chapter 2

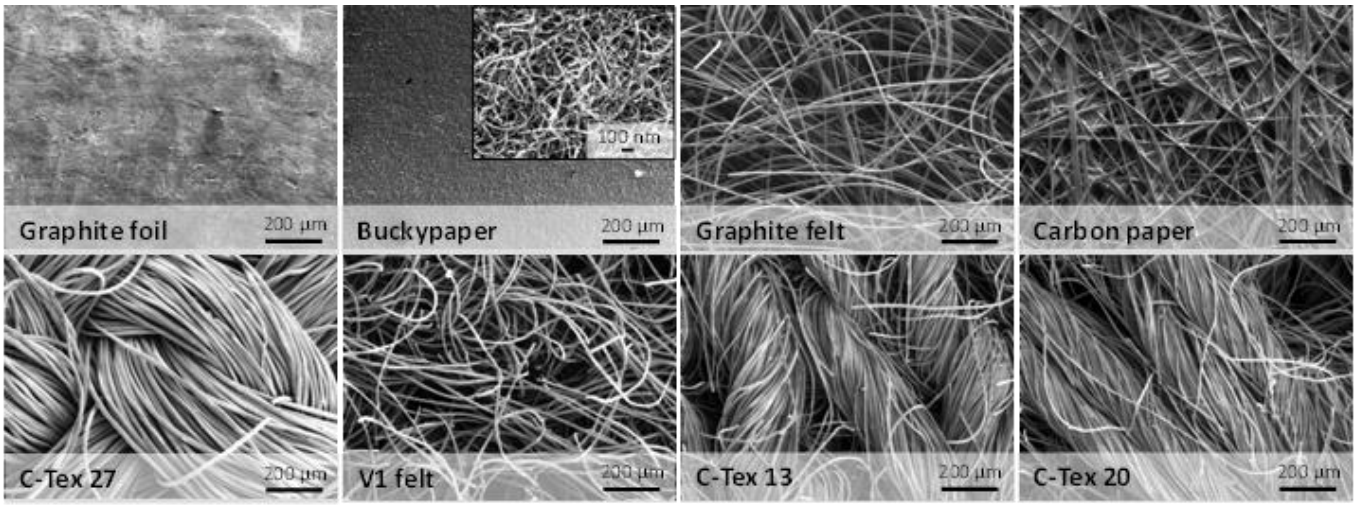

Figure A2.1: SEM images of the tested anode materials. Upper row from left to right: Graphite foil, Buckypaper in two magnifications, Graphite felt and Carbon paper. Lower row from left to right, the activated carbon cloth materials: C-Tex 27, V1felt, C-Tex 13 and C-Tex 20.

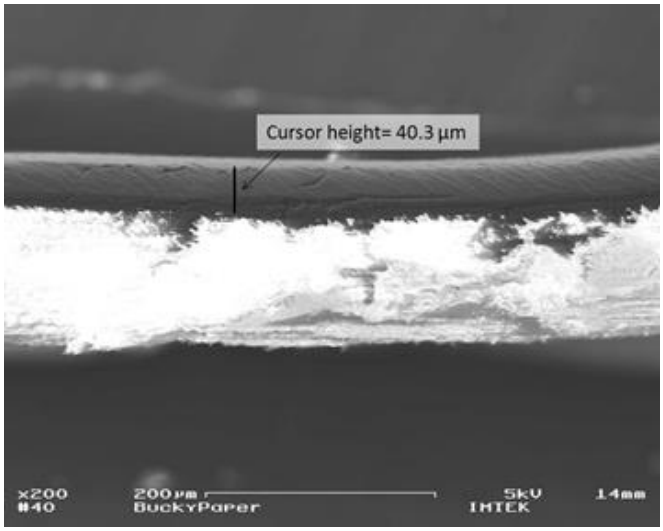

Figure A2.2: Cross-section of buckypaper in order to determine the thickness of the multi-walled carbon nanotube film.

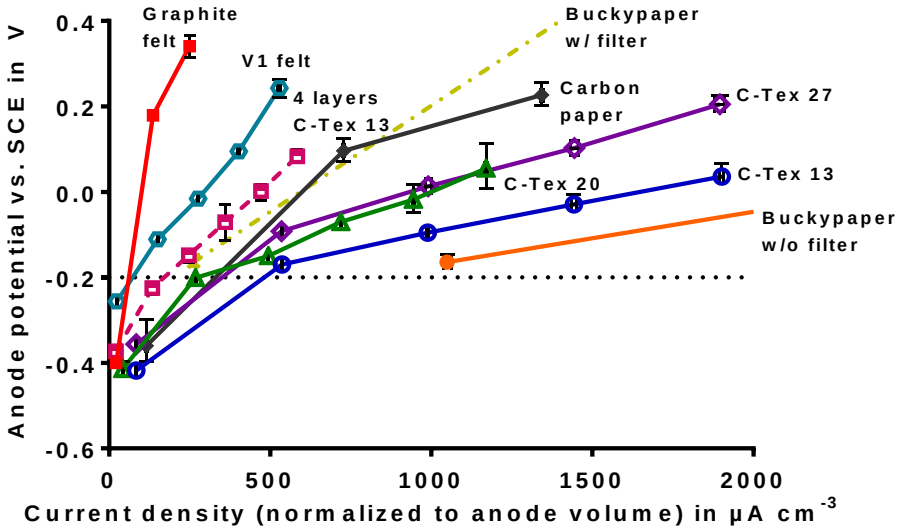

Figure A2.3: Anode polarization curves recorded with *S. oneidensis*. Current densities are normalized to the anode volume. Anode materials tested are: Buckypaper with supporting filter, Buckypaper without supporting filter, Carbon paper, Graphite felt, and the activated carbon materials: C-Tex 27, V1 felt, C-Tex 13, 4-layer composite of C-Tex 13 and C-Tex 20. Each data point depicts the mean value of 3 measurements; bars indicate the minimum and maximum values of the triplicates.

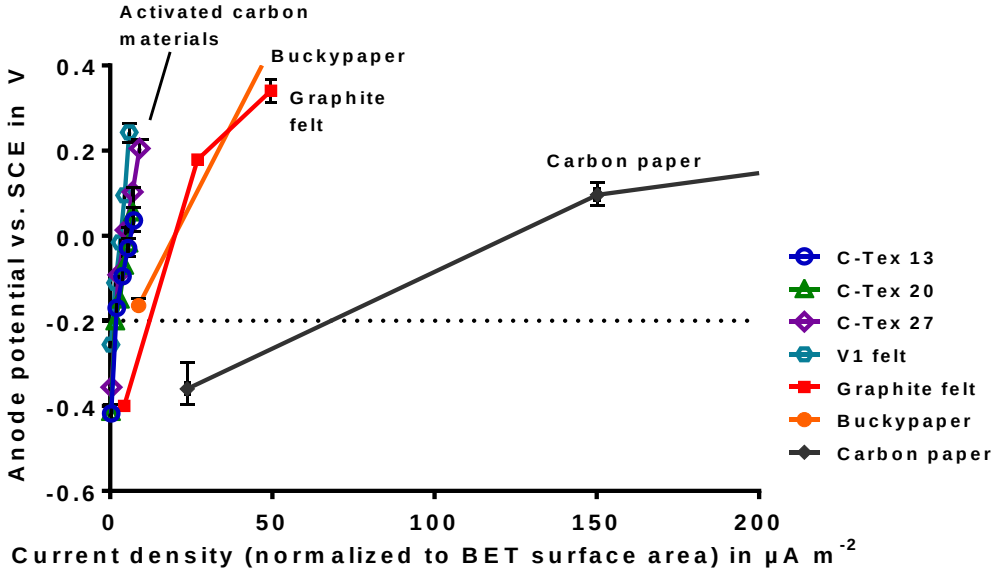

Figure A2.4: Anode polarization curves recorded with *S. oneidensis*. Current densities are normalized to the specific surface area of the anode materials, determined with the multiple-point nitrogen adsorption BET-method. Anode materials tested are: Buckypaper, Carbon paper, Graphite felt, and the activated carbon materials C-Tex 27, V1-Felt, C-Tex 13, and C-Tex 20. Each data point depicts the mean value of 3 measurements; bars indicate the minimum and maximum values of the triplicates.

A2.1 Procedure for the fabrication of buckypaper

Buckypaper consists of a thin film of multi-walled carbon nanotubes (MWCNTs) filtrated onto a filter membrane. This procedure is based on the publication of Hussein et al. (2011) [136]. In the first step, 550 mg MWCNTs (Baytubes C150 HP, Bayer Material Science AG, Germany) are dispersed in 1.1 L of a 1% aqueous solution of the surfactant Triton X-100 (11 g) (Carl Roth, Karlsruhe, Germany). Then the solution is stirred on a magnetic stirrer (15 min, 200-300 rpm) and afterwards agitated in the ultrasonic bath for 3 hours. Subsequently, the solution is centrifuged at 2000 g for 15 min to remove the agglomerates of MWCNTs, and the supernatant containing dispersed MWCNTs (without agglomerates) is filled into a glass column reservoir. In the next step, 135 mL of this MWCNT solution are vacuum-filtered through a nylon filter membrane with a pore size of 0.45 µm (Whatman, Maidstone, UK) using a glass vacuum filter holder (Sartorius AG, Göttingen, Germany). During this step a uniform MWCNT film forms on the filter membrane, from which excess Triton is removed by several washing steps as listed in the following:

- The coated membrane is washed with deionized water, isopropanol, and acetone (in this order).
- Each membrane is stored in 50 mL isopropanol for 2 h.
- Then the membranes are washed again as described in step 1.
- Each membrane is stored in 100 mL isopropanol overnight.
- Then the membranes are washed again as described in step 1.
- Each membrane is stored in 100 mL deionized water for 2 h.
- Then the membranes are washed again as described in step 1.
- Each membrane is stored in 100 mL acetone overnight.
- Then the membranes are washed again as described in step 1.
- Each membrane is stored in 100 mL isopropanol for 2h.
- At last the membranes are washed as described in step 1 and additionally with deionized water.

In order to keep the buckypaper film flat, each membrane is put carefully (after 5 minutes of drying) between two weighing pans (2150.1, Carl Roth, Karlsruhe, Germany) and is then dried in the oven at 70°C overnight. In the end, a stable MWCNT film without agglomerates should have formed on the nylon filter membrane. After weighing the filter

membrane before and after the filtration process, one should have obtained a MWCNT loading of 15 ± 2 mg per filter membrane.

A3 Appendix to Chapter 3

Redox potential of sulfate reduction

Reaction:	$SO_4^{2-} + 9H^+ + 8e^-$	→	$HS^- + 4H_2O$	(A3.1)

To calculate the *standard free energy* of the overall reaction ΔG_r^{0} only the net amount of protons (in this case 1) is considered, yielding:

$\Delta G_r^{0'}$ = (12.05 + 4*(-237.178)) kJ mol^{-1} – (-744.63 + 1*(-39.87)) kJ mol^{-1}

= -152.2 kJ mol^{-1}

$$\Delta E_r^{0'} = -\frac{\Delta G_r^{0'}}{nF} = \frac{152.2 \text{ kJ mol}^{-1}}{8 \cdot 96485 \text{ C mol}^{-1}} = 197 \text{ mV vs. SHE} = \textbf{-47 mV vs. SCE}$$

Energy gain per electron in the case of lactate oxidation by *S. oneidensis*

Lactate oxidation by *S. oneidensis* at an anode (sulfate as „virtual“ electron acceptor mimicking the anode potential, see above):

Oxidation:	$C_3H_5O_3^- + 2H_2O$	→	$C_2H_3O_2^- + HCO_3^- + 5H^+ + 4e^-$	(A3.2)
Reduction:	$SO_4^{2-} + 9H^+ + 8e^-$	→	$HS^- + 4H_2O$	(A3.3)
Overall:	$2C_3H_5O_3^- + SO_4^{2-}$	→	$2C_2H_3O_2^- + 2HCO_3^- + 1H^+ + HS^-$	(A3.4)

The *standard free energy* of the overall reaction ΔG_r^{0} is then calculated from the tabulated *standard free energy of formation* ΔG_f^{0} using the relation from Thauer et al. 1977 [161]:

$$\Delta G_r^{0} = \Sigma \Delta G_f^{0} \text{ (Products)} - \Sigma \Delta G_f^{0} \text{ (Educts)} \quad \text{(A3.5)}$$

For the overall reaction

$2C_3H_5O_3^- + SO_4^{2-}$ → $2C_2H_3O_2^- + 2HCO_3^- + 1H^+ + HS^-$

the *standard free en*ergy $\Delta G_r^{0'}$ (pH=7, T= 25 °C) calculates to

$\Delta G_r^{0'}$ = (2*(-369.41)+2*(-586.85) + (-39.87)+12.05)kJ mol^{-1} - (2*(-517.81)+(-744.63))kJ mol^{-1}

= -160.09 kJ mol^{-1}

➔ **- 20.0 kJ/mol electrons**

Energy gain per electron in the case of acetate oxidation by *G. sulfurreducens*

Analogous to the calculation above:

Oxidation:	$C_2H_3O_2^- + 4H_2O$	→	$2HCO_3^- + 9H^+ + 8e^-$	(A3.6)
Reduction:	$SO_4^{2-} + 9H^+ + 8e^-$	→	$HS^- + 4H_2O$	(A3.7)
Overall:	$C_2H_3O_2^- + SO_4^{2-}$	→	$2HCO_3^- + HS^-$	(A3.8)

$\Delta G_r^{0\prime}$ = (2*(-586.85) + 12.05) kJ mol^{-1} – (-369.41 + (-744.63)) kJ mol^{-1}
= -47.61 kJ mol^{-1}

➔ **-6.0 kJ/mol electrons**

A4 Appendix to Chapter 4

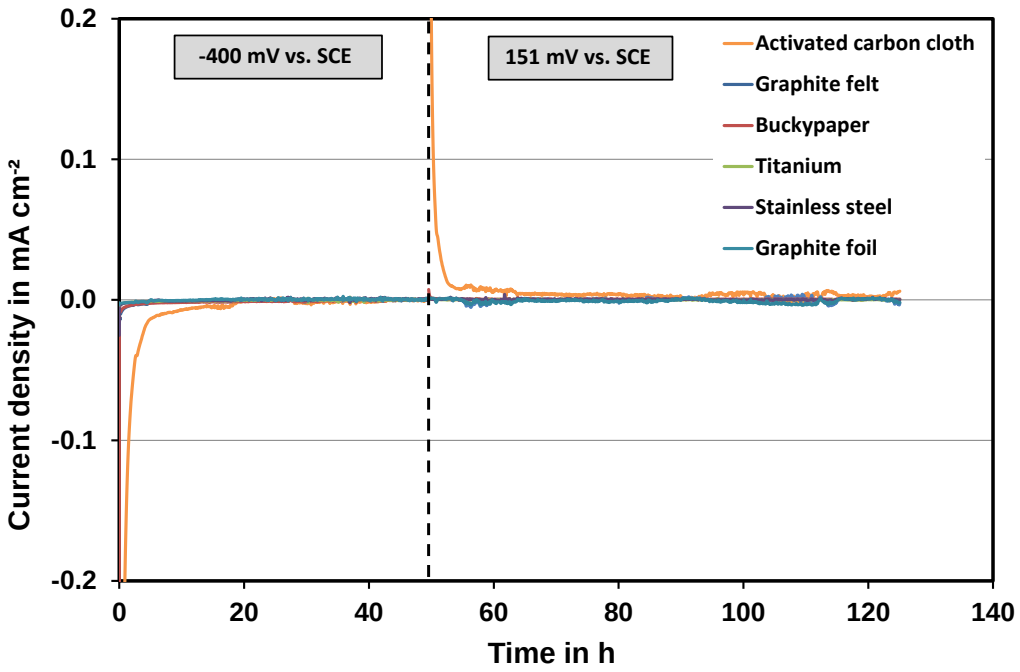

Figure A4.1: Current densities recorded with potentiostatic control filled only with sterile anode medium at +0.151 V and -0.400 V vs. SCE to measure the baseline current.

Table A4.1: Baseline current of each anode material measured in sterile anode medium after 40 h under potentiostatic control at -400 mV and +151 mV vs. SCE.

Anode materials	Baseline current after 40 h at -400 mV vs. SCE	Baseline current after 40 h at 151 mV vs. SCE
Activated carbon cloth	-2.6 µA	5.9 µA
Graphite felt	-1.2 µA	0.9 µA
Buckypaper	-1.5 µA	1.1 µA
Titanium	-0.4 µA	0.2 µA
Stainless steel	1.3 µA	0.2 µA
Graphite foil	-0.5 µA	-0.3 µA

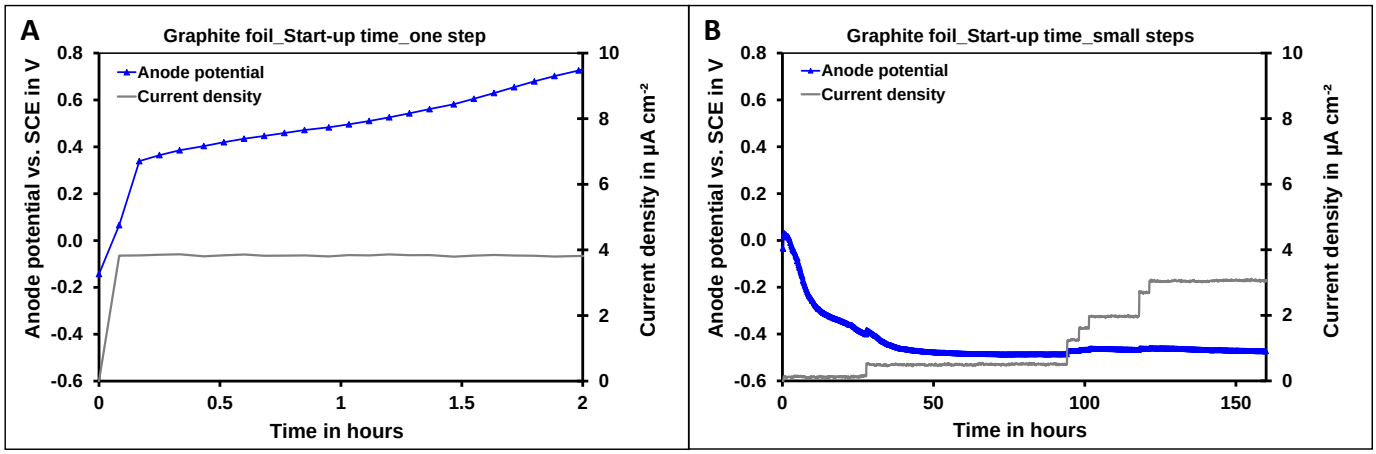

Figure A4.2: Start-up of the anode material graphite foil and the evolution of the corresponding anode potential depending on the size of the applied current density steps. A) A current density step of 3.8 µA cm^{-2} was applied. B) Current densities from 0 - 3.1 µA cm^{-2} were applied in small current density steps within one week.

Table A4.2: Limiting current densities (recorded using step-wise galvanostatic polarization) of the anode materials tested with *G. sulfurreducens* in ascending current density order and the corresponding potential vs. SCE. In addition, the total time until the limiting current density is reached (including the initial growth phase of one week) is shown.

Material	Limiting current density in µA cm^{-2}	Corresponding potential in V vs. SCE	Time until limiting current density is reached
Titanium	-	-	-
Titanium glass bead blasted	312 ± 21	-0.231 ± 0.042	561 ± 29 h
Stainless steel glass bead blasted	348 ± 21	-0.241 ± 0.040	603 ± 15 h
Buckypaper	590 ± 43	-0.273 ± 0.025	319 ± 12 h
Graphite felt	739 ± 103	-0.324 ± 0.010	357 ± 24 h
Untreated stainless steel	740 ± 18	-0.038 ± 0.026	1110 ± 19 h
Activated carbon cloth	749 ± 63	-0.322 ± 0.007	361 ± 16 h
Graphite foil	756 ± 15	-0.253 ± 0.037	1134 ± 19 h

Table A4.3: Comparison of the area-based current densities of *G. sulfurreducens* recorded with the step-wise galvanostatic technique and under potentiostatic control in triplicates (-0.400 V and +0.151 V vs. SCE) achieved with the different anode materials. Data for activated carbon cloth and graphite felt (step-wise galvanostatic technique) are cited from [167].

Anode material	Step-wise galvanostatic	Potentiostatic control	
	Current density at -0.400 V vs. SCE	Current density at -0.400 V vs. SCE	Current density at +0.151 V vs. SCE
Titanium	-	-	-
Titanium, glass bead blasted	185 ± 30 µA cm^{-2}	-	-
Stainless steel, glass bead blasted	225 ± 15 µA cm^{-2}	-	-
Buckypaper	336 ± 13 µA cm^{-2}	-	-
Stainless steel	67 ± 35 µA cm^{-2}	235 ± 13 µA cm^{-2}	38 ± 28 µA cm^{-2}
Graphite foil	310 ± 11 µA cm^{-2}	334 ± 39 µA cm^{-2}	653 ± 82 µA $cm^{-2\#}$
Graphite felt	398 ± 39 µA cm^{-2} *1990 ± 195 µA cm^{-3}**	492 ± 43 µA cm^{-2} *2460 ± 215 µA cm^{-3}**	1022 ± 66 µA cm^{-2} *5110 ± 330 µA cm^{-3}**
Activated carbon cloth	412 ± 19 µA cm^{-2} *8240 ± 380 µA cm^{-3}**	471 ± 12 µA cm^{-2} *9420 ± 240 µA cm^{-3}**	926 ± 21 µA cm^{-2} *18520 ± 420 µA cm^{-3}**

* Volume-based current density of the two porous materials graphite felt and activated carbon cloth

measured as duplicate.

Acknowledgements

First of all, I would like to thank Prof. Dr. Roland Zengerle for supervising and reviewing my PhD thesis, for scientific advice and for giving me the opportunity to work in his well-equipped laboratory.

I also would like to thank Prof. Dr. Johannes Gescher for scientific advice during my work and for agreeing to co-referee this thesis.

I would like to thank Prof. Dr. Sven Kerzenmacher for supervising my PhD thesis, and for many fruitful discussions and valuable support within my project work and our publications. Thank you for your trust in my work!

In addition, I want to thank the German Ministry of Education and Research (BMBF) for the funding programs “BioEnergie 2021” (Grant No. 03SF0382) and “BioProFi” (Grant No. 03SF0424) that built the basis for this PhD thesis.

Moreover, I would like to thank:

- The Bioelectrochemical systems group, especially my “old” group: Joana, Maxi, Christian, Jens, Sabine, Arne, Johannes, Marika and Steffi. Thank you for the great working atmosphere. I enjoyed working with you!
- Tobi H. for all the motivation and advice regarding my PhD thesis, and of course for all the important coffee breaks.
- All members of the Laboratory for MEMS Applications and Hahn-Schickard Freiburg, especially the APP-soccer and the IMTEK-Basketball group, I had a lot of fun with you!

I want to thank Ludi for your support, especially in times when writing this PhD thesis was very stressful! You are the best!

Finally, I want to thank my parents who always supported and believed in me and made it possible at all. Thank you for everything!

References

[1] Santoro, C.; Arbizzani, C.; Erable, B.; Ieropoulos, I. Microbial fuel cells: From fundamentals to applications. A review. *Journal of power sources* **2017**, *356*, 225–244.

[2] Kadier, A.; Simayi, Y.; Abdeshahian, P.; Azman, N.F.; Chandrasekhar, K.; Kalil, M.S. A comprehensive review of microbial electrolysis cells (MEC) reactor designs and configurations for sustainable hydrogen gas production. *Alexandria Engineering Journal* **2016**, *55*, 427–443.

[3] Kuppam Chandrasekhar, Abudukeremu Kadier, Gopalakrishnan Kumar, Rosa Anna Nastro, Velpuri Jeevitha. Challenges in Microbial Fuel Cell and Future Scope: Chapter 25. In *Microbial Fuel Cell*; Das, D., Ed.; Springer International Publishing: Cham, 2018.

[4] Chaturvedi, V.; Verma, P. Microbial fuel cell: A green approach for the utilization of waste for the generation of bioelectricity. *Bioresour. Bioprocess.* **2016**, *3*, 3388.

[5] Chouler, J.; Padgett, G.A.; Cameron, P.J.; Preuss, K.; Titirici, M.-M.; Ieropoulos, I.; Di Lorenzo, M. Towards effective small scale microbial fuel cells for energy generation from urine. *Electrochimica Acta* **2016**, *192*, 89–98.

[6] Kumar, R.; Singh, L.; Zularisam, A.W.; Hai, F.I. Microbial fuel cell is emerging as a versatile technology: A review on its possible applications, challenges and strategies to improve the performances. *Int J Energy Res* **2018**, *42*, 369–394.

[7] *Microbial Fuel Cells;* Logan, B.E., Ed.; John Wiley & Sons, Inc, 2008.

[8] Potter, M.C. Electrical Effects Accompanying the Decomposition of Organic Compounds. *Proceedings of the Royal Society of London. Series B, Containing Papers of a Biological Character* **1911**, *84*, 260–276.

[9] Logan, B.E.; Wallack, M.J.; Kim, K.-Y.; He, W.; Feng, Y.; Saikaly, P.E. Assessment of Microbial Fuel Cell Configurations and Power Densities. *Environ. Sci. Technol. Lett.* **2015**, *2*, 206–214.

[10] Koch, C.; Harnisch, F. Is there a Specific Ecological Niche for Electroactive Microorganisms? *ChemElectroChem* **2016**, *3*, 1282–1295.

[11] Myers, C.R.; Nealson, K.H. Bacterial manganese reduction and growth with manganese oxide as the sole electron acceptor. *Science (New York, N.Y.)* **1988**, *240*, 1319–1321.

[12] Heidelberg, J.F.; Paulsen, I.T.; Nelson, K.E.; Gaidos, E.J.; Nelson, W.C.; Read, T.D.; Eisen, J.A.; Seshadri, R.; Ward, N.; Methe, B.*; et al.* Genome sequence of the dissimilatory metal ion-reducing bacterium Shewanella oneidensis. *Nature biotechnology* **2002**, *20*, 1118–1123.

[13] Bücking, C.; Schicklberger, M.; Gescher, J. The Biochemistry of Dissimilatory Ferric Iron and Manganese Reduction in Shewanella oneidensis. In *Microbial Metal Respiration: From Geochemistry to Potential Applications*; Gescher, J., Kappler, A., Eds.; Springer Berlin Heidelberg: Berlin, Heidelberg, 2012; pp 49–82.

[14] Nealson, K.H.; Saffarini, D. Iron and manganese in anaerobic respiration: environmental significance, physiology, and regulation. *Annual review of microbiology* **1994**, *48*, 311–343.

[15] Richter, K.; Schicklberger, M.; Gescher, J. Dissimilatory reduction of extracellular electron acceptors in anaerobic respiration. *Applied and environmental microbiology* **2012**, *78*, 913–921.

[16] Golitsch, F.; Bücking, C.; Gescher, J. Proof of principle for an engineered microbial biosensor based on Shewanella oneidensis outer membrane protein complexes. *Biosensors & bioelectronics* **2013**, *47*, 285–291.

[17] Bücking, C.; Popp, F.; Kerzenmacher, S.; Gescher, J. Involvement and specificity of Shewanella oneidensis outer membrane cytochromes in the reduction of soluble and solid-phase terminal electron acceptors. *FEMS microbiology letters* **2010**, *306*, 144–151.

[18] Meyer, T.E.; Tsapin, A.I.; Vandenberghe, I.; Smet, L. de; Frishman, D.; Nealson, K.H.; Cusanovich, M.A.; van Beeumen, J.J. Identification of 42 possible cytochrome C genes in the Shewanella oneidensis genome and characterization of six soluble cytochromes. *Omics : a journal of integrative biology* **2004**, *8*, 57–77.

[19] Saffarini D., Brockman K., Beliaev A., Bouhenni R., Shirodkar S. Shewanella oneidensis and Extracellular Electron Transfer to Metal Oxides. In *Bacteria-Metal Interactions*; Saffarini, D., Ed.; Springer International Publishing: Cham, 2015.

[20] Kotloski, N.J.; Gralnick, J.A. Flavin electron shuttles dominate extracellular electron transfer by Shewanella oneidensis. *mBio* **2013**, *4*.

[21] Sydow, A.; Krieg, T.; Mayer, F.; Schrader, J.; Holtmann, D. Electroactive bacteria--molecular mechanisms and genetic tools. *Applied microbiology and biotechnology* **2014**, *98*, 8481–8495.

[22] Nevin, K.P.; Richter, H.; Covalla, S.F.; Johnson, J.P.; Woodard, T.L.; Orloff, A.L.; Jia, H.; Zhang, M.; Lovley, D.R. Power output and columbic efficiencies from biofilms of Geobacter sulfurreducens comparable to mixed community microbial fuel cells. *Environmental microbiology* **2008**, *10*, 2505–2514.

[23] Inoue, K.; Leang, C.; Franks, A.E.; Woodard, T.L.; Nevin, K.P.; Lovley, D.R. Specific localization of the c-type cytochrome OmcZ at the anode surface in current-producing biofilms of Geobacter sulfurreducens. *Environmental microbiology reports* **2011**, *3*, 211–217.

[24] Rosenbaum, M.A.; Bar, H.Y.; Beg, Q.K.; Segrè, D.; Booth, J.; Cotta, M.A.; Angenent, L.T. Shewanella oneidensis in a lactate-fed pure-culture and a glucose-fed co-culture with Lactococcus lactis with an electrode as electron acceptor. *Bioresource technology* **2011**, *102*, 2623–2628.

[25] Bond, D.R.; Lovley, D.R. Electricity Production by Geobacter sulfurreducens Attached to Electrodes. *Applied and environmental microbiology* **2003**, *69*, 1548–1555.

[26] Nevin, K.P.; Lovley, D.R. Lack of Production of Electron-Shuttling Compounds or Solubilization of Fe(III) during Reduction of Insoluble Fe(III) Oxide by Geobacter metallireducens. *Applied and environmental microbiology* **2000**, *66*, 2248–2251.

[27] Reguera, G.; McCarthy, K.D.; Mehta, T.; Nicoll, J.S.; Tuominen, M.T.; Lovley, D.R. Extracellular electron transfer via microbial nanowires. *Nature* **2005**, *435*, 1098–1101.

[28] Rosenbaum, M.; Cotta, M.A.; Angenent, L.T. Aerated Shewanella oneidensis in continuously fed bioelectrochemical systems for power and hydrogen production. *Biotechnology and bioengineering* **2010**, *105*, 880–888.

[29] Reguera, G.; Nevin, K.P.; Nicoll, J.S.; Covalla, S.F.; Woodard, T.L.; Lovley, D.R. Biofilm and nanowire production leads to increased current in Geobacter sulfurreducens fuel cells. *Applied and environmental microbiology* **2006**, *72*, 7345–7348.

[30] Methé, B.A.; Nelson, K.E.; Eisen, J.A.; Paulsen, I.T.; Nelson, W.; Heidelberg, J.F.; Wu, D.; Wu, M.; Ward, N.; Beanan, M.J.*; et al.* Genome of Geobacter sulfurreducens: metal reduction in subsurface environments. *Science (New York, N.Y.)* **2003**, *302*, 1967–1969.

[31] Rollefson, J.B.; Stephen, C.S.; Tien, M.; Bond, D.R. Identification of an extracellular polysaccharide network essential for cytochrome anchoring and biofilm formation in Geobacter sulfurreducens. *Journal of bacteriology* **2011**, *193*, 1023–1033.

[32] Jung, S.; Regan, J.M. Comparison of anode bacterial communities and performance in microbial fuel cells with different electron donors. *Applied microbiology and biotechnology* **2007**, *77*, 393–402.

[33] Holmes, D.E.; Bond, D.R.; O'Neil, R.A.; Reimers, C.E.; Tender, L.R.; Lovley, D.R. Microbial communities associated with electrodes harvesting electricity from a variety of aquatic sediments. *Microbial ecology* **2004**, *48*, 178–190.

[34] Sun, J.; Hu, Y.; Bi, Z.; Cao, Y. Improved performance of air-cathode single-chamber microbial fuel cell for wastewater treatment using microfiltration membranes and multiple sludge inoculation. *Journal of power sources* **2009**, *187*, 471–479.

[35] Janicek, A.; Fan, Y.; Liu, H. Design of microbial fuel cells for practical application: A review and analysis of scale-up studies. *Biofuels* **2014**, *5*, 79–92.

[36] Speers, A.M.; Reguera, G. Electron donors supporting growth and electroactivity of Geobacter sulfurreducens anode biofilms. *Applied and environmental microbiology* **2012**, *78*, 437–444.

[37] Kim, J.R.; Min, B.; Logan, B.E. Evaluation of procedures to acclimate a microbial fuel cell for electricity production. *Applied microbiology and biotechnology* **2005**, *68*, 23–30.

[38] Cusick, R.D.; Kiely, P.D.; Logan, B.E. A monetary comparison of energy recovered from microbial fuel cells and microbial electrolysis cells fed winery or domestic wastewaters. *International Journal of Hydrogen Energy* **2010**, *35*, 8855–8861.

[39] Mohan, S.V.; Pandey, A.; Varjani, S. *Microbial Electrochemical Technology*. *Sustainable Platform for Fuels, Chemicals and Remediation;* Elsevier: Netherlands, 2018.

[40] Torres, C.I.; Krajmalnik-Brown, R.; Parameswaran, P.; Marcus, A.K.; Wanger, G.; Gorby, Y.A.; Rittmann, B.E. Selecting anode-respiring bacteria based on anode potential: phylogenetic, electrochemical, and microscopic characterization. *Environmental science & technology* **2009**, *43*, 9519–9524.

[41] Rosenbaum, M.; Angenent, L.T. Genetically modified microorganisms for bioelectrochemical systems. In *Bioelectrochemical systems*: *From extracellular electron transfer to biotechnological application*; Rabaey, K., Ed.; IWA Publishing: London, New York, 2010; pp 101–118.

[42] Torres, C.I.; Marcus, A.K.; Lee, H.-S.; Parameswaran, P.; Krajmalnik-Brown, R.; Rittmann, B.E. A kinetic perspective on extracellular electron transfer by anode-respiring bacteria. *FEMS microbiology reviews* **2010**, *34*, 3–17.

[43] Schlegel, H.G.; Eitinger, T. *Allgemeine Mikrobiologie*, 8., vollst. überarb. und erw. Aufl.; Thieme: Stuttgart [u.a.], 2007.

[44] Myers, C.R.; Myers, J.M. Localization of cytochromes to the outer membrane of anaerobically grown Shewanella putrefaciens MR-1. *Journal of bacteriology* **1992**, *174*, 3429–3438.

[45] Beliaev, A.S.; Saffarini, D.A.; McLaughlin, J.L.; Hunnicutt, D. MtrC, an outer membrane decahaem c cytochrome required for metal reduction in Shewanella putrefaciens MR-1. *Mol Microbiol* **2001**, *39*, 722–730.

[46] Newman, D.K.; Kolter, R. A role for excreted quinones in extracellular electron transfer. *Nature* **2000**, *405*, 94–97.

[47] Canstein, H. von; Ogawa, J.; Shimizu, S.; Lloyd, J.R. Secretion of flavins by Shewanella species and their role in extracellular electron transfer. *Applied and environmental microbiology* **2008**, *74*, 615–623.

[48] Taskan, E.; Ozkaya, B.; Hasar, H. Combination of a novel electrode material and artificial mediators to enhance power generation in an MFC. *Water science and technology : a journal of the International Association on Water Pollution Research* **2015**, *71*, 320–328.

[49] Park, D.H.; Zeikus, J.G. Electricity Generation in Microbial Fuel Cells Using Neutral Red as an Electronophore. *Applied and environmental microbiology* **2000**, *66*, 1292–1297.

[50] Gorby, Y.A.; Yanina, S.; McLean, J.S.; Rosso, K.M.; Moyles, D.; Dohnalkova, A.; Beveridge, T.J.; Chang, I.S.; Kim, B.H.; Kim, K.S.*; et al.* Electrically conductive bacterial nanowires produced by Shewanella oneidensis strain MR-1 and other microorganisms. *Proceedings of the National Academy of Sciences of the United States of America* **2006**, *103*, 11358–11363.

[51] Polizzi, N.F.; Skourtis, S.S.; Beratan, D.N. Physical constraints on charge transport through bacterial nanowires. *Faraday Discuss* **2012**, *155*, 43–61.

[52] Okamoto, A.; Hashimoto, K.; Nealson, K.H.; Nakamura, R. Rate enhancement of bacterial extracellular electron transport involves bound flavin semiquinones. *Proceedings of the National Academy of Sciences of the United States of America* **2013**, *110*, 7856–7861.

[53] Logan, B.E.; Hamelers, B.; Rozendal, R.; Schröder, U.; Keller, J.; Freguia, S.; Aelterman, P.; Verstraete, W.; Rabaey, K. Microbial Fuel Cells: Methodology and Technology †. *Environ. Sci. Technol.* **2006**, *40*, 5181–5192.

[54] O'Hayre, R.P.; Cha, S.-W.; Colella, W.G.; Prinz, F.B. *Fuel cell fundamentals;* John Wiley & Sons Inc: Hoboken, New Jersey, 2016.

[55] Kerzenmacher, S.; Mutschler, K.; Kräling, U.; Baumer, H.; Ducrée, J.; Zengerle, R.; Stetten, F. von. A complete testing environment for the automated parallel performance characterization of biofuel cells: Design, validation, and application. *J Appl Electrochem* **2009**, *39*, 1477–1485.

[56] Rabaey, K. Bioelectrochemical Systems: a new approach towards environmental and industrial biotechnology. In *Bioelectrochemical systems*: *From extracellular electron transfer to biotechnological application*; Rabaey, K., Ed.; IWA Publishing: London, New York, 2010; pp 1–16.

[57] Logan, B.E. Voltage Generation. In *Microbial Fuel Cells*; Logan, B.E., Ed.; John Wiley & Sons, Inc, 2008; pp 29–43.

[58] Schröder, U.; Harnisch, F. Electrochemical losses. In *Bioelectrochemical systems*: *From extracellular electron transfer to biotechnological application*; Rabaey, K., Ed.; IWA Publishing: London, New York, 2010; pp 119–133.

[59] Logan, B.E. Power Generation. In *Microbial Fuel Cells*; Logan, B.E., Ed.; John Wiley & Sons, Inc, 2008; pp 44–60.

[60] Rozendal, R.A.; Hamelers, H.V.M.; Buisman, C.J.N. Effects of Membrane Cation Transport on pH and Microbial Fuel Cell Performance †. *Environ. Sci. Technol.* **2006**, *40*, 5206–5211.

[61] Popat, S.C.; Torres, C.I. Critical transport rates that limit the performance of microbial electrochemistry technologies. *Bioresource technology* **2016**, *215*, 265–273.

[62] Helder, M.; Strik, D.P.; Hamelers, H.V.; Buisman, C.J. The flat-plate plant-microbial fuel cell: the effect of a new design on internal resistances. *Biotechnology for biofuels* **2012**, *5*, 70.

[63] Kerzenmacher, S. Engineering of Microbial Electrodes. In *Bioelectrosynthesis*; Harnisch, F., Holtmann, D., Eds.; Springer International Publishing: Cham, 2019; pp 135–180.

[64] Logan, B.E. Architecture. In *Microbial Fuel Cells*; Logan, B.E., Ed.; John Wiley & Sons, Inc, 2008; pp 85–110.

[65] Oliot, M.; Etcheverry, L.; Mosdale, R.; Bergel, A. Microbial fuel cells connected in series in a common electrolyte underperform: Understanding why and in what context such a set-up can be applied. *Electrochimica Acta* **2017**, *246*, 879–889.

[66] Mustakeem. Electrode materials for microbial fuel cells: Nanomaterial approach. *Mater Renew Sustain Energy* **2015**, *4*, 9.

[67] Guo, K.; Prévoteau, A.; Patil, S.A.; Rabaey, K. Engineering electrodes for microbial electrocatalysis. *Current opinion in biotechnology* **2015**, *33*, 149–156.

[68] Cheng, S.; Logan, B.E. Ammonia treatment of carbon cloth anodes to enhance power generation of microbial fuel cells. *Electrochemistry Communications* **2007**, *9*, 492–496.

[69] Picot, M.; Lapinsonnière, L.; Rothballer, M.; Barrière, F. Graphite anode surface modification with controlled reduction of specific aryl diazonium salts for improved microbial fuel cells power output. *Biosensors & bioelectronics* **2011**, *28*, 181–188.

[70] Guo, K.; Freguia, S.; Dennis, P.G.; Chen, X.; Donose, B.C.; Keller, J.; Gooding, J.J.; Rabaey, K. Effects of surface charge and hydrophobicity on anodic biofilm formation, community composition, and current generation in bioelectrochemical systems. *Environmental science & technology* **2013**, *47*, 7563–7570.

[71] Santoro, C.; Guilizzoni, M.; Correa Baena, J.P.; Pasaogullari, U.; Casalegno, A.; Li, B.; Babanova, S.; Artyushkova, K.; Atanassov, P. The effects of carbon electrode surface properties on bacteria attachment and start up time of microbial fuel cells. *Carbon* **2014**, *67*, 128–139.

[72] Chen, S.; He, G.; Hu, X.; Xie, M.; Wang, S.; Zeng, D.; Hou, H.; Schröder, U. A three-dimensionally ordered macroporous carbon derived from a natural resource as anode for microbial bioelectrochemical systems. *ChemSusChem* **2012**, *5*, 1059–1063.

[73] Karthikeyan, R.; Wang, B.; Xuan, J.; Wong, J.W.C.; Lee, P.K.H.; Leung, M.K.H. Interfacial electron transfer and bioelectrocatalysis of carbonized plant material as effective anode of microbial fuel cell. *Electrochimica Acta* **2015**, *157*, 314–323.

[74] Yuan, Y.; Zhou, S.; Liu, Y.; Tang, J. Nanostructured macroporous bioanode based on polyaniline-modified natural loofah sponge for high-performance microbial fuel cells. *Environmental science & technology* **2013**, *47*, 14525–14532.

[75] Chen, S.; He, G.; Liu, Q.; Harnisch, F.; Zhou, Y.; Chen, Y.; Hanif, M.; Wang, S.; Peng, X.; Hou, H.*; et al.* Layered corrugated electrode macrostructures boost microbial bioelectrocatalysis. *Energy Environ. Sci.* **2012**, *5*, 9769.

[76] Chen, S.; Hou, H.; Harnisch, F.; Patil, S.A.; Carmona-Martinez, A.A.; Agarwal, S.; Zhang, Y.; Sinha-Ray, S.; Yarin, A.L.; Greiner, A.*; et al.* Electrospun and solution blown three-dimensional carbon fiber nonwovens for application as electrodes in microbial fuel cells. *Energy Environ. Sci.* **2011**, *4*, 1417–1421.

[77] Logan, B.E. Materials for BES. In *Bioelectrochemical systems*: *From extracellular electron transfer to biotechnological application*; Rabaey, K., Ed.; IWA Publishing: London, New York, 2010; pp 185–204.

[78] Baudler, A.; Schmidt, I.; Langner, M.; Greiner, A.; Schröder, U. Does it have to be carbon?: Metal anodes in microbial fuel cells and related bioelectrochemical systems. *Energy Environ. Sci.* **2015**, *8*, 2048–2055.

[79] Dumas, C.; Basseguy, R.; Bergel, A. Electrochemical activity of Geobacter sulfurreducens biofilms on stainless steel anodes. *Electrochimica Acta* **2008**, *53*, 5235–5241.

[80] Pocaznoi, D.; Calmet, A.; Etcheverry, L.; Erable, B.; Bergel, A. Stainless steel is a promising electrode material for anodes of microbial fuel cells. *Energy Environ. Sci.* **2012**, *5*, 9645.

[81] Ketep, S.F.; Bergel, A.; Calmet, A.; Erable, B. Stainless steel foam increases the current produced by microbial bioanodes in bioelectrochemical systems. *Energy Environ. Sci.* **2014**, *7*, 1633–1637.

[82] Dumas, C.; Mollica, A.; Féron, D.; Basseguy, R.; Etcheverry, L.; Bergel, A. Checking graphite and stainless anodes with an experimental model of marine microbial fuel cell. *Bioresource technology* **2008**, *99*, 8887–8894.

[83] Baudler, A.; Langner, M.; Rohr, C.; Greiner, A.; Schröder, U. Metal-Polymer Hybrid Architectures as Novel Anode Platform for Microbial Electrochemical Technologies. *ChemSusChem* **2017**, *10*, 253–257.

[84] Xie, X.; Ye, M.; Hu, L.; Liu, N.; McDonough, J.R.; Chen, W.; Alshareef, H.N.; Criddle, C.S.; Cui, Y. Carbon nanotube-coated macroporous sponge for microbial fuel cell electrodes. *Energy Environ. Sci.* **2012**, *5*, 5265–5270.

[85] Erbay, C.; Pu, X.; Choi, W.; Choi, M.-J.; Ryu, Y.; Hou, H.; Lin, F.; Figueiredo, P. de; Yu, C.; Han, A. Control of geometrical properties of carbon nanotube electrodes towards high-performance microbial fuel cells. *Journal of power sources* **2015**, *280*, 347–354.

[86] Logan, B.; Cheng, S.; Watson, V.; Estadt, G. Graphite Fiber Brush Anodes for Increased Power Production in Air-Cathode Microbial Fuel Cells. *Environ. Sci. Technol.* **2007**, *41*, 3341–3346.

[87] Zheng, S.; Yang, F.; Chen, S.; Liu, L.; Xiong, Q.; Yu, T.; Zhao, F.; Schröder, U.; Hou, H. Binder-free carbon black/stainless steel mesh composite electrode for high-performance anode in microbial fuel cells. *Journal of power sources* **2015**, *284*, 252–257.

[88] Lanas, V.; Logan, B.E. Evaluation of multi-brush anode systems in microbial fuel cells. *Bioresource technology* **2013**, *148*, 379–385.

[89] Peng, L.; You, S.-J.; Wang, J.-Y. Carbon nanotubes as electrode modifier promoting direct electron transfer from Shewanella oneidensis. *Biosensors & bioelectronics* **2010**, *25*, 1248–1251.

[90] Sanchez, D.; Jacobs, D.; Gregory, K.; Huang, J.; Hu, Y.; Vidic, R.; Yun, M. Changes in Carbon Electrode Morphology Affect Microbial Fuel Cell Performance with Shewanella oneidensis MR-1. *Energies* **2015**, *8*, 1817–1829.

[91] TerAvest, M.A.; Rosenbaum, M.A.; Kotloski, N.J.; Gralnick, J.A.; Angenent, L.T. Oxygen allows Shewanella oneidensis MR-1 to overcome mediator washout in a continuously fed bioelectrochemical system. *Biotechnology and bioengineering* **2014**, *111*, 692–699.

[92] Zhao, Y.; Nakanishi, S.; Watanabe, K.; Hashimoto, K. Hydroxylated and aminated polyaniline nanowire networks for improving anode performance in microbial fuel cells. *Journal of bioscience and bioengineering* **2011**, *112*, 63–66.

[93] Blanchet, E.; Erable, B.; Solan, M.-L. de; Bergel, A. Two-dimensional carbon cloth and three-dimensional carbon felt perform similarly to form bioanode fed with food waste. *Electrochemistry Communications* **2016**, *66*, 38–41.

[94] Harnisch, F.; Schröder, U. From MFC to MXC: chemical and biological cathodes and their potential for microbial bioelectrochemical systems. *Chemical Society reviews* **2010**, *39*, 4433–4448.

[95] Wang, Z.; Mahadevan, G.D.; Wu, Y.; Zhao, F. Progress of air-breathing cathode in microbial fuel cells. *Journal of power sources* **2017**, *356*, 245–255.

[96] Rismani-Yazdi, H.; Carver, S.M.; Christy, A.D.; Tuovinen, O.H. Cathodic limitations in microbial fuel cells: An overview. *Journal of power sources* **2008**, *180*, 683–694.

[97] Yuan, H.; Hou, Y.; Abu-Reesh, I.M.; Chen, J.; He, Z. Oxygen reduction reaction catalysts used in microbial fuel cells for energy-efficient wastewater treatment: A review. *Mater. Horiz.* **2016**, *3*, 382–401.

[98] Zhao, F.; Harnisch, F.; Schröder, U.; Scholz, F.; Bogdanoff, P.; Herrmann, I. Challenges and Constraints of Using Oxygen Cathodes in Microbial Fuel Cells. *Environ. Sci. Technol.* **2006**, *40*, 5193–5199.

[99] Cheng, S.; Liu, H.; Logan, B.E. Power Densities Using Different Cathode Catalysts (Pt and CoTMPP) and Polymer Binders (Nafion and PTFE) in Single Chamber Microbial Fuel Cells. *Environ. Sci. Technol.* **2006**, *40*, 364–369.

[100] Rozendal, R.A.; Hamelers, H.V.M.; Rabaey, K.; Keller, J.; Buisman, C.J.N. Towards practical implementation of bioelectrochemical wastewater treatment. *Trends in biotechnology* **2008**, *26*, 450–459.

[101] Roche, I.; Katuri, K.; Scott, K. A microbial fuel cell using manganese oxide oxygen reduction catalysts. *J Appl Electrochem* **2010**, *40*, 13–21.

[102] Bajracharya, S.; Vanbroekhoven, K.; Buisman, C.J.N.; Pant, D.; Strik, David P B T B. Application of gas diffusion biocathode in microbial electrosynthesis from carbon dioxide. *Environmental science and pollution research international* **2016**, *23*, 22292–22308.

[103] Brandon, N.P.; Brett, D.J. Engineering porous materials for fuel cell applications. *Philosophical transactions. Series A, Mathematical, physical, and engineering sciences* **2006**, *364*, 147–159.

[104] SU, A.; WENG, F.; HSU, C.; CHEN, Y. Studies on flooding in PEM fuel cell cathode channels. *International Journal of Hydrogen Energy* **2006**, *31*, 1031–1039.

[105] Ahn, Y.; Zhang, F.; Logan, B.E. Air humidity and water pressure effects on the performance of air-cathode microbial fuel cell cathodes. *Journal of power sources* **2014**, *247*, 655–659.

[106] Wright, M.R. *An introduction to aqueous electrolyte solutions;* John Wiley: Chichester, England, Hoboken, NJ, 2007.

[107] Luo, Y.; Zhang, F.; Wei, B.; Liu, G.; Zhang, R.; Logan, B.E. Power generation using carbon mesh cathodes with different diffusion layers in microbial fuel cells. *Journal of power sources* **2011**, *196*, 9317–9321.

[108] Harnisch, F.; Wirth, S.; Schröder, U. Effects of substrate and metabolite crossover on the cathodic oxygen reduction reaction in microbial fuel cells: Platinum vs. iron(II) phthalocyanine based electrodes. *Electrochemistry Communications* **2009**, *11*, 2253–2256.

[109] Bergel, A.; Féron, D.; Mollica, A. Catalysis of oxygen reduction in PEM fuel cell by seawater biofilm. *Electrochemistry Communications* **2005**, *7*, 900–904.

[110] Clauwaert, P.; van der Ha, D.; Boon, N.; Verbeken, K.; Verhaege, M.; Rabaey, K.; Verstraete, W. Open Air Biocathode Enables Effective Electricity Generation with Microbial Fuel Cells. *Environ. Sci. Technol.* **2007**, *41*, 7564–7569.

[111] Rhoads, A.; Beyenal, H.; Lewandowski, Z. Microbial Fuel Cell using Anaerobic Respiration as an Anodic Reaction and Biomineralized Manganese as a Cathodic Reactant. *Environ. Sci. Technol.* **2005**, *39*, 4666–4671.

[112] Rabaey, K.; Read, S.T.; Clauwaert, P.; Freguia, S.; Bond, P.L.; Blackall, L.L.; Keller, J. Cathodic oxygen reduction catalyzed by bacteria in microbial fuel cells. *The ISME journal* **2008**, *2*, 519–527.

[113] Erable, B.; Vandecandelaere, I.; Faimali, M.; Delia, M.-L.; Etcheverry, L.; Vandamme, P.; Bergel, A. Marine aerobic biofilm as biocathode catalyst. *Bioelectrochemistry (Amsterdam, Netherlands)* **2010**, *78*, 51–56.

[114] Rubenwolf, S.; Sané, S.; Hussein, L.; Kestel, J.; Stetten, F. von; Urban, G.; Krueger, M.; Zengerle, R.; Kerzenmacher, S. Prolongation of electrode lifetime in biofuel cells by periodic enzyme renewal. *Applied microbiology and biotechnology* **2012**, *96*, 841–849.

[115] Sané, S.; Jolivalt, C.; Mittler, G.; Nielsen, P.J.; Rubenwolf, S.; Zengerle, R.; Kerzenmacher, S. Overcoming bottlenecks of enzymatic biofuel cell cathodes: crude fungal culture supernatant can help to extend lifetime and reduce cost. *ChemSusChem* **2013**, *6*, 1209–1215.

[116] Schaetzle, O.; Barrière, F.; Schröder, U. An improved microbial fuel cell with laccase as the oxygen reduction catalyst. *Energy Environ. Sci.* **2009**, *2*, 96–99.

[117] Willner, I.; Yan, Y.-M.; Willner, B.; Tel-Vered, R. Integrated Enzyme-Based Biofuel Cells-A Review. *Fuel Cells* **2009**, *9*, 7–24.

[118] Minteer, S.D.; Liaw, B.Y.; Cooney, M.J. Enzyme-based biofuel cells. *Current opinion in biotechnology* **2007**, *18*, 228–234.

[119] Meredith, M.T.; Minteer, S.D. Biofuel cells: enhanced enzymatic bioelectrocatalysis. *Annual review of analytical chemistry (Palo Alto, Calif.)* **2012**, *5*, 157–179.

[120] Zulic, Z.; Minteer, S.D. Enzymatic fuel cells and their complementarities relative to BES/MFC. In *Bioelectrochemical systems*: *From extracellular electron transfer to biotechnological application*; Rabaey, K., Ed.; IWA Publishing: London, New York, 2010; pp 39–57.

[121] Falk, M.; Blum, Z.; Shleev, S. Direct electron transfer based enzymatic fuel cells. *Electrochimica Acta* **2012**, *82*, 191–202.

[122] Cooney, M.J.; Svoboda, V.; Lau, C.; Martin, G.; Minteer, S.D. Enzyme catalysed biofuel cells. *Energy Environ. Sci.* **2008**, *1*, 320.

[123] Kim, B.H.; Chang, I.S.; Gil, G.C.; Park, H.S.; Kim, H.J. Novel BOD (biological oxygen demand) sensor using mediator-less microbial fuel cell. *Biotechnology letters* **2003**, *25*, 541–545.

[124] Myers, C.R.; Myers, J.M. Outer membrane cytochromes of Shewanella putrefaciens MR-1: Spectral analysis, and purification of the 83-kDa c-type cytochrome. *Biochimica et Biophysica Acta (BBA)-Biomembranes* **1997**, *1326*, 307–318.

[125] Marsili, E.; Baron, D.B.; Shikhare, I.D.; Coursolle, D.; Gralnick, J.A.; Bond, D.R. Shewanella secretes flavins that mediate extracellular electron transfer. *Proceedings of the National Academy of Sciences of the United States of America* **2008**, *105*, 3968–3973.

[126] Nealson, K.H.; Belz, A.; McKee, B. Breathing metals as a way of life: Geobiology in action. *Antonie van Leeuwenhoek* **2002**, *81*, 215–222.

[127] Biffinger, J.C.; Byrd, J.N.; Dudley, B.L.; Ringeisen, B.R. Oxygen exposure promotes fuel diversity for Shewanella oneidensis microbial fuel cells. *Biosensors & bioelectronics* **2008**, *23*, 820–826.

[128] Watson, V.J.; Logan, B.E. Power production in MFCs inoculated with Shewanella oneidensis MR-1 or mixed cultures. *Biotechnology and bioengineering* **2010**, *105*, 489–498.

[129] Wang, X.; Cheng, S.; Feng, Y.; Merrill, M.D.; Saito, T.; Logan, B.E. Use of Carbon Mesh Anodes and the Effect of Different Pretreatment Methods on Power Production in Microbial Fuel Cells. *Environ. Sci. Technol.* **2009**, *43*, 6870–6874.

[130] Ringeisen, B.R.; Henderson, E.; Wu, P.K.; Pietron, J.; Ray, R.; Little, B.; Biffinger, J.C.; Jones-Meehan, J.M. High Power Density from a Miniature Microbial Fuel Cell Using Shewanella oneidensis DSP10. *Environ. Sci. Technol.* **2006**, *40*, 2629–2634.

[131] Lanthier, M.; Gregory, K.B.; Lovley, D.R. Growth with high planktonic biomass in Shewanella oneidensis fuel cells. *FEMS microbiology letters* **2008**, *278*, 29–35.

[132] Zhu, N.; Chen, X.; Zhang, T.; Wu, P.; Li, P.; Wu, J. Improved performance of membrane free single-chamber air-cathode microbial fuel cells with nitric acid and ethylenediamine surface modified activated carbon fiber felt anodes. *Bioresource technology* **2011**, *102*, 422–426.

[133] Sun, M.; Zhang, F.; Tong, Z.-H.; Sheng, G.-P.; Chen, Y.-Z.; Zhao, Y.; Chen, Y.-P.; Zhou, S.-Y.; Liu, G.; Tian, Y.-C.*; et al.* A gold-sputtered carbon paper as an anode for improved electricity generation from a microbial fuel cell inoculated with Shewanella oneidensis MR-1. *Biosensors & bioelectronics* **2010**, *26*, 338–343.

[134] Wei, J.; Liang, P.; Huang, X. Recent progress in electrodes for microbial fuel cells. *Bioresource technology* **2011**, *102*, 9335–9344.

[135] Biffinger, J.C.; Ray, R.; Little, B.J.; Fitzgerald, L.A.; Ribbens, M.; Finkel, S.E.; Ringeisen, B.R. Simultaneous analysis of physiological and electrical output changes in an operating microbial fuel cell with Shewanella oneidensis. *Biotechnology and bioengineering* **2009**, *103*, 524–531.

[136] Hussein, L.; Urban, G.; Krüger, M. Fabrication and characterization of buckypaper-based nanostructured electrodes as a novel material for biofuel cell applications. *Physical chemistry chemical physics : PCCP* **2011**, *13*, 5831–5839.

[137] Sengupta, R.; Bhattacharya, M.; Bandyopadhyay, S.; Bhowmick, A.K. A review on the mechanical and electrical properties of graphite and modified graphite reinforced polymer composites. *Progress in Polymer Science* **2011**, *36*, 638–670.

[138] Auer, E.; Freund, A.; Pietsch, J.; Tacke, T. Carbons as supports for industrial precious metal catalysts. *Applied Catalysis A: General* **1998**, *173*, 259–271.

[139] Bretschger, O.; Obraztsova, A.; Sturm, C.A.; Chang, I.S.; Gorby, Y.A.; Reed, S.B.; Culley, D.E.; Reardon, C.L.; Barua, S.; Romine, M.F.*; et al.* Current production and metal oxide reduction by Shewanella oneidensis MR-1 wild type and mutants. *Applied and environmental microbiology* **2007**, *73*, 7003–7012.

[140] Huang, Y.-X.; Liu, X.-W.; Xie, J.-F.; Sheng, G.-P.; Wang, G.-Y.; Zhang, Y.-Y.; Xu, A.-W.; Yu, H.-Q. Graphene oxide nanoribbons greatly enhance extracellular electron transfer in bio-electrochemical systems. *Chemical communications (Cambridge, England)* **2011**, *47*, 5795–5797.

[141] Torres, C.I.; Kato Marcus, A.; Rittmann, B.E. Proton transport inside the biofilm limits electrical current generation by anode-respiring bacteria. *Biotechnology and bioengineering* **2008**, *100*, 872–881.

[142] Flexer, V.; Chen, J.; Donose, B.C.; Sherrell, P.; Wallace, G.G.; Keller, J. The nanostructure of three-dimensional scaffolds enhances the current density of microbial bioelectrochemical systems. *Energy Environ. Sci.* **2013**, *6*, 1291.

[143] Rabaey, K.; Rozendal, R.A. Microbial electrosynthesis - revisiting the electrical route for microbial production. *Nature reviews. Microbiology* **2010**, *8*, 706–716.

[144] Bennetto, H.P.; Stirling, J.L.; Tanaka, K.; Vega, C.A. Anodic reactions in microbial fuel cells. *Biotechnology and bioengineering* **1983**, *25*, 559–568.

[145] Habermann, W.; Pommer, E.H. Biological fuel cells with sulphide storage capacity. *Appl Microbiol Biotechnol* **1991**, *35*.

[146] Borole, A.P.; Reguera, G.; Ringeisen, B.; Wang, Z.-W.; Feng, Y.; Kim, B.H. Electroactive biofilms: Current status and future research needs. *Energy Environ. Sci.* **2011**, *4*, 4813.

[147] Liu, H.; Logan, B.E. Electricity Generation Using an Air-Cathode Single Chamber Microbial Fuel Cell in the Presence and Absence of a Proton Exchange Membrane. *Environ. Sci. Technol.* **2004**, *38*, 4040–4046.

[148] Benson, D.A.; Karsch-Mizrachi, I.; Lipman, D.J.; Ostell, J.; Wheeler, D.L. GenBank. *Nucleic acids research* **2007**, *35*, D21-5.

[149] Lovley, D.R. Bug juice: harvesting electricity with microorganisms. *Nature reviews. Microbiology* **2006**, *4*, 497–508.

[150] Caccavo, F.; Lonergan, D.J.; Lovley, D.R.; Davis, M.; Stolz, J.F.; McInerney, M.J. Geobacter sulfurreducens sp. nov., a hydrogen- and acetate-oxidizing dissimilatory metal-reducing microorganism. *Applied and environmental microbiology* **1994**, *60*, 3752–3759.

[151] Lin, W.C.; Coppi, M.V.; Lovley, D.R. Geobacter sulfurreducens Can Grow with Oxygen as a Terminal Electron Acceptor. *Applied and environmental microbiology* **2004**, *70*, 2525–2528.

[152] Kipf, E.; Koch, J.; Geiger, B.; Erben, J.; Richter, K.; Gescher, J.; Zengerle, R.; Kerzenmacher, S. Systematic screening of carbon-based anode materials for microbial fuel cells with Shewanella oneidensis MR-1. *Bioresource technology* **2013**, *146*, 386–392.

[153] Call, D.F.; Logan, B.E. Lactate oxidation coupled to iron or electrode reduction by Geobacter sulfurreducens PCA. *Applied and environmental microbiology* **2011**, *77*, 8791–8794.

[154] Jung, S. Impedance Analysis of Geobacter sulfurreducens PCA, Shewanella oneidensis MR-1, and their Coculture in Bioeletrochemical Systems. *Int J Electrochem Sci* **2012**, *7*.

[155] Marsili, E.; Rollefson, J.B.; Baron, D.B.; Hozalski, R.M.; Bond, D.R. Microbial biofilm voltammetry: direct electrochemical characterization of catalytic electrode-attached biofilms. *Applied and environmental microbiology* **2008**, *74*, 7329–7337.

[156] Dolch, K.; Danzer, J.; Kabbeck, T.; Bierer, B.; Erben, J.; Förster, A.H.; Maisch, J.; Nick, P.; Kerzenmacher, S.; Gescher, J. Characterization of microbial current production as a function of microbe-electrode-interaction. *Bioresource technology* **2014**, *157*, 284–292.

[157] Coppi, M.V.; Leang, C.; Sandler, S.J.; Lovley, D.R. Development of a genetic system for Geobacter sulfurreducens. *Applied and environmental microbiology* **2001**, *67*, 3180–3187.

[158] Balch, W.E.; Fox, G.E.; Magrum, L.J.; Woese, C.R.; Wolfe, R.S. Methanogens: reevaluation of a unique biological group. *Microbiological Reviews* **1979**, *43*, 260–296.

[159] Lowell, S.; Shields, J.E.; Thomas, M.A. *Characterization of porous solids and powders*. *Surface area, pore size and density;* Springer: Dordrecht, 2004.

[160] Soussan, L.; Erable, B.; Delia, M.-L.; Bergel, A. The open circuit potential of Geobacter sulfurreducens bioanodes depends on the electrochemical adaptation of the strain. *Electrochemistry Communications* **2013**, *33*, 35–38.

[161] Thauer, R.K.; Jungermann, K.; Decker, K. Energy conservation in chemotrophic anaerobic bacteria. *Bacteriological reviews* **1977**, *41*, 100–180.

[162] Mahadevan, R.; Bond, D.R.; Butler, J.E.; Esteve-Nuñez, A.; Coppi, M.V.; Palsson, B.O.; Schilling, C.H.; Lovley, D.R. Characterization of metabolism in the Fe(III)-reducing organism Geobacter sulfurreducens by constraint-based modeling. *Applied and environmental microbiology* **2006**, *72*, 1558–1568.

[163] Rahimnejad, M.; Adhami, A.; Darvari, S.; Zirepour, A.; Oh, S.-E. Microbial fuel cell as new technology for bioelectricity generation: A review. *Alexandria Engineering Journal* **2015**, *54*, 745–756.

[164] Okamoto, A.; Saito, K.; Inoue, K.; Nealson, K.H.; Hashimoto, K.; Nakamura, R. Uptake of self-secreted flavins as bound cofactors for extracellular electron transfer in Geobacter species. *Energy Environ. Sci.* **2014**, *7*, 1357–1361.

[165] Kumar, R.; Singh, L.; Wahid, Z.A.; Din, M.F.M. Exoelectrogens in microbial fuel cells toward bioelectricity generation: A review. *Int. J. Energy Res.* **2015**, *39*, 1048–1067.

[166] Lovley, D.R.; Ueki, T.; Zhang, T.; Malvankar, N.S.; Shrestha, P.M.; Flanagan, K.A.; Aklujkar, M.; Butler, J.E.; Giloteaux, L.; Rotaru, A.-E.*; et al.* Geobacter: the microbe electric's physiology, ecology, and practical applications. *Advances in microbial physiology* **2011**, *59*, 1–100.

[167] Kipf, E.; Zengerle, R.; Gescher, J.; Kerzenmacher, S. How Does the Choice of Anode Material Influence Electrical Performance?: A Comparison of Two Microbial Fuel Cell Model Organisms. *CHEMELECTROCHEM* **2014**, *1*, 1849–1853.

[168] Nord, F.F. *Advances in Enzymology and Related Areas of Molecular Biology;* John Wiley & Sons, Inc: Hoboken, NJ, USA, 1970.

[169] Richter, H.; Nevin, K.P.; Jia, H.; Lowy, D.A.; Lovley, D.R.; Tender, L.M. Cyclic voltammetry of biofilms of wild type and mutant Geobacter sulfurreducens on fuel cell anodes indicates possible roles of OmcB, OmcZ, type IV pili, and protons in extracellular electron transfer. *Energy Environ. Sci.* **2009**, *2*, 506.

[170] ter Heijne, A.; Hamelers, H.V.M.; Saakes, M.; Buisman, C.J.N. Performance of non-porous graphite and titanium-based anodes in microbial fuel cells. *Electrochimica Acta* **2008**, *53*, 5697–5703.

[171] Pons, L.; Délia, M.-L.; Basséguy, R.; Bergel, A. Effect of the semi-conductive properties of the passive layer on the current provided by stainless steel microbial cathodes. *Electrochimica Acta* **2011**, *56*, 2682–2688.

[172] *Bioelectrochemical systems*. *From extracellular electron transfer to biotechnological application;* Rabaey, K., Ed.; IWA Publishing: London, New York, 2010.

[173] Lovley, D.R. The microbe electric: conversion of organic matter to electricity. *Current opinion in biotechnology* **2008**, *19*, 564–571.

[174] Esteve-Núñez, A.; Sosnik, J.; Visconti, P.; Lovley, D.R. Fluorescent properties of c-type cytochromes reveal their potential role as an extracytoplasmic electron sink in Geobacter sulfurreducens. *Environmental microbiology* **2008**, *10*, 497–505.

[175] Malvankar, N.S.; Mester, T.; Tuominen, M.T.; Lovley, D.R. Supercapacitors based on c-type cytochromes using conductive nanostructured networks of living bacteria. *Chemphyschem : a European journal of chemical physics and physical chemistry* **2012**, *13*, 463–468.

[176] Fernandes, A.P.; Nunes, T.C.; Paquete, C.M.; Salgueiro, C.A. Interaction studies between periplasmic cytochromes provide insights into extracellular electron transfer pathways of Geobacter sulfurreducens. *The Biochemical journal* **2017**, *474*, 797–808.

[177] Bonanni, P.S.; Schrott, G.D.; Robuschi, L.; Busalmen, J.P. Charge accumulation and electron transfer kinetics in Geobacter sulfurreducens biofilms. *Energy Environ. Sci.* **2012**, *5*, 6188.

[178] Madjarov, J.; Popat, S.C.; Erben, J.; Götze, A.; Zengerle, R.; Kerzenmacher, S. Revisiting methods to characterize bioelectrochemical systems: The influence of uncompensated resistance (iR u -drop), double layer capacitance, and junction potential. *Journal of power sources* **2017**, *356*, 408–418.

[179] Yoho, R.A.; Popat, S.C.; Torres, C.I. Dynamic potential-dependent electron transport pathway shifts in anode biofilms of Geobacter sulfurreducens. *ChemSusChem* **2014**, *7*, 3413–3419.

[180] Wagner, R.C.; Call, D.F.; Logan, B.E. Optimal set anode potentials vary in bioelectrochemical systems. *Environmental science & technology* **2010**, *44*, 6036–6041.

[181] Dennis, P.G.; Virdis, B.; Vanwonterghem, I.; Hassan, A.; Hugenholtz, P.; Tyson, G.W.; Rabaey, K. Anode potential influences the structure and function of anodic electrode and electrolyte-associated microbiomes. *Scientific reports* **2016**, *6*, 39114.

[182] Patil, S.A.; Harnisch, F.; Kapadnis, B.; Schröder, U. Electroactive mixed culture biofilms in microbial bioelectrochemical systems: the role of temperature for biofilm formation and performance. *Biosensors & bioelectronics* **2010**, *26*, 803–808.

[183] Logan, B.E. Simultaneous wastewater treatment and biological electricity generation. *Water science and technology : a journal of the International Association on Water Pollution Research* **2005**, *52*, 31–37.

[184] Cracknell, J.A.; Vincent, K.A.; Armstrong, F.A. Enzymes as working or inspirational electrocatalysts for fuel cells and electrolysis. *Chemical reviews* **2008**, *108*, 2439–2461.

[185] Ivnitski, D.; Atanassov, P. Electrochemical Studies of Intramolecular Electron Transfer in Laccase from Trametes versicolor. *Electroanalysis* **2007**, *19*, 2307–2313.

[186] Piontek, K.; Antorini, M.; Choinowski, T. Crystal structure of a laccase from the fungus Trametes versicolor at 1.90-A resolution containing a full complement of coppers. *The Journal of biological chemistry* **2002**, *277*, 37663–37669.

[187] Christenson, A.; Dimcheva, N.; Ferapontova, E.E.; Lo Gorton; Ruzgas, T.; Stoica, L.; Shleev, S.; Yaropolov, A.I.; Haltrich, D.; Thorneley, R.N.F.*; et al.* Direct Electron Transfer Between Ligninolytic Redox Enzymes and Electrodes. *Electroanalysis* **2004**, *16*, 1074–1092.

[188] Rasmussen, M.; Abdellaoui, S.; Minteer, S.D. Enzymatic biofuel cells: 30 years of critical advancements. *Biosensors & bioelectronics* **2016**, *76*, 91–102.

[189] Rubenwolf, S.; Kerzenmacher, S.; Zengerle, R.; Stetten, F. von. Strategies to extend the lifetime of bioelectrochemical enzyme electrodes for biosensing and biofuel cell applications. *Applied microbiology and biotechnology* **2011**, *89*, 1315–1322.

[190] Leech, D.; Kavanagh, P.; Schuhmann, W. Enzymatic fuel cells: Recent progress. *Electrochimica Acta* **2012**, *84*, 223–234.

[191] Santoro, C.; Babanova, S.; Erable, B.; Schuler, A.; Atanassov, P. Bilirubin oxidase based enzymatic air-breathing cathode: Operation under pristine and contaminated conditions. *Bioelectrochemistry (Amsterdam, Netherlands)* **2016**, *108*, 1–7.

[192] Kipf, E.; Messinger, T.; Sané, S.; Kerzenmacher, S. An air-breathing cathode based on buckypaper electrodes with reversibly adsorbed laccase. In *Proceedings EU-ISMET 2014.* 2nd European Meeting of the International Society for Microbial Electrochemistry and Technology, 3-5 September 2014: Alcala, Spain, 2014; p 166.

[193] Kipf, E.; Morse, D.; Messinger, T.; Sané, S.; Kerzenmacher, S. An air-breathing enzymatic cathode with extended lifetime by continuous laccase supply. In *Proceedings of EFC 2015.* European Fuel Cell Technology & Applications Conference - Piero Lunghi Conference, Naples, Italy, 16-18 December 2015, 2015; pp 123–124.

[194] Wetser, K.; Dieleman, K.; Buisman, C.; Strik, D. Electricity from wetlands: Tubular plant microbial fuels with silicone gas-diffusion biocathodes. *Applied Energy* **2017**, *185*, 642–649.

[195] Kipf, E.; Thissen, D.; Kerzenmacher, S. Air-breathing cathodes for microbial fuel cells based on activated carbon cloth and spin-coated PDMS membranes as hydrophobic diffusion layer. In *Proceedings of the 4th microbial fuel cell conference.* 4th Microbial fuel cell conference, Cairns, Australia, 1.-4. September 2013, 2013; pp 58–59.

[196] An, J.; Li, N.; Wan, L.; Zhou, L.; Du, Q.; Li, T.; Wang, X. Electric field induced salt precipitation into activated carbon air-cathode causes power decay in microbial fuel cells. *Water research* **2017**, *123*, 369–377.

[197] Hussein, L.; Rubenwolf, S.; Stetten, F. von; Urban, G.; Zengerle, R.; Krueger, M.; Kerzenmacher, S. A highly efficient buckypaper-based electrode material for mediatorless laccase-catalyzed dioxygen reduction. *Biosensors & bioelectronics* **2011**, *26*, 4133–4138.

[198] Kontani, R.; Tsujimura, S.; Kano, K. Air diffusion biocathode with CueO as electrocatalyst adsorbed on carbon particle-modified electrodes. *Bioelectrochemistry (Amsterdam, Netherlands)* **2009**, *76*, 10–13.

[199] Ciniciato, G.P.M.K.; Lau, C.; Cochrane, A.; Sibbett, S.S.; Gonzalez, E.R.; Atanassov, P. Development of paper based electrodes: From air-breathing to paintable enzymatic cathodes. *Electrochimica Acta* **2012**, *82*, 208–213.

[200] Gupta, G.; Lau, C.; Branch, B.; Rajendran, V.; Ivnitski, D.; Atanassov, P. Direct bio-electrocatalysis by multi-copper oxidases: Gas-diffusion laccase-catalyzed cathodes for biofuel cells. *Electrochimica Acta* **2011**, *56*, 10767–10771.

[201] Xavier, Ana Maria Rebelo Barreto; Mora Tavares, A.P.; Ferreira, R.; Amado, F. Trametes versicolor growth and laccase induction with by-products of pulp and paper industry. *Electron. J. Biotechnol.* **2007**, *10*, 444–451.

[202] Moldes, D.; Lorenzo, M.; Sanromán, M.A. Different proportions of laccase isoenzymes produced by submerged cultures of Trametes versicolor grown on lignocellulosic wastes. *Biotechnology letters* **2004**, *26*, 327–330.

[203] Xu, S.; Jangir, Y.; El-Naggar, M.Y. Disentangling the roles of free and cytochrome-bound flavins in extracellular electron transport from Shewanella oneidensis MR-1. *Electrochimica Acta* **2016**, *198*, 49–55.

[204] Rosenbaum, M.A.; Bar, H.Y.; Beg, Q.K.; Segrè, D.; Booth, J.; Cotta, M.A.; Angenent, L.T. Transcriptional analysis of Shewanella oneidensis MR-1 with an electrode compared to Fe(III)citrate or oxygen as terminal electron acceptor. *PloS one* **2012**, *7*, e30827.

[205] Bursac, T.; Gralnick, J.A.; Gescher, J. Acetoin production via unbalanced fermentation in Shewanella oneidensis. *Biotechnology and bioengineering* **2017**, *114*, 1283–1289.

[206] Flynn, J.M.; Ross, D.E.; Hunt, K.A.; Bond, D.R.; Gralnick, J.A. Enabling unbalanced fermentations by using engineered electrode-interfaced bacteria. *mBio* **2010**, *1*.

[207] Webster, D.P.; TerAvest, M.A.; Doud, D.F.R.; Chakravorty, A.; Holmes, E.C.; Radens, C.M.; Sureka, S.; Gralnick, J.A.; Angenent, L.T. An arsenic-specific biosensor with genetically engineered Shewanella oneidensis in a bioelectrochemical system. *Biosensors & bioelectronics* **2014**, *62*, 320–324.

[208] Okamoto, A.; Nakamura, R.; Nealson, K.H.; Hashimoto, K. Bound Flavin Model Suggests Similar Electron-Transfer Mechanisms in Shewanella and Geobacter. *CHEMELECTROCHEM* **2014**, *1*, 1808–1812.

[209] Dwevedi, A. Basics of Enzyme Immobilization. In *Enzyme Immobilization*; Dwevedi, A., Ed.; Springer International Publishing: Cham, 2016; pp 21–44.

[210] Gupta, G.; Lau, C.; Rajendran, V.; Colon, F.; Branch, B.; Ivnitski, D.; Atanassov, P. Direct electron transfer catalyzed by bilirubin oxidase for air breathing gas-diffusion electrodes. *Electrochemistry Communications* **2011**, *13*, 247–249.

[211] Li, B.; Zhou, J.; Zhou, X.; Wang, X.; Li, B.; Santoro, C.; Grattieri, M.; Babanova, S.; Artyushkova, K.; Atanassov, P.*; et al.* Surface Modification of Microbial Fuel Cells Anodes: Approaches to Practical Design. *Electrochimica Acta* **2014**, *134*, 116–126.

[212] Margot, J.; Bennati-Granier, C.; Maillard, J.; Blánquez, P.; Barry, D.A.; Holliger, C. Bacterial versus fungal laccase: potential for micropollutant degradation. *AMB Express* **2013**, *3*, 63.